

Dissertation zur Erlangung des Doktorgrades der Fakultät für Chemie und Pharmazie
der Ludwig-Maximilians-Universität München

RNA polymerase I

structure and transcription regulation



Christoph Engel

aus

Leipzig

2013

Erklärung

Diese Dissertation wurde im Sinne von § 7 der Promotionsordnung vom 28. November 2011 von Herrn Prof. Dr. Patrick Cramer betreut.

Eidesstattliche Versicherung

Diese Dissertation wurde eigenständig und ohne unerlaubte Hilfe erarbeitet.

München, den

.....
Christoph Engel

Dissertation eingereicht am 12.12.2013

1. Gutachter: Prof. Dr. Patrick Cramer

2. Gutachter: PD Dr. Dietmar Martin

Mündliche Prüfung am 21.01.2014

Summary

Transcription of ribosomal RNA by RNA polymerase (Pol) I initiates ribosome biogenesis and regulates eukaryotic cell growth. Obtaining the crystal structure of Pol I would improve our understanding of the enzymes regulation and its functional properties. It has therefore been a target of investigation over the past 10 years. Within this work, a number of strategies were pursued to obtain a novel Pol I crystal form that allows for solving a high-resolution structure. Purification of Pol I from the fission yeast *Schizosaccharomyces pombe* was established and its crystallization assayed for this purpose. For the baker's yeast *Saccharomyces cerevisiae*, new strains were established, the fermentation and purification adapted and a new crystal form obtained. This allowed for solving the structure of the 590-kilodalton (kDa) enzyme at a resolution of 2.8 Å. For phasing, intrinsically bound zinc atoms were used. An atomic model of Pol I was built and refined to an R-free factor of 21% with excellent stereochemistry. The model revealed all 14 subunits of the enzyme with exception of the tandem winged helix domain of subunit A49 and several unstructured surface residues. The structure shows differences to Pol II. The dimerization domain of the Pol-I-specific A49/A34.5 subcomplex is anchored on the polymerase by an elongated, well ordered, lysine-rich tail. The Pol-I- and Pol-III-specific subunit complex AC40/AC19 is first described structurally. Furthermore, the C-terminal domain of subunit A12.2 is shown to resemble the fold and positioning of TFIIS, thereby explaining the intrinsic cleavage activity of Pol I. A novel 'expander' element occupies the DNA template site and stabilizes an expanded active centre cleft with an unwound bridge helix. A 'connector' element invades the cleft of an adjacent polymerase and stabilizes an inactive polymerase dimer. The connector and expander must detach during Pol I activation to enable transcription initiation and cleft contraction by convergent movement of the polymerase 'core' and 'shelf' modules. Conversion between an inactive expanded and an active contracted polymerase state may generally underlie transcription. Regulatory factors can modulate the core–shelf interface that includes a 'composite' active site for RNA chain initiation, elongation, proofreading and termination.

Acknowledgments

First and foremost I would like to thank Patrick Cramer, the master of polymerases, for his excellent supervision. His overseeing of general strategies and support of even somewhat outrageous ideas have contributed a great deal to this work's success. Consistent support and encouragement even throughout the extended dry-patches of this work alongside managing an immense machinery, that is his lab and the Gene Center itself, were truly inspiring for me. To learn from Patrick's presentation skills in speech and writing, his open-mindedness and his general attitude towards science contributed to shaping my own ideas. Thank you Patrick.

I thank all past and present members of the Cramer lab and would like to highlight some that were especially important to this work's success and to me personally. Starting off as a master student under my supervision, walking to Spain and then returning despite better knowledge of what was to come, Tobias Gubbey contributed a great deal. Not only did he perform many experiments and made the lab an increasingly happy place, but also did his assistance in daily work help to take my mind off the short-term problems in favour of more general strategies. Also thanks to Sarah Sainsbury for consistent discussion throughout all stages of the project and for not taking me for a lunatic (at least in the beginning). Sarah's efforts to teach me computational crystallography and her help during preparation of the paper were most important. I would like to thank Carlo "Radioactive Man" Bäjén for helping me with endless fermentations, all assays involving radioactivity, daily lab business, coffee, "Buse" and general discussions about the world. If friendship and moral support would count, Carlo would be co-author of this work.

Thanks to Schulzi for searching, finding, having, celebrating, going and being NUTs. Also thanks to Alan Cheung for advice on data-collection strategies and computational crystallography training and support. Thanks to Stefan Benkert for fermentation and help with establishing the *S. pombe* protocols. Thanks to Stefan Jennebach for introduction to the topic of Pol I and for not losing his nerves with me in the early stages. Thanks to Simon Neyer for work on the Elp1 project and being crazy enough to come back for Pol I. Also thanks to Sebastian Geiger, Claus Kuhn and Claudia Blattner, the past Pol I team as well as Kerstin Maier and Stefanie Etzold for help with yeast cloning. Thanks to Franz Herzog for crosslinking and Kathrin "Gollum" Schwinghammer for the best synchrotron trips. And of course thanks to all members of the lab and the positive interactions: Youwei "Eier", Carrie, Rike, Else, Merle, Anna and Bruno, Kerstin K., Daniel R., Fuen, Clemens, Jürgen, Sofia, Anselm, Wolfgang, Michi, Mai, Poony, Phillipp "Fallout Boy", Carina, Pölli, Dietmar, Tobias

K., Lutz Z., Claudia Bu., as well as “our” students Saskia, Silva, Katharina and everyone I forgot.

I would also like to thank my external colleagues for help, input and discussions: Steve Hahn and Bruce Knutson, Alessandro Vannini, Ana Lisica and Stephan Grill as well as Herbert Tschochner and his lab, Christoph Carles, Oliver Gadal and Achim Griesenbeck. Thanks to Sebastian Hogl for the occasional late-night mass spec and Skat session and to Malte Kock and Petra Wendler for electron microscopy. SLS and ESRF staff were most kind and very helpful. Also thanks to Karina, Sabine and Laura from the MPI crystallization facility and Stefan Uebel of the Core facility as well as the ZfP mass spectrometry facility. Many thanks also to Irina Heckmann and Max Kern from the Stefan Jentsch Department of the MPI for Biochemistry for sharing a great A190-shuffle strain with me.

Furthermore, I am most grateful to the Boehringer Ingelheim Fonds for personal and financial support as well as a travel grant. Special thanks to Claudia Walther, Anja Hoffmann and Sandra Schedler who are the heart of the organization. Also thanks to the Bavarian Elite Network program “Protein dynamics in health and disease” and all its members for great retreats and scientific exchange. Furthermore, I thank the SFB960 graduate school “RNA Biology”.

To my past mentors Gert Bange and Irmgard Sinning I am still grateful for an exciting start into the real world of Biochemistry during my master thesis and consistent discussions and support also past my graduation. Further thanks to the members of my thesis advisory committee: Herbert Tschochner and Petra Wendler.

Also thanks to Andrea, Sarah, Tobias and Sebastian for carefully reading this thesis.

Last but not least, I thank my family for their constant support: My sister Lydia, my parents Lutz and Simone as well as grand parents Christa and Klaus, Liesel and Rolf and the cousins, uncles, aunts, ... Especially thanks to Andrea for putting up with all that (me) and for bringing proper language into this thesis.

Contributions

During the preparation of this thesis, I was trained and assisted by many great researchers in our institute who I hereby acknowledge for their respective contributions:

- Patrick Cramer designed and supervised all research and wrote the manuscript of the publication associated with this thesis with input from all authors
- Claus Kuhn initially established the Pol I fermentation and purification in our laboratory and obtained an initial crystal form
- Sebastian Geiger solved the structures of Pol I subunit complexes A14/A43, and A49/A34.5
- Claudia Blattner established the recombinant expression and purification of Rrn3 and was able to solve its crystal structure
- Stefan Jennebach positioned Pol-I-specific subunits and Rrn3 on a Pol-II-based homology model of Pol I
- Stefan Benkert performed all yeast fermentations with the help of Carlo Bäjén or Tobias Gubbey
- Malte Kock performed electron microscopy of Pol I samples together with Petra Wendler
- Franz Herzog carried out mass spectrometry following crosslinking and evaluated the results
- Sarah Sainsbury, Alan Cheung and Dirk Kostrewa aided in processing and interpretation of crystallographic data
- Sarah Sainsbury and Alan Cheung helped preparing Figures for the associated publication
- Alan Cheung produced movies of crystal structures associated with this thesis and the publication
- Carlo Bäjén performed all radioactive work presented in this thesis
- Simon Neyer and Silva Bussemer contributed to the Elp1 project
- Tobias Gubbey aided in or carried out work associated with the Core Factor
- Sarah Sainsbury and Alan Cheung advised on crystallographic work
- Polymerase purification, strain establishment, cloning, crystallographic work, data collection, structure solution and model building and all experiments were planned and performed by Christoph Engel

Publication

Engel, C., Sainsbury, S., Cheung, A. C., Kostrewa, D. & Cramer, P.

RNA polymerase I structure and transcription regulation.

Nature 502, 650-655, Oct. 31 (2013)

Author Contributions: C.E. planned and carried out experiments and crystal structure determination. S.S. advised on experimental and crystallographic work. A.C.C. performed computational crystallographic analysis. D.K. contributed to computational crystallography and model building. P.C. designed and supervised research and prepared the manuscript, with contributions from all authors.

List of Figures

Figure 1. The nucleolus and rDNA repeat organization	15
Figure 2. Pol I initiation in yeast	16
Figure 3. Structure-guided sequence alignment	19
Figure 4. Crystal structures of multi-subunit DNA-dependent RNA polymerases.....	21
Figure 5. Electron microscopy structures of the complete RNA polymerase I and known crystal structures of Pol I subunits	22
Figure 6. Purification of Pol I.....	44
Figure 7. Purified Pol I is active in elongation and cleavage of a preannealed elongation scaffold	44
Figure 8. Initial Pol I crystals of form A in the PEG 6000 condition	45
Figure 9. Crystal form B in a PEG 3350 condition.....	46
Figure 10. Crystal form C, initial diffraction and crystal optimization.....	47
Figure 11. X-ray diffraction of crystal form C.....	48
Figure 12. Phasing Pol I with intrinsically bound zincs.....	50
Figure 13. Crystal structure of Pol I.....	51
Figure 14. Structure of the two largest Pol I subunits.....	52
Figure 15. Structure of the subassembly AC40/AC19/Rpb10/Rpb12	53
Figure 16. Subunit A12.2 - Structure and sequence comparison.....	53
Figure 17. Structure and location of the TFIIIF-like subcomplex A49/A34.5.....	54
Figure 18. Expanded cleft, expander and unwound bridge helix.....	56
Figure 19. Shift in domain positions between Pol I and Pol II	56
Figure 20. Composite active site and A12.2 hairpin.....	57
Figure 21. Connector and Pol I dimerization	58
Figure 22. Activity of Pol I and re-evaluation of expander crosslinking data	59
Figure 23. Model for Pol I initiation regulation.....	60
Figure 24. Generation <i>S. pombe</i> strains with tagged Pol I subunits.....	81
Figure 25. Purification of <i>S. pombe</i> Pol I.....	82
Figure 26. Elongation/cleavage assay of <i>S. pombe</i> Pol I	83
Figure 27. Crystallization of <i>S. pombe</i> Pol I.....	84
Figure 28. <i>S. pombe</i> Pol I crystals in a PEG 4000 condition	85
Figure 29. Purification of <i>S. pombe</i> Pol IΔ	87

Figure 30. Proteolytic digest of <i>S. pombe</i> Pol I.....	88
Figure 31. Crystallization of a chymotrypsin-digested <i>S. pombe</i> Pol I variant.....	89
Figure 32. Structure-based alignment of A190 and Rpb1.....	97
Figure 33. Structure-based alignment of A135 and Rpb2.....	98
Figure 34. Structure-based sequence alignment of the sub complex AC40/AC19 with Rpb3/Rpb1	99
Figure 35. Detailed comparison of A190–A135 domains with their Rpb1–Rpb2 counterparts	101
Figure 36. Sequence conservation of the expander and the connector element.....	102
Figure 37. Mutation of the expander element does not result in a growth defect on YPD medium.....	103

Table of contents

Summary	3
Acknowledgments	4
Contributions	6
Publication.....	7
List of Figures	8
Table of contents	10
1. Introduction	13
1.1 General importance and composition of RNA polymerases	13
1.2 The rDNA gene and its organization.....	14
1.3 Pol I transcription cycle.....	16
1.4 Regulation of Pol I activity.....	17
1.5 Structural information on DNA-dependent RNA polymerases and their general transcription factors	18
1.6 Scope of this study.....	21
2. Materials and Methods	24
2.1 Materials	24
2.1.1 Strains.....	24
2.1.2 Oligonucleotides.....	25
2.1.3 Media.....	29
2.1.4 Plasmids	30
2.1.5 Buffers for the purification of RNA polymerase I	33
2.2 Molecular Biology Methods	34
2.2.1 Polymerase Chain reaction.....	34
2.2.2 Preparation of competent <i>E. coli</i> cells.....	34
2.2.3 Transformation in <i>E. coli</i> and plasmid purification	35
2.2.4 DNA digest and ligation.....	35

2.2.5 Preparation of competent yeast cells and DNA transformation	35
2.3 Biochemical Methods	37
2.3.1 Fermentation of <i>S. cerevisiae</i>	37
2.3.2 Fermentation of <i>S. pombe</i>	37
2.3.3 Pol I purification.....	38
2.3.4 Expression and purification of recombinant proteins.....	39
2.3.5 Protein analysis	39
2.3.6 Transcription assays	40
2.4 Crystallization and structure solution	40
2.4.1 Pol I crystallization and microseeding	40
2.4.2 Data collection and processing.....	41
2.4.3 Phasing	41
2.4.4 Model building and refinement	42
3. Results and Discussion.....	43
3.1 Purification of <i>S. cerevisiae</i> Pol I	43
3.2 <i>S. cerevisiae</i> Pol I crystallizes in three different forms, of which one is suitable for structure determination	43
3.3 Data collection and processing	47
3.4 Solving the structure of Pol I.....	48
3.5 Pol I structure.....	51
3.6 Composite active centre and the A49/A34.5 subcomplex.....	54
3.7 Expander and cleft expansion.....	55
3.8 Connector and polymerase dimerization	57
3.9 Transcription regulation	58
4. Conclusion and Outlook.....	61
4.1 Conclusions	61
4.2 Evaluation of previously obtained structural information on Pol I	62
4.3 RNA polymerase I from an evolutionary point of view	64

4.4 Future perspectives	66
5. References	70
6. Appendix	79
6.1 <i>Schizosaccharomyces pombe</i> RNA polymerase I	79
6.1.1 Construction and cultivation of <i>S. pombe</i> strains with tagged Pol I subunits	79
6.1.2 <i>S. pombe</i> Pol I - purification and activity	81
6.1.3 Attempts to crystallize <i>S. pombe</i> Pol I	83
6.1.4 Conclusion of the <i>S. pombe</i> Pol I project	89
6.2 Scripts for crystallographic data processing	91
6.2.1 XDS script for data integration	91
6.2.2 XSCALE script for the combination of five datasets from four crystals	92
6.2.3 XSCALE – Selected output parameters	92
6.3 Scripts and parameterization files for structure refinement.....	93
6.3.1 Refinement strategy file for phenix.refine	93
6.3.2 Definition of bond lengths for one coordinated Zinc atom.....	93
6.3.3 Definition file for NCS refinement	94
6.3.4 Definition file for Rigid body refinement	95
6.3.5 Definition file for TLS refinement	96
6.3.6 Solvent definition file for refinement.....	96
6.4 Structure-based alignment of A190 and Rpb1	97
6.5 Structure-based alignment of A135 and Rpb2	98
6.6 Structure-based alignment of AC40/AC19 and the Rpb3/Rpb11 subcomplex	99
6.7 Conservation of Pol I and Pol II subunits.....	100
6.8 Domain differences between the polymerase subunits A190/Rpb1 and A135/Rpb2 ..	101
6.9 Evolutionary conservation of expander and connector elements	102
6.10 Expander mutations do not display a growth defect in <i>S. cerevisiae</i> on YPD medium	103
7. Abbreviations	104

1. Introduction

1.1 General importance and composition of RNA polymerases

Every cell needs to perform a series of metabolic processes in order to stay alive. Among them, the transcription of DNA into RNA plays a central role. This task is performed by DNA-dependent RNA polymerases (Pols). Whereas viruses and organelles use a single subunit polymerase, all other cell types have evolved one or more mutli-subunit polymerases¹. In bacteria and archaea, one single polymerase transcribes all forms of RNA^{2,3}. However, in eukaryotes, three different polymerases have evolved to perform specific tasks: (1) Pol I transcribes ribosomal RNA (rRNA); (2) Pol II produces messenger RNA (mRNA) and several small, functional RNAs; and (3) Pol III transcribes transfer RNA (tRNA), one small rRNA and others⁴. In plants, two additional polymerases (IV and V) exist and have a function in RNA interference and gene silencing^{5,6}. The three general eukaryotic Pols share a common core of the five subunits Rpb5, Rpb6, Rpb8, Rpb10 and Rpb12. Furthermore, the large subunits are homologous: A190 and A135 in Pol I, Rpb1 and Rpb2 in Pol II and C160 and C128 in Pol III⁷. All Pols contain a protruding element that is called stalk and consists of two strongly associated subunits that have related counterparts: A14/A43 in Pol I⁸, Rpb4/Rpb7 in Pol II⁹ and C17/C25 in Pol III¹⁰. Additionally, the Pols include a heterodimeric subcomplex that is shared between Pol I and III (AC40/AC19) and homologous to Rpb3/Rpb11 in Pol II⁷. Apart from the 12 homologous, shared or common subunits, Pol I and III contain an additional subcomplex that consists of the two subunits A49/A34.5 or C37/C53, respectively¹¹. Finally, the trimeric C82/C34/C31 subcomplex is unique to Pol III¹². Table 1 displays all subunits of the three eukaryotic polymerases and their relation to each other. Throughout this thesis, the nomenclature will refer to the yeast *Saccharomyces cerevisiae* and might differ from other organisms.

Table 1. Yeast RNA Polymerase Subunits and Homologues⁴.

Pol II	Pol I	Pol III
Polymerase Core		
Rpb1	A190	C160
Rpb2	A135	C128
Rpb3	AC40	AC40
Rpb11	AC19	AC19
Rpb9	AC12.2 N-ribbon	C11 N-ribbon
TFIIS C-ribbon ^a	AC12.2 C-ribbon	C11 C-ribbon
Rpb5	Rpb5	Rpb5
Rpb6	Rpb6	Rpb6
Rpb8	Rpb8	Rpb8
Rpb10	Rpb10	Rpb10
Rpb12	Rpb12	Rpb12
Polymerase Stalk		
Rpb4	A14	C17
Rpb7	A43	C25
General Transcription Factors and Their Counterparts		
Tfg1 (TFIIF α)	A49 (N-terminal domain)	C37
Tfg2 (TFIIF β)	A34.5	C53
Tfa1 (TFIIE α) ^b		C82 ^b
Tfa2 (TFIIE β) ^c	A49 (C-terminal domain) ^c	C34 ^c
		C31

a TFIIS is a dissociable factor that is not part of the polymerase core. Its C-terminal ribbon domain (C ribbon) is however structurally and functionally related to the corresponding domains of A12.2 and C11.

b These proteins share "extended" WH domains but their evolutionary relationship remains at present tentative.

c These proteins share two subsequent WH domains but their evolutionary relationship remains at present tentative.

1.2 The rDNA gene and its organization

Apart from transcription of DNA into RNA, the translation of mRNA into proteins is another central cellular process that is common to all organisms. It is performed by ribosomes which themselves consist of RNA and proteins¹³. The large ribosomal subunit is termed 60S and contains the 24S, the 5.8S and the 5S rRNAs as well as 42 ribosomal proteins. The small subunit, called 40S, consists of the 18S rRNA and 32 additional proteins¹³. Biogenesis of ribosomes starts with processing of the 35S rRNA precursor which is produced by Pol I from multiple copies of the rDNA gene. From the 35S precursor, the three ribosomal RNAs 24S, 18S and 5.8S are processed. The smallest rRNA (5S) is transcribed by Pol III¹⁴.

In quantitative terms, the production of rRNA is one of the most energy-consuming processes in the cell. It accounts for up to 60% of overall transcription rates and results in up to 80% of total RNA in exponentially growing cells^{15,16}. The factories of rRNA transcription are the nucleoli, which are the most prominent substructure of the nucleus. Multiple copies of the rDNA gene (~150 in yeast) are located in the same genomic region and are, if they are active, each transcribed by several Pol I molecules. This results in the formation of “Christmas-tree-like” structures that can be visualized by electron microscopy in so-called “Miller-spreads”¹⁷. Figure 1 displays a nucleolus as the most prominent substructure of the nucleus (a)¹⁸ as well as a Miller spread (b)¹⁷. In yeast, rDNA repeats are clustered at one single position on chromosome XII whereas human cells have five separate rDNA clusters^{19,20}. Each of those clusters can form a nucleolus and is therefore termed nucleolar organizer region (NOR)²¹. All NORs share a conserved organization that is depicted in Figure 1c²²: The rDNA genes are tandemly repeated and separated by an intergenic spacer (IGS) that plays a role in silencing. Each yeast repeat contains the 35S rRNA precursor gene, its promoter, an enhancer, a terminator, the Pol III transcribed 5S rRNA gene and elements that regulate replication²².

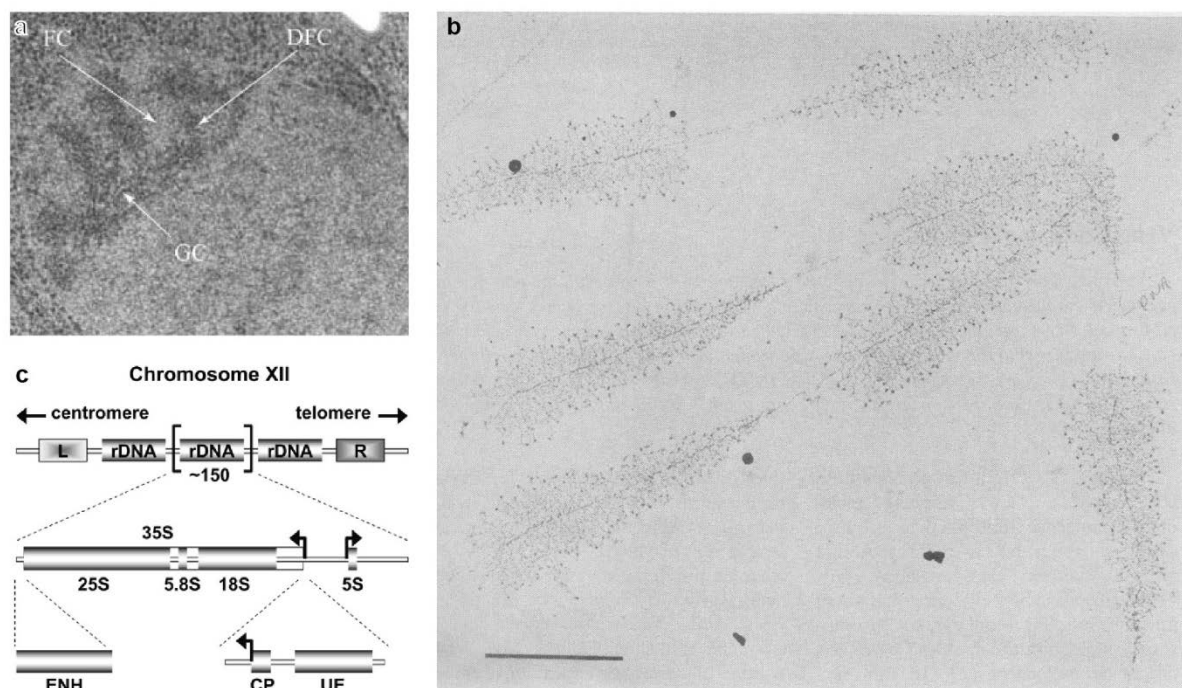


Figure 1. The nucleolus and rDNA repeat organization.

a Electron microscopic representation of a *S. cerevisiae* nucleolus¹⁸. FC, Fibrillar centre; DFC, Dense fibrillar centre; GC, Granular centre. **b** Miller spread of a *Triturus viridescens* oocyte displays rDNA transcription by multiple Pol I molecules resulting in a christmas-tree-like representation¹⁷. The bar corresponds to 1 μ m. **c** Schematic representation of the *S. cerevisiae* rDNA locus²². The position of the rDNA repeat cluster on chromosome XII including the left (L) and the right (R) flanking regions with respect to the centromere and telomere is shown. Each rDNA repeat consists of the Pol I-transcribed 35S rRNA gene (precursor for the 18S, 5.8S, and 25S rRNAs) and the RNA Pol III-transcribed 5S rRNA gene. Arrows mark the transcription start sites and direction. The positions of three regulatory DNA elements ENH (enhancer), CP (core promoter), and UE (upstream element) are indicated.

1.3 Pol I transcription cycle

In general, rDNA promoters are 140-160 base pair (bp) long stretches which are not well conserved throughout different organisms²³. Nevertheless, all of them seem to contain two regulatory elements, the so-called upstream element (UE) and the core element (CE), as displayed in Figure 1 and Figure 2. The UE is bound by the upstream activation factor (UAF) that consists of Rrn5, Rrn9, Rrn10, UAF30 and the associated histones H3 and H4²³. The UAF is then bound by the TATA binding protein (TBP) and the core factor (CF) which in turn interacts with the core element of the promoter²⁴. CF is a heterotrimer that consists of the proteins Rrn6, Rrn7 and Rrn11^{25,26}. Upon interaction of CF with the initiation factor Rrn3, Pol I is recruited²⁷. It has been shown that this recruitment is dependent on the binding of Rrn3 to the Pol I stalk subunit A43 on the one hand, and an interaction with the CF component Rrn6 on the other hand²⁷. Following initiation, Pol I starts transcribing and the initiation factors Rrn3, CF as well as TBP dissociate from the complex. The complete process of initiation is schematically depicted in Figure 2²³.

Once in elongation mode, Pol I transcribes the complete 35S rRNA precursor. The Pol I elongation complex contains several components including a number of general Pol II elongation factors. It has been shown that the Spt4/5 complex can interact with Pol I and has a regulatory effect^{28,29}. Additionally, the Paf1 complex has been shown to associate with elongating Pol I³⁰. The Paf1 complex is associated with chromatin remodelling and was mainly studied in the Pol II system³¹. Recent work from this system demonstrated that the subunit Rtf1 of the Paf1 complex binds the C-terminal repeat (CTR) of Spt5 if this CTR carries a specific phosphorylation^{32,33}. By homology, this strongly argues for elongating Pol I to be associated with both, the Paf1 complex as well as Spt4/5. Independently, a head-to-tail dimerization of elongating polymerases has been proposed from EM studies³⁴. This would agree with the high loading rate of Pol I and might contribute to Rrn3 release. However, it is

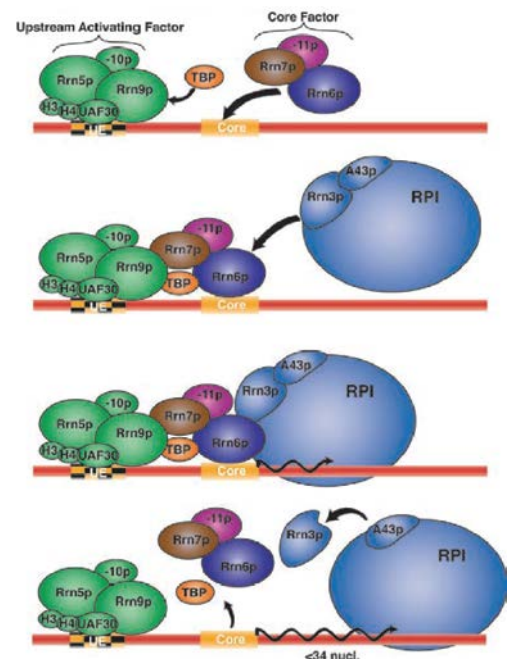


Figure 2. Pol I initiation in yeast^{21,23,24}.

The Upstream Activating Factor (UAF) binds to the upstream element (UE) and recruits TBP (TATA binding protein) as well as the Core Factor (CF). Pol I (RPI) itself binds Rrn3 via its subunit A43 and is subsequently recruited to CF, partly by interaction of Rrn3 with Rrn6.

unclear how backtracking and/or RNA cleavage would take place in such a scenario. Furthermore, a strain with Rrn3 fused to the C-terminus of A43 is still able to elongate at wild type levels.

The termination of Pol I transcription has been a focus of numerous studies. Whereas a 61 bp T-rich sequence is sufficient to terminate Pol I *in vivo*, the involved players and their respective roles remain to be defined. In any case, the endonuclease Rnt1 as well as the exonuclease Rat1 and the helicase Sen1 seem to be involved³⁵⁻³⁷. The action of Rat1 in a “torpedo-like” fashion has been discussed but does not seem to be sufficient for termination in an *in vitro* system³⁸. A binding site for the protein Reb1 has been found at the 3’ end of the 25S rRNA sequence and is situated only 16 bp 5’ of the T-rich sequence³⁹. Binding of the Reb1 homologue Nsi1 was suggested to slow down elongating Pol I before it hits the T-rich termination patch³⁹. However, the rRNA precursor still needs to be cleaved off and released. Which nuclease performs this task or if the Pol I subunit A12.2 is involved in that process remains to be resolved.

1.4 Regulation of Pol I activity

Despite the presence of numerous rDNA copies, only half of them are actively transcribed at one point in time, even in exponentially growing cells⁴⁰. The reason for rDNA gene inactivation can mostly be found in epigenetic silencing which is characterized by DNA hyper-methylation and deacetylation of histones (eg. H4)⁴¹. Additionally, silencing of rDNA genes in higher eukaryotes requires a transcript of the IGS which is incorporated into a nucleolar remodelling complex that subsequently associates with the IGS itself⁴².

Independent of the epigenetic state of rDNA repeats and hence the number of active genes, Pol I loading rate seems to have a high importance in regulating rDNA transcription⁴⁰. Meaning, Pol I activity can be regulated via the availability of Pol I / Rrn3 complexes since the formation of a stable complex of Pol I with Rrn3 was shown to be a prerequisite for efficient initiation⁴³. Rrn3 binds to the Pol I stalk subunit A43 in a phosphorylation dependent manner^{27,44,45}. Thus, one of the main mechanisms controlling Pol I activity is based on phosphorylation and dephosphorylation of Pol I subunits and Rrn3 itself⁴⁵ and thereby the manipulation of available Pol I / Rrn3 complex. Rrn3 forms a homodimer in solution but binds Pol I as a monomer, for which it needs to be dephosphorylated⁴⁴. In contrast, site specific Pol I phosphorylation is required for binding Rrn3^{45,46}. The two main Pol I phosphorylation sites cluster around the stalk⁴⁶ and around A190 residue 1415⁴⁷. The

phosphorylation of those sites and hence the amount of Pol I / Rrn3 complex formation was shown to be dependent on signalling via the target of rapamycin (TOR) pathway⁴⁸. The TOR pathway also links the production of rRNA to ribosomal protein transcription by Pol II⁴⁹. In line with this, the level of Rrn3 is decreased by down-regulated expression coupled to targeted proteasomal degradation upon starvation-induced impairment of TOR signalling⁵⁰. On the other hand, if the amount of Pol I / Rrn3 complex is artificially increased by a covalent fusion of Rrn3 to A43, regulation defects occur¹⁶. This further strengthens the role of Pol I / Rrn3 complex number to be important for rRNA transcription regulation.

Independent of Rrn3, an inactive dimeric form of Pol I was observed in yeast^{43,51}. Similarly, a human version of Pol I was described to be inactive and is most likely dimeric as well⁵². To summarize, it is known that Pol I regulation takes place (1) at an epigenetic level, (2) via a phosphorylation-dependent influence on the abundance of Pol I / Rrn3 complexes, and (3) by changing the level of available Rrn3. A dimerization of Pol I does take place and might have an additional regulatory role. Also, further phosphorylations on Pol I subunits might have additional influences. However, none of these appear to account for rRNA expression changes on their own. It seems rather likely that a complex interplay occurs which orchestrates the efficient and tight regulation of rRNA transcription. Supporting the special requirement of tight regulation, it has been shown that deregulation of rRNA transcription in humans is largely observed in cancer cells and is correlated to tumour malignancy^{53,54}. This also means, that Pol I - dependent transcription emerges as a novel target for cancer therapy⁵⁴. The availability of a Pol I structure with atomic resolution would be the ideal starting point for designing specific inhibitors, comparable to the structure-based design of antibiotics influencing the bacterial RNA polymerase^{55,56}.

1.5 Structural information on DNA-dependent RNA polymerases and their general transcription factors

At the beginning of this work, the structure of RNA polymerase II 10-subunit-core from yeast had been solved for a decade^{57,58} and the 12-subunit-structure was known^{9,59}. Despite intense work on Pol I, the only available data on the complete polymerase originated from electron microscopy. This included a negative stain reconstruction from Patrick Schultz's lab⁶⁰ as well as a cryo EM map from our group⁸. In addition, the crystal structure of the heterodimeric stalk-subunit-complex A14/A43 has been reported^{8,61}. Later on, the crystal structures of the Pol-specific subunit complex A49/A34.5 and the initiation factor Rrn3 were solved in our

lab⁴⁴. Finally, the architecture of the complete 14-subunit Pol I has been further elucidated by lysine-lysine crosslinking coupled to mass spectrometry⁶². This did not only display the location of the A49/A34.5 subcomplex on the A135 lobe and the top of the cleft (not entirely complying with the cryo-EM⁸), but also showed that the C-terminus of A12.2 folds like the Pol II elongation and cleavage factor TFIIIS. The TFIIIS-like fold explains the strong intrinsic cleavage activity which Pol I exhibits in contrast to Pol II⁸. According to their structural and functional properties, domains were assigned to the different polymerase subunits⁵⁸. Despite the notable differences between the three eukaryotic multi-subunit polymerases, most domains are apparently conserved⁸. Figure 3 displays the domain assignment for Pol II and the suspected Pol I homology, which largely originated from sequence analysis of all subunits⁸. In the case of A12.2, information regarding homology to TFIIIS was added later on according to crosslinking/mass spectrometry results⁶². The sequence comparison shows that A190 contains the main elements of the Pol II subunit Rpb1. Most strikingly, it displays large insertions in the clamp head and the jaw domains, as well as a prominent deletion in the foot domain. Furthermore, Pol I does not contain the C-terminal domain (CTD) of Rpb1 with its regulatory, repetitive sequence elements⁸. A135 and Rpb2 are overall conserved, as are AC40 and Rpb3 as well as AC19 and Rpb11. The latter two, however, display differences in their N- or C-terminal regions.

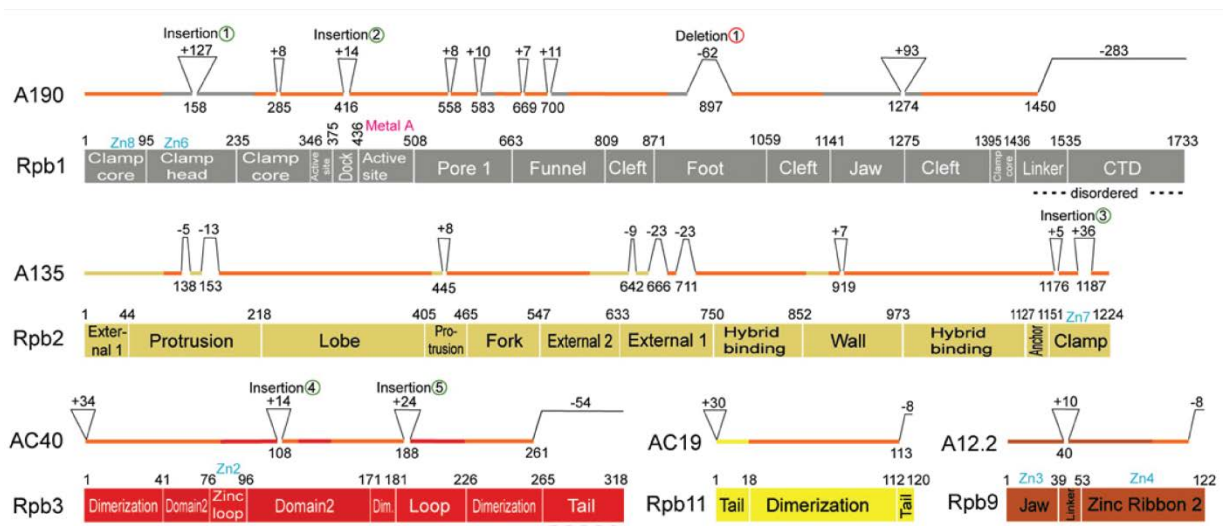


Figure 3. Structure-guided sequence alignment⁸.

Pol II structure-guided sequence alignment of five Pol I subunits with their homologs in Pol II. The domain organization of Pol II subunits Rpb1, Rpb2, Rpb3, Rpb11, and Rpb9 is shown as diagrams⁸. Insertions and deletions exceeding five amino acid residues are indicated. Conserved folds are indicated by orange highlighting of the bar above the diagrams. CTD: C-terminal domain.

The structure of the N-terminal so-called dimerization domain of A49 shows a strong homology to the dimerization domain of Tfg1 and Tfg2, subunits of the Pol II initiation factor TFIIF^{11,63}. Furthermore, the A49 C-terminal tandem-winged helix (tWH) domain displays similarities with the winged helix domain of the Pol II initiation factor TFIIE¹¹. Overall, the homologies between Pol I subunits and Pol II transcription factors seem quite striking but also make a lot of sense: While Pol II transcribes a larger number of different target genes, it requires a high variability in levels of regulation. In contrast, Pol I only needs to perform one single task and may well have perfectly adapted to it, including the permanent incorporation of transcription factors. Pol III exhibits some of the respective elements as well, and also contains an additional heterotrimeric subcomplex C82/C34/C31 that displays similarities to TFIIE⁶⁴⁻⁶⁶.

In the past years, the development of novel structure and domain prediction algorithms such as “HHPred” by the Soeding group⁶⁷ led to the discovery that the Core factor subunit Rrn7 (TAF1B in humans), one of the main Pol I initiation factors, is homologous to the general Pol II initiation factor TFIIB^{68,69}. The consistent discovery of homologies between Pol II transcription factors and Pol I subunits or initiation factors is a striking feature that confirms the close evolutionary relationship between all multi-subunit polymerases⁴. This suggests that, when working with Pol I, structural and functional features of other polymerases and their transcription factors should be studied and constantly considered. Figure 4 displays the crystal structures of 12-subunit RNA polymerase II from the yeasts *S. cerevisiae*⁷⁰ and *S. pombe*⁷¹ as well as bacterial polymerase from *Thermus aquaticus*⁷² and the archeal polymerase from *Sulfolobus solfataricus*^{3,73}. Pol I subunit crystal structures and EM reconstructions of the complete enzyme are displayed in Figure 5. Known crystal structures of Pol I subunits are the A14/A43 stalk subcomplex, the A49/A34.5 dimerization domain and the A49 C-terminal tandem winged helix domain. Solved crystal structures of Pol II transcription factors include TFIIB, TFIIS, the human TFIIF homologue as well as parts of TFIIE, TFIID and TFIIH.

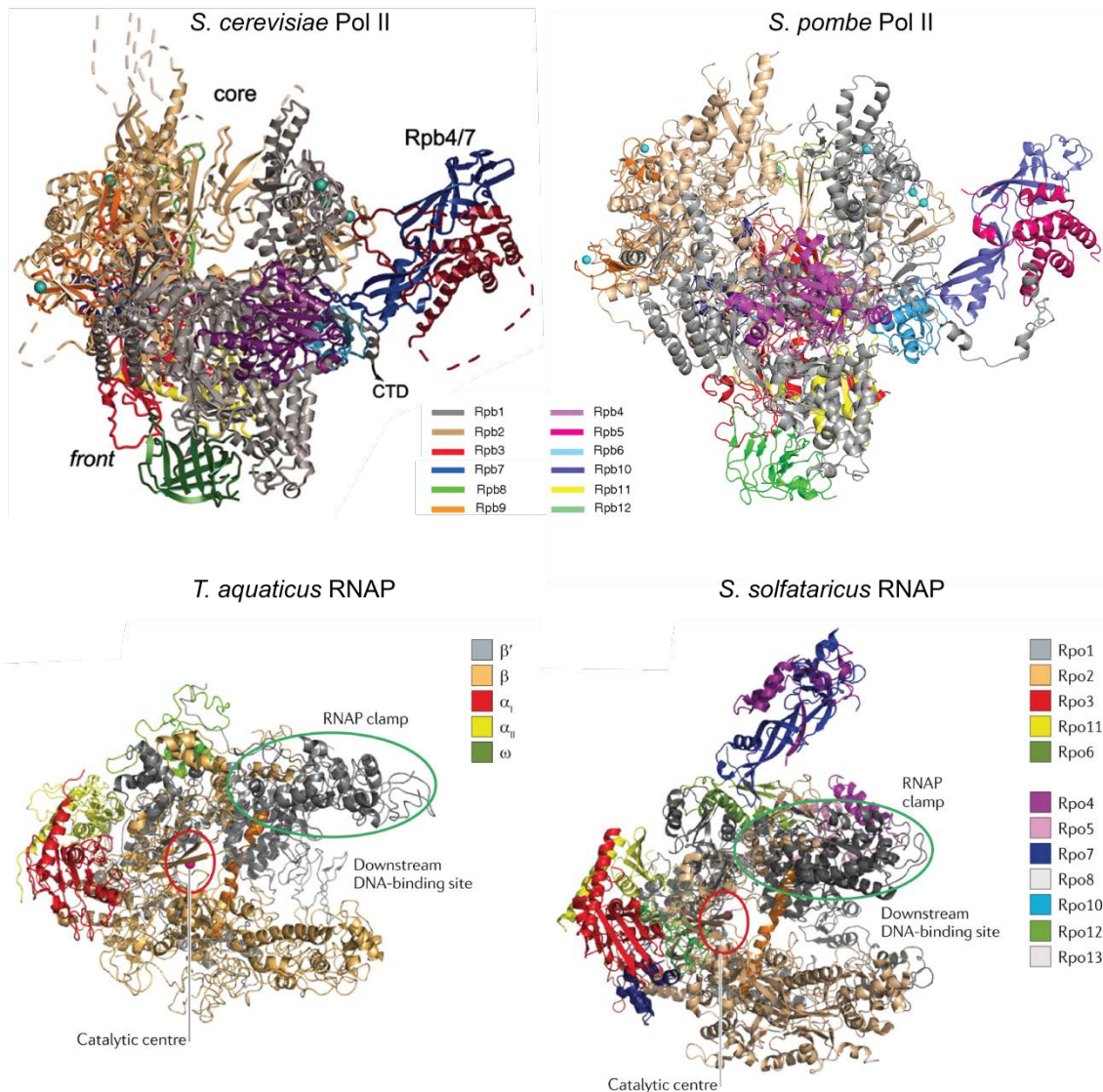


Figure 4. Crystal structures of multi-subunit DNA-dependent RNA polymerases^{3,70-74}. The crystal structures of eukaryotic Pol II from *S. cerevisiae* (1WCM)⁷⁰ and *S. pombe* (3H0G)⁷¹ are displayed in front view. The bacterial polymerase from *T. aquaticus* (1I6V)⁷² and the archaeal polymerase from *S. solfataricus* (2WAQ)⁷³ are displayed in back view (Figures modified from ⁷⁴). The core and overall shape are conserved throughout evolution. Bacterial polymerase does not contain a stalk and organism- or polymerase-specific subunits exist in all organisms. Subunit colour code as indicated.

1.6 Scope of this study

Solving the structure of Pol II at an atomic level led to a much more detailed and well-founded understanding of transcription. Furthermore, it induced a boost of work targeted at specific polymerase features that were elucidated by the structure, giving the complete transcription field a significant boost. Since then, one focus of Patrick Cramer's group was to solve the structure of another eukaryotic polymerase to validate, compare and deepen our understanding of transcription in general. Independently, its role as a major player in ribosome synthesis and its apparently well-defined structure made Pol I an appealing target.

Claus Dieter Kuhn was the first “Pol-I-PhD-student” who implicated a novel protocol for the large scale purification of *S. cerevisiae* Pol I in collaboration with the group of Herbert Tschochner in Regensburg. Claus succeeded in obtaining a cryo-EM map and elucidating the functional architecture of Pol I as well as in crystallizing the 14-subunit Pol I⁷⁵. Unfortunately, it was never possible to solve the Pol I structure from the initial crystals due to a number of reasons, such as poor reproducibility, an extremely large unit cell and enormous radiation damage of the crystals during data collection, a high number of molecules in the

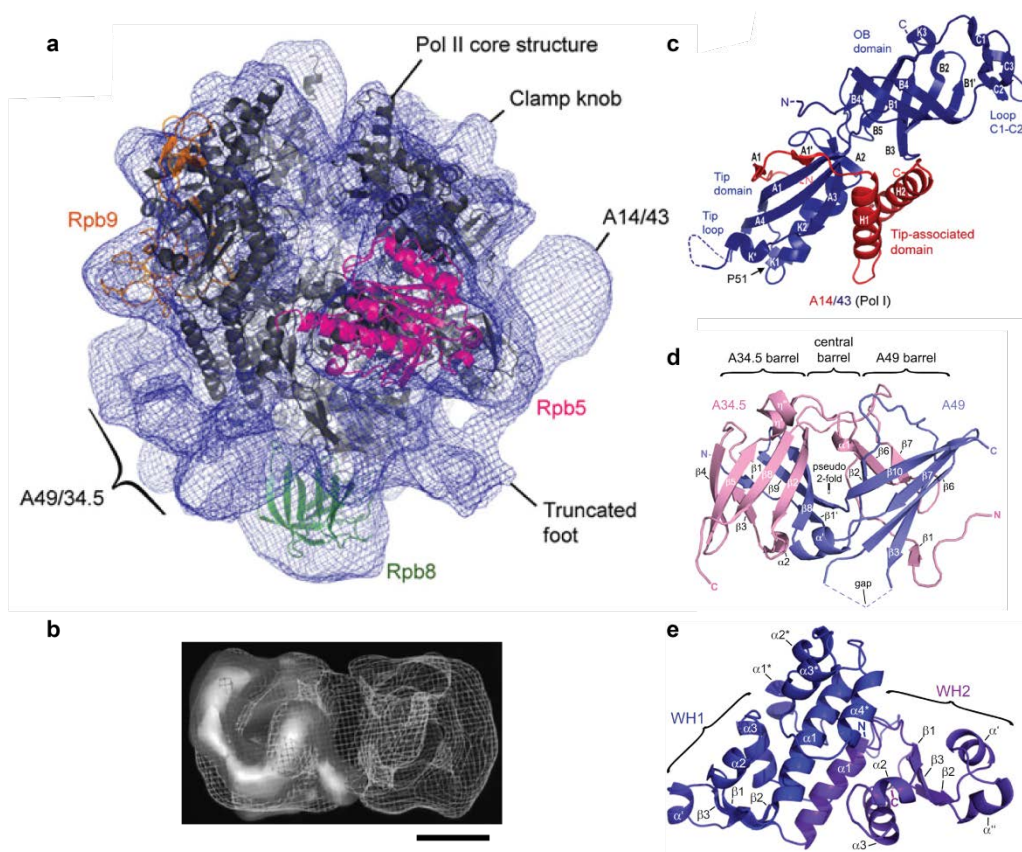


Figure 5. Electron microscopy structures of the complete RNA polymerase I and known crystal structures of Pol I subunits⁸.

a Cryo EM envelope of Pol I with fitted Pol II 10-subunit-core crystal structure⁸. The fit demonstrates that the overall shape is conserved between Pol I and Pol II. However, solvent exposed parts display significant differences. The position of the A49/A34.5 dimerization module is proposed to be outside the funnel domain (bottom left in the panel). **b** Negative stain EM reconstruction of Pol I⁶⁰. Under specific conditions, Pol I forms a dimer which is characterized by interaction of the stalk from one polymerase with the cleft of another. The indicated bar corresponds to 10 nm. **c** Crystal structure of the *S. cerevisiae* Pol I stalk⁸. A43 (blue) and A14 (red) correspond to the Pol II subunits Rpb7 and Rpb4, respectively. However, a domain swap seems to have taken place and the overall shape of the Pol I stalk is less bulky than the one of its Pol II counterpart. Upon limited proteolysis, flexible regions have been removed, including the C-terminal (presumably unstructured) region of A43 in order to improve crystallization behaviour⁶¹. **d** The structure of the A49/A34.5 (slate and pink, respectively; solved from the yeast *Candida glabrata*) dimerization domain is similar to the Tfg1/Tfg2 dimerization domain of the Pol II initiation factor TFIIIF¹¹. Both engage in a double beta-barrel fold that results in a tight association of the two subunits. A34.5 contains an additional, charged C-terminal tail and A49 has a C-terminal domain that is displayed in (e). **e** Crystal structure of the tandem winged helix domain (tWH) situated at the C-terminus of A49¹¹. By structural and functional homology, it likely is related to the winged helix domain of the Pol II initiation factor TFIIIE.

asymmetric unit and difficulties with phasing. Therefore, a second PhD student, Stefan Jennebach, took over the project and continued to work on Pol I crystallization and structure determination. Whereas he managed to increase our understanding of Pol I by applying lysine-lysine crosslinking coupled to mass spectrometry, solving the Pol I crystal structure from the initial crystal form still failed. From Stefan's work it became clear that a different crystal form needed to be obtained for solving the structure. Thus, multiple ideas were raised which all had the common goal of obtaining a novel crystal form: (1) Purification of Pol I from a different organism could lead to an altered crystallization behaviour. Pol II had been recently endogenously purified from *Schizosaccharomyces pombe* and its structure solved in a novel crystal form by the Kornberg lab⁷¹. After a proof of principle by this work, a comparable approach was intended for *S. pombe* Pol I. (2) The deletion of Pol I subunits or addition of transcription factors and/or nucleic acid scaffolds in either organism may also drive an alternative crystallization and hence yield a different crystal form. In line with this, proteolytic digest was intended in order to obtain a minimal Pol I. (3) Solving the structure from the initial crystal form using up-to-date approaches. X-ray detectors, beamline setups and data collection strategies had been improved since the first description of Pol I crystals and so have programs for processing and molecular replacement. Additionally, a novel, higher resolution EM map could in principle be used in order to obtain novel results for molecular replacement which might enable us to solve the structure or at least elucidate the backbone Pol I architecture from the original crystal form.

Firstly, the establishment of novel strains with tagged *S. pombe* Pol I subunits was required, since no tagged strains existed. Furthermore, large-scale fermentation and purification approaches as well as crystallization protocols needed to be put in place and optimized. For the first Pol I purification protocol, a *S. cerevisiae* strain was used, which originated from a cloning strain and harboured a genomic knockout of the stalk subunit A43 as well as a plasmid for the expression of an A43 variant containing a 6x histidine tag at its N-terminus. In order to circumvent potential issues arising from the tag-location at the exposed stalk, expression differences due to plasmid-based A43 expression or proteolytic degradation during purification, a novel *S. cerevisiae* strain containing a genomic 10x histidine tag at the C-terminus of A190 and a triple protease knock-out was established.

With the changes in organism, expression and purification, the aim of this study was to produce novel Pol I crystals in order to solve the structure. From the structure, deductions for transcriptional mechanisms in general and the synthesis of ribosomal RNA in specific as well as for the evolutionary relation between different transcriptions systems were intended.

2. Materials and Methods

2.1 Materials

2.1.1 Strains

Table 2. Strains used in this study

Strain	Genotype	Source
<i>E. coli</i> XL-1 Blue	rec1A; endA1, gyrA96; thi-1; supE44; elA1; lac[F'proAB lacI ^q ZDM15 Tn10(Tet ^r)]	Stratagene
<i>E. coli</i> BL21(DE3)RIL	B; F-; <i>ompT</i> ; <i>hsdS</i> (r _B ⁻ m _B ⁻); <i>dcm</i> ⁺ ; Tet ^r ; <i>gal</i> λ(DE3); <i>endA</i> ; Hte [argU, ileY, leuW, Cam ^r]	Stratagene
<i>S. cerevisiae</i> CB010	MATa pep4::HIS3; prb1::LEU2; prc1::HISG; can1; ade2; trp1; ura3; his3; leu2-3	Cramer et al. 2000
<i>S. cerevisiae</i> CB010 A190-his/flag	MATa pep4::HIS3; prb1::LEU2; prc1::HISG; can1; ade2; trp1; ura3; his3; leu2-3; A190::A190-his/flag_G418 ^R	This study
<i>S. cerevisiae</i> CB010 ΔA12.2(75-C) A190-his/flag	MATa pep4::HIS3; prb1::LEU2; prc1::HISG; can1; ade2; trp1; ura3; his3; leu2-3; A190::A190-his/flag_G418 ^R ; A12.2::A12.2Δ75-125_Clonat ^R	This study
<i>S. cerevisiae</i> CARA (Rrn3 fused to A43)	Δrrn3::his5 ⁺ ; Δrpa43::kan ^r ; pGEN-RRN3-A43	Laferte et al. 2006
<i>S. cerevisiae</i> DF5 ΔA190 ycPLAC33-A190	ΔA190::hyg; ycPLAC-A190 +/-250bp	Jentsch lab
<i>S. cerevisiae</i> DF5 ΔA190 pRS314-A190	ΔA190::hyg; pRS314-A190	This study
<i>S. cerevisiae</i> DF5 ΔA190 pRS314-A190 Δ1337-1441	ΔA190::hyg; pRS314-A190 Δ1337-1441	This study
<i>S. cerevisiae</i> DF5 ΔA190 pRS314-A190 Δ1361-1395	ΔA190::hyg; pRS314-A190 Δ1361-1395	This study
<i>S. cerevisiae</i> DF5 ΔA190 pRS314-A190 D1388R	ΔA190::hyg; pRS314-A190 D1388R	This study
<i>S. cerevisiae</i> DF5 ΔA190 pRS314-A190 R1015E	ΔA190::hyg; pRS314-A190 R1015E	This study
<i>S. cerevisiae</i> DF5 ΔA190 ycPLAC33-A190 pRS314-A190Δ981-C	ΔA190::hyg; ycPLAC33-A190; pRS314-A190Δ981-C	This study
<i>S. pombe</i> 972h- (WT)	Wild type	Evolution
<i>S. pombe</i> 972h- A49-his/flag	A49::A49-FLAG/10xHIS-kanMX4	This study
<i>S. pombe</i> 972h- AC40-his/flag	AC40::AC40-FLAG/10xHIS-kanMX4	This study
<i>S. pombe</i> 972h- A14-his/flag	A14::A14-FLAG/10xHIS-kanMX4	This study
<i>S. pombe</i> T611	ade6-M210; ura4-D18; leu1-32; mating type h-	Albert et al. 2011
<i>S. pombe</i> T611 ΔRpa34	ade6-M210; ura4-D18; leu1-32; rpa34::kan-MX4	Albert et al. 2011
<i>S. pombe</i> T611 ΔRpa51	ade6-M210; ura4-D18; leu1-32; rpa51::URA4	Albert et al. 2011
<i>S. pombe</i> T611 ΔRpa51/AC40-his/flag	ade6-M210; ura4-D18; leu1-32; rpa51::URA4; AC40::AC40-FLAG/10xHIS-kanMX4	This study

2.1.2 Oligonucleotides

Table 3. Primers used in this study - part I of V

Primer name	Sequence
Spo-ac40-f01	CCTAAAGGAGTCATCGAGCTTG
Spo-ac40-r03	GCATCAATTAAGGCGTCGC
Spo-a14-f01	CCACCTGAAGAAATGTTGGAA
Spo-a14-r03	AATATGCAAACCTCAAGTACTG
Spo-a49-f01	TTACTCAACTGATGTTCTTACC
Spo-a49-r03	CACCTTTAATCCCGTATTCCC
Hsa-AID-f01	TACCATGGACAGCCTCTTGATGAAC
Hsa-AID-f02	TACCATGGGGTGCCACGTGGAATTGCTCT
Hsa-AID-r01h	TAGGATCCTCAGTGATGGTGATGGTGATGAAGTCCCAAAGTACGAAATGCG
Hsa-AID-r02h	TAGGATCCTCAATGGTGATGGTGATGGTGCTCATAACAGGGGCAAAAGGAT
pGEX_mut_Nco_fw	CTGGTTCCGCGTGGATCCATGGAATCCCGGGTCTGACTC
pGEX_mut_Nco_rev	GAGTCGACCCGGGAATCCATGGATCCACGCGGAACCAG
pGEX_mut_Nde_fw	CTGGTTCCGCGTGGATCCCATATGTTCCCGGGTCTGACTCGAG
pGEX_mut_Nde_rev	CTCGAGTCGACCCGGGAACATATGGGATCCACGCGGAACCAG
Spo_Elp1_f_Nde	TACATATGAAAAATTTGGTAACACACCTGCATC
Spo_Elp1_N600_6h_r_Not	TAGCGGCCGCTTAGTGATGGTGATGGTGATGTCTTTTCGGTGCAGAAAAACGATAAGAC
Spo_Elp1_N662_6h_r_Not	TAGCGGCCGCTTAGTGATGGTGATGGTGATGAGGCATTTGTAAAACCACTGCC
Spo_Elp1_delN632_f_Nde	TACATATGCGACACGATGAGCGATGCCGC
Spo_Elp1_r_8h_Not	TAGCGGCCGCTAGTGATGGTGATGGTGATGGTGATGTATTAATAACTCAATTTTTCAAAAGG
Spo_Elp1_N1218_6h_r_Not	TAGCGGCCGCTAGTGATGGTGATGGTGATGGGGAATAACTTTTCTCACCAATAGTAC
Spo_tag_control_r	GTTGGAATTTAATCGCGCCTCG
Spo_A14_tag_control	CTGGAAGTGAGAGTGTCTATCCC
Spo_A49_tag_control	CCGGTATTGGTAGCGTCCAAG
Spo_AC40_tag_control	CCTACCGCTTATTGCCTACTATAC
Spo_Elp1_M1	TCTGGATCCGTTTGTAGCAACAATTAAG
Spo_Elp1_M2	TTTAAAGCTTTAATATACGTACTACTCCG
Elp1_Nde_f2	GACATCCATATGAAAAATTTGGTAACACACCTGC
Elp1_BamH_rev	GTTGCTAAAACGGATCCAGATGG
Elp1_Not_rev	AGCCTGCGGCCGCTATTAATAACTCAATTTTTCAAAAGG
Elp1_fw_HR	AGGAGATATACCATGAAAAATTTGGTAACACACCTGCATC
Elp1_fw_HR_2	AGGAGATATACCATGGTAACACACCTGCATCATG
Elp1_rev_HR	GTGATGGTGATGTTTTATTAATAACTCAATTTTTCAAAAGG
CDC48_Nde_fw	ATCACATATGAACGCACCATCCACCATG
CDC48_Not_rev	TAATTGGATCCTGCATACAAATCATCAGCACCATC
Spo_RRN3_xho_r	TGCTCTCGAGAAAGGGAGATTCACCCAACATTACGG
Spo_Elp1_tap_fw	CCACAAGCACCGGTTGTTCCAAACGTTAAACCTTTTGAAAAATTGAGTATTTTAATATCCATGGAAAAGAGAAG
Spo_Elp1_tap_rev	GTAATCTATATGTAATGAAAAATTTCCCATTTATCCAAAACCAATCCTAACCTACGACTCACTATAGGG
Spo_Elp1_tap_control	GGAGGTTGATCGCTCGTGTG
Spo_Elp1_tap_control2	TTTCATCGTGTGCGCAAGAGCCG

Table 4. Primers used in this study - part II of V

Primer name	Sequence
Sce_A190_10his_fw	GGGTAAATTGAACAATGTTGGTACGGGTTTCATTTGATGTGTTAGCAAAGGTTCCAAATGCGGCTGAT TACAAAGATGACGATGACAAGCATC
Sce_A190_10his_rev	CTTCTGACCTTCTCCTTCAAATAAACTAATATTAATCGTAATAATATATGGGACCTTTTGCCTGCTT GCATAGGCCACTAGTGGATCTG
Sce_A190_tag_control	GAGCGTGAACAATTGGACAGTCC
Elp1_seq_1	GCAACAATTAAGTCAGATAGTTCCG
Elp1_seq_2	GTCTTGAAACTTTTGGCTTCCG
Elp1_seq_3	CAGTGATACATCCAAGTCACAGTC
Spo_Elp1_tap_f2	CCACAAGCACCAGGTTGTTCCAAACGTTAAACCTTTTGAAAAATGAGTATTTTAATACAGCTGAAGCTTCGTACGCTG
Spo_Elp1_tap_r2	CAGATCCACTAGTGGCCTATGCGGTTAGGATTGGTTTTGATAAATGGGGAAATTTTTTCATTACATATAGATTTAC
GST_Nco_fw	TAATCCATGGGCAGCTCCCCTATACTAGGTTATTGG
GST_Nde_rev	TATATACATATGCGATCCACGCGGAACCAGATCCG
Spo_Elp1_tap_r3	GTAAATCTATATGTAAATGAAAAATTTCCCATTTATCCAAAACCAATCCTAACCGCATAGGCCACTAGTGGATCTG
elp2-nhe-fw	CGCGCGGCAGCCATATGGGCTTTCAGTATGAGGCTTTAC
elp2-nhe-rev	GTCCACCAGTCATGCTAGTTATCCCAACGTAACGTTT
elp3-nhe-fw	CGCGCGGCAGCCATATGGGCTCGACTTCCAGTTTGGCC
elp3-nhe-rev	GTCCACCAGTCATGCTAGCTAAAGCCATTTAGACATG
elp4-nhe-fw	CGCGCGGCAGCCATATGGGCTCGTTCAAAGGAAAGCAGC
elp4-nhe-rev	GTCCACCAGTCATGCTAGCTAAAAATCCAAAGATTTAACAG
elp5-nhe-fw	CGCGCGGCAGCCATATGGGCTCGAAATTCCTTTTGAACCG
elp5-nhe-rev	GTCCACCAGTCATGCTAGTTAAATTAGTAAATCTTCATCAGC
elp6-nhe-fw	CGCGCGGCAGCCATATGGGCTCTTCTTACACGAGCAFTTACG
elp6-nhe-rev	GTCCACCAGTCATGCTAGTTAGAGTTGCAGCGTCACC
SpE1-nhe-fw	CGCGCGGCAGCCATATGGGCAAAAAATTTGGTAACACACCTGC
SpE1-delN208-fw	CGCGCGGCAGCCATATGGGCGGCAAACTTATATTTGCTGG
SpE1-delN421-fw	CGCGCGGCAGCCATATGGGCGTACAAATGACTTCGATAAACG
SpE1-delN668-fw	CGCGCGGCAGCCATATGGGCATTTACCTAGAATTATGGTTC
SpE1-delN762-fw	CGCGCGGCAGCCATATGGGCATTGACAATAAAGTTAATTTATTG
SpE1-nhe-rev	GTCCACCAGTCATGCTAGCTATATTAATAACTCAATTTTTCAAAGG
SpE1-N1153-rev	GTCCACCAGTCATGCTAGCTATCCTCTCGCGGTTTTCTCTC
SpE1-N1092-rev	GTCCACCAGTCATGCTAGCTAATCTTCTTTTTTCTTCTCTC
SpE1-N1044-rev	GTCCACCAGTCATGCTAGCTAACCGTGGCGGAGCAATCCG
SpE1-N737-rev	GTCCACCAGTCATGCTAGCTATAAAGAAGTGAGAAACAAGTC
SpE1-N661-rev	GTCCACCAGTCATGCTAGCTACATTTGTAAAACCACTGCC
SpE1-N617-rev	GTCCACCAGTCATGCTAGCTAAACCAAGTGACAAAATTTAAG
SpE1-N400-rev	GTCCACCAGTCATGCTAGCTATGTGACCAACAGCGAAGAGC
SpE1-19-rev1	CAATAAATTAACCTTTATGTCAATAACCAAGTGACAAATTTAAG
SpE1-19-fw2	CTTAAATTTGTACACTTGGTTATTGACAATAAAGTTAATTTATTG
CtE1-nhe-fw	CGCGCGGCAGCCATATGGGCCGTAACCTGCGCAACATCAG
CtE1-nhe-rev	GTCCACCAGTCATGCTAGTCACACCTTGCCCTCCTTCC
SpE1-not-r-no-tag	TAGCGCCGCTATATTAATAACTCAATTTTTCAAAGG
CtE1-seq-1	CGAGCTGGATAGTGTGAGTGAGC
CtE1-seq-2	GCCATGATTTCTCCGCGTCGAAG
CtE1-seq-3	GATCAATACCATCTGCGATGC
Hp_A190_fw	GGACGTCGACGCGCCAAG

Table 5. Primers used in this study - part III of V

Primer name	Sequence
Hp_A190_rev	ACGCATGAAACCGTTCGGCCG
Hp_A190_c1fw	CCGAGTCCGACGACGAAGACG
Hp_A190_c1r	GAACACTGCCAGCGCATCAAC
Hp_A190_c2fw	GTTGATGCGCTGGCAGTGTTC
Hp_A190_c2r	AAGGCTTGAAGTTAGACACAAC
Spo-elp3-f-sac	AAGAGCTCAATAATTTTGTTTAACTTTAAGAAGGAGATATAATGTGACTTCCAGTTTGGCC
Spo-elp3-r-xho	ATCTCGAGCTAAAGCCATTTAGACATG
Spo-elp2-f-nde	AACATATGTTTCAGTATGAGGCTTTAC
Spo-elp2-r-sac	TAGAGCTCTTATCCCAACGTAACGTTT
scrrn6-f-e	AGGAGATATACCATGAGTGAGGGACAAATTCGAAG
scrrn6-r-e	GTGATGGTGATGTTTTTATCCAAACCCCGGATCC
scrrn7-f-bk	AAGTTCTGTTTCAGGGCCCGATGTCTACTTTTCATAAGAGGTCCC
scrrn7-r-bk	ATGGTCTAGAAAGCTTCAATTCATCCTATGCAGACAGGC
sc7n210-r-b	ATGGTCTAGAAAGCTTCAATAATTTGGCAGCTGGATCCTCC
scrrn11-f-nco	AACCATGGGUTTTGAAGTCCCTATAACTTTAAC
scrrn11-r-xho	AACTCGAGTCACTCACTTGAGTCTTCATCAC
scrrn6-fw-k	AAGTTCTGTTTCAGGGCCCGATGAGTGAGGGACAAATTCGAAG
scrrn6-rev-k	ATGGTCTAGAAAGCTTTATCCAAACCCCGGATCC
scrrn11-f-k	AAGTTCTGTTTCAGGGCCCGATGTTTGAAGTCCCTATAACTTTAAC
scrrn11-r-k	ATGGTCTAGAAAGCTTCACTCACTTGAGTCTTCATCAC
sc7-rbs-r	AATAATTTTGTTTAACTTTAAGAAGGAGATATACAGTCAATTCATCCTATGCAGACAGGC
sc6-rbs-f	AATAATTTTGTTTAACTTTAAGAAGGAGATATACAGATGAGTGAGGGACAAATTCGAAGC
sc6-r	TTATCCAAACCCCGGATCC
sc6-rbs-r	CTGTATATCTCCTTCTTAAAGTTAAACAAAATTTTTATCCAAACCCCGGATCC
sc11-rbs-f	AATAATTTTGTTTAACTTTAAGAAGGAGATATACAGATGTTTGAAGTCCCTATAACTTTAAC
sprn6-f-e	AGGAGATATACCATGTCAACATGGCCTATTGATGC
sprn6-r-e	GTGATGGTGATGTTTTTAAATCCGCTCTTTTCTTTTTTC
sprn7-f-bk	AAGTTCTGTTTCAGGGCCCGATGGAAGCAATTTGGTTTGAAGG
sprn7-r-bk	ATGGTCTAGAAAGCTTTAATCTTGATTGTGTATACCGG
sp7n232-r-b	ATGGTCTAGAAAGCTTCAAGTTTTTTTGAAGCCTTTTAAATATTTTAGAGG
sprn11-f-nco	AACCATGGGATTCTCTCCTTGTACCGTTAAAG
sprn11-r-xho	AACTCGAGCTACAATTCGACGTCAATTCCTG
sp11dn32-f-bam	AAGGATCCGTCAAGAAGGTATAAAACAAGAC
sprn6-f-k	AAGTTCTGTTTCAGGGCCCGATGTCAACATGGCCTATTGATGC
sprn6-r-k	ATGGTCTAGAAAGCTTTTAAATCCGCTCTTTTCTTTTTTC
sprn11-f-k	AAGTTCTGTTTCAGGGCCCGATGTCTCTCCTTGTACCGTTAAAG
sprn11-r-k	ATGGTCTAGAAAGCTTACAATTCGACGTCAATTCCTG
sp7-rbs-r	CTGTATATCTCCTTCTTAAAGTTAAACAAAATTTTTAATCTTGATTGTGTATACCGG
sp6-rbs-f	AATAATTTTGTTTAACTTTAAGAAGGAGATATACAGATGTCAACATGGCCTATTGATGC
sp6-r	TTAAATCCGCTCTTTTTCTTTTTTC
sp6-rbs-r	CTGTATATCTCCTTCTTAAAGTTAAACAAAATTTTTTAAATCCGCTCTTTTTCTTTTTTC
sp11-rbs-f	AATAATTTTGTTTAACTTTAAGAAGGAGATATACAGATGTTCTCTCCTTGTACCGTTAAAG
scrrn6-dn182-fw-e	AGGAGATATACCATGGGCAGCCTGGACTCTCAATATATTCAGAC

Table 6. Primers used in this study - part IV of V

Primer name	Sequence
scrm6-n557-rev-e	GTGATGGTGATGTTTTTGTGAGTGTGATAAAGCATAG
scCF-seq-1	GGGAAAGAACGGACGAACG
scCF-seq-2	TTAGGCTCGCAATTGGGTG
scCF-seq-3	GGTGGTAGATTTTGCATTC
scCF-seq-4	GATTCACAACCGCGTAATTC
spCF-seq-1	CTTAGAAATCTTCATACCTGC
spCF-seq-2	CTAGTGTAAGTTTGGATTATGG
spCF-seq-3	CATCTGGCAATTCTTAGATG
sc7dn320-f-b	AAGTTCTGTTTTCAGGGCCCCGGATAGAGACCGACAATACCC
sp7dn343-f-b	AAGTTCTGTTTTCAGGGCCCCGAATGTATGTTATGGGTTTGATG
pOPINK-sequ	TTTGGTGGTGGCGACCATCC
sc190hisCNfw1	AAGGTTCCAAATGCGGCTCTGGTGCCGCGCGGAGCCATCACCATCACCATCACCATCACCAT CACTGACCTTATGTATCATAACATACG
sc190TAGfw2	CGCTAGAATTGTGGTGGGTAATTAACAATGTGGTACGGGTTTCATTTGATGTGTTAGCAAA GGTTCCAAATGCGGCT
sc190cnTAGrev	CTTCTGACCTTCTCCTTCAAATAAACTAATATTAATCGTAATAATTATGGGACCTTTTGCCT GCTTTTAGGGGCAGGGCATGCTCATGTAG
sc190bioKANfw1	AAGGTTCCAAATGCGGCTAGCAACAGCGGCTGAACGATATTTTGAAGCGCAGAAAATTGAA TGGCATGATTACAAAGATGACGATGAC
sc6dN197-e-fw	AGGAGATATACCATGGACGGAACCGAAATCATAGC
sc6dN576-e-fw	AGGAGATATACCATGCTTTTCAATAACGCTGATGAAC
sc6N763-e-re	GTGATGGTGATGTTTGCTGCCGCGCGGACCAGTGATCGTGAATTTTCGTTTTG
sc6-e-re-tag	GTGATGGTGATGTTTGCTGCCGCGCGGACCAGTCCAAACCCCCGGATCC
sp6-e-re-tag	GTGATGGTGATGTTTGCTGCCGCGCGGACCAGAAATCCGCTTCTTTTCTTTTTTC
sc7dN96-b-fw	AAGTTCTGTTTCAGGGCCCCGGTTCATGAGCCAAATTAC
sc7N319-b-re	ATGGTCTAGAAAGCTTCAAGAAAGCATCCAATTTATTGTG
sc7N416-b-re	ATGGTCTAGAAAGCTTCAAATCTTGACAGTTTCCTTCTAG
sc11dN92-f-nco	AACCATGGGAAGCGAAACAGACTCTCAAG
sc11N322-r-xho	AACTCGAGTCATTTTTGGCAATTAATTAAGAAGACC
scpoll_prom_fw	GTTAAGGCAGAGCGACAGAG
scpoll_prom_re	GTCTTCAACTGCTTTTCGCAT
scRPA12_n75_fw	AAGAAATCCGTGGTTAAAACCTTCTTTGAAGAAGAACGAAGATTACAAAGATGACGATGACAAGTGACCTTAT GTATCATAACACATACG
scRPA12_n75_re	AAAGCGGGGATGATATTAATGTACAAATTTGTAATATGTGCGAACACAACCCAATTAGGGGCAGGGCATGCTC ATGTAG
sc_dRPA12c_c_f	CTTGGACTGTGGTGATCTCCTG
sc_dRPA12c_c_r	TCGGTGGTGAAGGACCCATCC
scRPA12_n75_f2	CGTCACCACGACGGCAGACGATGCGTTTCCATCTTCTCTTAGAGCCAAGAAATCCGTGGTTAAAAC
A190_dEXP_1_f	AAATCAAAAAACAAAAGAGAATACAGGAGTTGACATGAATGAACAAATTAATAAGAG
A190_dEXP_1_r	CTCTTATTAATTTGTTTATTTCATGTCACCTCCTGTAGTTCTCTTTTGTTTTTTGATTT
A190_dEXP_2_f	AGATGTTGCAAATAGTTCTTCGAGAGAAGCTGAAAAGTCTTCTG
A190_dEXP_2_r	CAGAAGACTTTTCAGCTTCTCTCGAAGAAGTATTTGCAACATCT
A190_K1377A_f	TAATGATGAAGAACAAGTCATAAGGCAACTAAAACAGCGGTTTCGTATGAC
A190_K1377A_r	GTCATACGAAACCGCTTGTGTTAGTTGCTTATGACTTTGTTCTTCATCATT
A190_Y1384A_f	AAACTAAACAAGCGGTTTCGGCTGACGAGCCAGATGAAGATG
A190_Y1384A_r	CATCTTCATCTGGCTCGTCAGCCGAAACCGCTTGTGTTAGTTT
A190_D1388R_f	GCGGTTTCGTATGACGAGCCACGTGAAGATGAAATTGAAAC

Table 7. Primers used in this study - part V of V

Primer name	Sequence
A190_D1388R_r	GTTTCAATTTTCATCTTCACGTGGCTCGTCATACGAAACCGC
A190_KYD_AAR_f	GAACAAAGTCATAAGGCAACTAAACAAGCGTTTCGGCTGACGAGCCACGTGAAGATG
A190_KYD_AAR_r	CATCTTCACGTGGCTCGTCAGCCGAAACCGCTTGTTTTAGTTGCCTTATGACTTTGTTC
A190_R1015E_f	GAAGGTTTAATTGATACGGCCGTTAAACATCTGAGTCCGGTTATTTGCAACGT
A190_R1015E_r	ACGTTGCAAATAACCGACTCAGATGTTTTAACGGCCGTATCAATTAACCTTC
A190_1380-91A_f	GTCATAAGAAAATAAAGCTGCAGCCGCGGCTGCCGAGCTGCCGCCGAGCTATTGAAACTATGAGAGAAG
A190_1380-91A_r	CTTCTCTCATAGTTTCAATAGCTGCGGCCGAGCTGCCGCCGAGCCGCGGCTGCAGCTTTAGTTTTCTTATGAC
A190_c1_r	GCTGATAGATTTCTAATCTC
A190_c2_f	ATGGATATTTCTAAACCGG
A190_c3_f	GAAGCATCTGCAAATGACG
A190_c4_f	ATTGACACCATCTTCAAACG
A190_c5_f	CATCTTGAAGACGTCTGTTG
A190_c6_f	GTTTTAGCTAAGTATAATCC
A190_c7_f	TGAGAGAAGCTGAAAAGTC
A190_c8_f	GGTTCATTGATGTGTTAGC
A190_insert_f	GATGCCATGGCTGGTGGTTATG
A190_insert_r	AATTGGAGCTCCACCGCGG
polyA_ins_1_r	AGCTGCGGCCGAGCTGCGGCAGCCGCGGCTGCAGCTTTAGTTTTCTTATGACTTTG
polyA_ins_2_f	GCTGCAGCCGCGGCTGCCGAGCTGCGGCCGAGCTATTGAAACTATGAGAGAAGC
KYD_AAR_ins_1_r	CGAAACCGCTTGTTTTAGTTGCCTTATGACTTTGTTC
KYD_AAR_ins_2_f	ACTAAACAAGCGTTTTTCGGCTGACGAGCCACGTGAAGATGAAATG

2.1.3 Media

Table 8. Media and additives used in this study

Name	Description
Lysogeny broth (LB)	1% (w/v) Tryptone , 0.5 % (w/v) Yeast extract, 8.6 mM NaCl
ZY	1% (w/v) Tryptone , 0.5 % (w/v) Yeast extract
20x NPS	170 mM Potassium dihydrogen phosphate, 720 mM Dipotassium hydrogen phosphate
LB plates	1% (w/v) Tryptone , 0.5 % (w/v) Yeast extract, 8.6 mM NaCl, 1.5 % (w/v) agar, 1x Antibiotic
X-Gal plates	1% (w/v) Tryptone, 0.5 % (w/v) Yeast extract, 8.6 mM NaCl, 1.5 % (w/v) agar, 1x Antibiotic, 0.02% X-Gal dissolved in N,N-Dimethylformamide (DMF)
YPD	2 % (w/v) Peptone, 2 % (w/v) Glucose, 1 % Yeast extract
YPD plates	2 % (w/v) Peptone, 2 % (w/v) Glucose, 1 % Yeast extract, 2 % (w/v) Agar
Autoinduction “5052”	25 % (v/v) Glycerol, 2.5 % (w/v) Glucose, 10 % (w/v) α -Lactose
Ampicillin	100 μ g/ml final concentration
Kanamycin	30 μ g/ml final concentration
Chloramphenicol	30 μ g/ml final concentration
Tertacyclin	12.5 μ g/ml final concentration
Streptomycin	50 μ g/ml final concentration
Geneticin	200 μ g/ml final concentration
IPTG	0.1 mM - 1.0 mM final concentration

2.1.4 Plasmids

Table 9. Plasmids used in this study - part I of III

No.	Plasmid	Resistance	Organism	Insert	Comment
1	pET24d	Kan			
2	pET24a	Amp			
3	pET24d	Kan	<i>H. sapiens</i>	AID	Full length
4	pANY	Amp	<i>S.pombe</i>	A14-FLAG-10xHIS	Template for genomic insertion
5	pANY	Amp	<i>S.pombe</i>	A49-FLAG-10xHIS	Template for genomic insertion
6	pANY	Amp	<i>S.pombe</i>	AC40-FLAG-10xHIS	Template for genomic insertion
7	pET24d	Kan	<i>H. sapiens</i>	AID	Construct 2
8	pET24d	Kan	<i>H. sapiens</i>	AID	Construct 4
9	pGEX-4T-1	Amp	hybrid		N-term GST-tag
10	pGEX-4T-1-CE	Amp	hybrid		NcoI site inserted to "9"
11	pET24a	Kan	<i>S. pombe</i>	Elp1.4	
12	pGEX	Amp	<i>H. sapiens</i>	AID	Full length
13	pGEX	Amp	<i>H. sapiens</i>	AID	Construct 2
14	pGEX	Amp	<i>H. sapiens</i>	AID	Construct 4
15	pET21a	Amp			
16	pET21d	Amp			
17	pET21a	Amp	<i>S. pombe</i>	RPA21/ker1	A14/43 homologue; S. Geiger
18	pOPINE	Amp			
19	pBS1539	Amp			from M. Seizl
20	pOPINE	Amp	<i>S. pombe</i>	Elp1	Full length
21	pET28b	Kan			
22	pET28b	Kan	<i>S. pombe</i>	Elp1-N600	
23	pET28b	Kan	<i>S. pombe</i>	Elp1-N662	
24	pET28b	Kan	<i>S. pombe</i>	Elp1	Full length
25	pYM13	Amp			
26	pET21a	Amp	<i>S. pombe</i>	Rrn3	Full length
27	GFP-Amp	Amp	hybrid	GFP	from H. Feldmann
28	pET28b	Kan	<i>S. pombe</i>	Elp3	Full length
29	pET28b	Kan	<i>S. pombe</i>	Elp4	Full length
30	pET28b	Kan	<i>S. pombe</i>	Elp6	Full length
31	pET28b	Kan	<i>S. pombe</i>	Elp1.2	
32	pET28b	Kan	<i>S. pombe</i>	Elp1.7	
33	pET28b	Kan	<i>S. pombe</i>	Elp1.12	
34	pET28b	Kan	<i>S. pombe</i>	Elp1.13	
35	pET28b	Kan	<i>S. pombe</i>	Elp1.16	
36	pET28b	Kan	<i>S. pombe</i>	Elp1.8	
37	pET28b	Kan	<i>S. pombe</i>	Elp1.9	

Table 10. Plasmids used in this study - part II of III

No.	Plasmid	Resistance	Organism	Insert	Comment
38	pET28b	Kan	<i>S. pombe</i>	Elp1.15	
39	pET28b	Kan	<i>S. pombe</i>	Elp1.17	
40	pET28b	Kan	<i>S. pombe</i>	Elp2	Full length
41	pET28b	Kan	<i>S. pombe</i>	Elp5	Full length
42	pET28b	Kan	<i>S. pombe</i>	Elp1.6	
43	pET28b	Kan	<i>S. pombe</i>	Elp1.18	
44	pET28b	Kan	<i>S. pombe</i>	Elp1.5	
45	pET28b	Kan	<i>S. pombe</i>	Elp1.21	
46	pET28b	Kan	<i>S. pombe</i>	Elp1.1	
47	pET28b	Kan	<i>S. pombe</i>	Elp1.3	
48	pET28b	Kan	<i>S. pombe</i>	Elp1.10	
49	pET28b	Kan	<i>S. pombe</i>	Elp1.11	
50	pET28b	Kan	<i>S. pombe</i>	Elp1.14	
51	pET28b	Kan	<i>S. pombe</i>	Elp1.4	
52	pANY	Amp	<i>H. polymorpha</i>	A190-FLAG-10xHIS	Template for genomic insertion
53	pOPINB	Kan			
54	pOPINK	Kan			
55	pOPINE	Amp			
56	pCDF-Duet	Strep			
57	pET-TBP	Amp	<i>S. cerevisiae</i>	TBP core	from S. Sainsbury
58	pET28b	Kan	<i>S. cerevisiae</i>	A49/A34.5	both full length; from S. Geiger
59	pET28b	Kan	<i>S. cerevisiae</i>	Rrn3	Full length; from C. Blattner
60	pET21b	Amp	<i>S. cerevisiae</i>	A14/A43	both full length; from C. Blattner
61	pOPINE	Amp	<i>S. cerevisiae</i>	Rrn6	No tag
62	pOPINB	Kan	<i>S. cerevisiae</i>	Rrn7	N-term 6xhis
63	pOPINB	Kan	<i>S. cerevisiae</i>	Rrn7-N210	N-term 6xhis
64	pOPINB	Kan	<i>S. cerevisiae</i>	Rrn6/7/11	N-term 6xhis on Rrn7 / ongoing
65	pCDFDuet	Strep	<i>S. cerevisiae</i>	Rrn11	No tag
66	pOPINK	Kan	<i>S. cerevisiae</i>	Rrn6	N-term GST-tag
67	pOPINK	Kan	<i>S. cerevisiae</i>	Rrn7	N-term GST-tag
68	pOPINK	Kan	<i>S. cerevisiae</i>	Rrn11	N-term GST-tag
69	pOPINE	Amp	<i>S. pombe</i>	Rrn6	No tag
70	pOPINB	Kan	<i>S. pombe</i>	Rrn7	N-term 6xhis
71	pOPINB	Kan	<i>S. pombe</i>	Rrn7-N232	N-term 6xhis
72	pOPINB	Kan	<i>S. pombe</i>	Rrn6/7/11	N-term 6xhis on Rrn7 / ongoing
73	pCDFDuet	Strep	<i>S. pombe</i>	Rrn11	No tag
74	pCDFDuet	Strep	<i>S. pombe</i>	Rrn11ΔN32	N-term 6xhis
75	pOPINK	Kan	<i>S. pombe</i>	Rrn6	N-term GST-tag

Table 11. Plasmids used in this study - part III of III

No.	Plasmid	Resistance	Organism	Insert	Comment
76	pOPINK	Kan	<i>S. pombe</i>	Rrn7	N-term GST-tag
77	pOPINK	Kan	<i>S. pombe</i>	Rrn11	N-term GST-tag
78	pOPINE	Amp	<i>S. cerevisiae</i>	Rrn6 182-557	C-term 6xhis
79	pOPINK	Kan	<i>S. cerevisiae</i>	Rrn7-N210	N-term GST-tag
80	pOPINK	Kan	<i>S. pombe</i>	Rrn7-N232	N-term GST-tag
81	pF6A-NT2	Amp	hybrid	Clonat resistance	Template for genomic insertion
82	pOPINA	Kan			
83	pRS314	Amp/Trp	<i>S. cerevisiae</i>	A190 +/- ca. 250bp	Wittekin 1988
84	pET28	Kan	<i>S. cerevisiae</i>	Rrn7	from S. Jennebach
85	pET21	Amp	<i>S. cerevisiae</i>	Rrn7	from S. Jennebach
86	pET28	Kan	<i>S. cerevisiae</i>	Rrn6 and Rrn11	from C. Blattner
87	pET21	Amp	<i>S. cerevisiae</i>	Rrn6 and Rrn11	from C. Blattner
88	YCplac33	Amp/Ura	<i>S. cerevisiae</i>	A190 +/- 250bp	from I. Heckmann (Jentsch)
89	YCplac111	Amp/Leu	<i>S. cerevisiae</i>	A190 +/- 250bp	from I. Heckmann (Jentsch)
90	pRS314	Amp	<i>S. cerevisiae</i>	A190 Δexpander1_1	originates from 83
91	pRS314	Amp	<i>S. cerevisiae</i>	A190 Δexpander1_2	originates from 83
92	pRS314	Amp	<i>S. cerevisiae</i>	A190 Δexpander1_3	originates from 83
93	pRS314	Amp	<i>S. cerevisiae</i>	A190 Δexpander2_1	originates from 83
94	pRS314	Amp	<i>S. cerevisiae</i>	A190 D1388R_1	originates from 83
95	pRS314	Amp	<i>S. cerevisiae</i>	A190 R1015E_2	originates from 83
96	pRS314	Amp	<i>S. cerevisiae</i>	A190 Δ981-C	originates from 83
97	pOPINE	Amp	<i>S. cerevisiae</i>	Rrn6	C-term 6xHis
98	pOPINE	Amp	<i>S. cerevisiae</i>	Rrn6 197-763	C-term 6xHis
99	pOPINE	Amp	<i>S. cerevisiae</i>	Rrn6 577-763	C-term 6xHis
100	pOPINB	Kan	<i>S. cerevisiae</i>	Rrn7 97-319	N-term 6xHis
101	pOPINB	Kan	<i>S. cerevisiae</i>	Rrn7 97-416	N-term 6xHis
102	pCDF	Strep	<i>S. cerevisiae</i>	Rrn11 92-322	No tag
103	pETDuet	Amp	<i>S. cerevisiae</i>	Rrn7-Rrn11-Rrn6	From B. Knutson & S. Hahn

2.1.5 Buffers for the purification of RNA polymerase I

Table 12. Buffers for Pol I purification

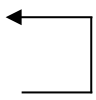
Buffer	Component	Concentration
Buffer A	HEPES pH 7.8	150 mM
	MgCl ₂	60 mM
	Glycerol	20 % v/v
	DTT	5 mM
	PMSF	1 mM
	Benzamidine	1 mM
	Leupeptin	60 μM
	Pepstatin	200 μM
Buffer B	Potassium acetate	50 mM
	HEPES pH 7.8	20 mM
	MgCl ₂	1 mM
	Glycerol	10 % v/v
	PMSF	1 mM
	Benzamidine	1 mM
	β-mercapto-ethanol	10 mM
Buffer C	Potassium acetate	1.5 M
	HEPES pH 7.8	20 mM
	MgCl ₂	1 mM
	Imidazol	10 mM
	Glycerol	10 % v/v
	PMSF	1 mM
	Benzamidine	1 mM
	β-mercapto-ethanol	10 mM
Buffer D	Potassium acetate	300 mM
	HEPES pH 7.8	20 mM
	MgCl ₂	1 mM
	Imidazol	25 mM
	Glycerol	10 % v/v
	β-mercapto-ethanol	10 mM
Buffer E	Potassium acetate	300 mM
	HEPES pH 7.8	20 mM
	MgCl ₂	1 mM
	Imidazol	200 mM
	Glycerol	10 % v/v
	β-mercapto-ethanol	10 mM
Buffer F	HEPES pH 7.8	20 mM
	MgCl ₂	1 mM
	Glycerol	10 % v/v
	DTT	5 mM
Buffer G	Ammonium sulfate	60 mM
	HEPES pH 7.8	5 mM
	MgCl ₂	1 mM
	ZnCl ₂	10 μM
	DTT	5 mM

Additional buffers are described within the methods they are used for.

2.2 Molecular Biology Methods

2.2.1 Polymerase Chain reaction

Relevant genes were amplified by polymerase chain reaction (PCR) from genomic DNA of *Saccharomyces cerevisiae* or cDNA from *Schizosaccharomyces pombe*. Primers are listed in Table 3-7 and were purchased from Thermo Fisher Scientific. Colony-PCR was performed with self-made *Thermus aquaticus* polymerase. The total PCR reaction volume was 50 μ l using Phusion High-Fidelity PCR Master Mix (general lab production; 2x concentrated). Each primer was used at a final concentration of 250 nM. In each case, dNTP concentration was 0.2 mM. Generally, the following protocol was used for initial trials:

180 s	98 °C		Initial denaturation
15 s	98 °C		Denaturation
60 s	55 °C		Primer annealing
120 s	72 °C		Elongation
600 s	72 °C		Final elongation
∞	8 °C		Storage

2.2.2 Preparation of competent *E. coli* cells

Two different strains of chemically competent bacteria cells were used in this study: *E. coli* XL1-Blue and BL21-CodonPlus(DE3)-RIL (see Table 2). For preparation of chemically competent cells, a 400 ml culture was grown to an optical density at 600 nm (OD₆₀₀) of 0.5, chilled on ice and centrifuged (Centrifuge 5810 R with an A-4-81 rotor; Eppendorf) for 10 min at 4,000 rpm and 4°C. The supernatant was removed and the pellet resuspended in 100 ml of buffer TFB-I (30 mM Potassium acetate pH 5.8, 50 mM MnCl₂, 100 mM RbCl, 10 mM CaCl₂, 15% (v/v) Glycerol) on ice. Subsequently, cells were centrifuged, the supernatant was removed and the pellet resuspended in TFB-II (10 mM MOPS pH 7.0, 75 mM CaCl₂, 10 mM RbCl, 15% (v/v) Glycerol). Finally, 50 μ l portions of cell suspension were aliquoted in precooled 1.5 ml tubes on ice, flash frozen in liquid nitrogen and stored at -80 °C.

2.2.3 Transformation in *E. coli* and plasmid purification

Plasmids were transformed in the two *E. coli* strains BL21-CodonPlus(DE3)-RIL and XL1-Blue for protein expression and plasmid amplification, respectively. For transformation, chemically competent cells were thawed on ice and 0.5 µl of pure plasmid, 2.5 µl of infusion reaction product (Clontech) or 5 µl of plasmid ligation product were added (according to the respective task). Cells were mixed and placed on ice for 15 min, followed by heat shock for 40 s at 42 °C and chilling on ice for 2 min. Subsequently, 0.5 ml LB medium was added and cells were shaken for 1 h at 37 °C. Cells were then harvested by centrifugation, resuspended in fresh LB and plated on LB agar plates with the respective antibiotics. Colonies were picked and used to start 5 ml overnight cultures for cloning. Those cultures were used to perform a miniprep (Qiagen Kit), which was carried out as recommended by the manufacturer.

2.2.4 DNA digest and ligation

Plasmids and amplified DNA were digested dependent on the respective cutting sites and their application. For in-fusion cloning, reactions were performed in a total volume of 200 µl with 5 µg of vector, 1x NEBuffer 4 (NEB), 1x Bovine Serum Albumin (BSA) and 40U of each restriction enzyme. For classical cloning, reaction volumes of 50 µl were used. The reactions were incubated at 37 °C for 3 h and purified via Agarose gels (Gel extraction, Qiagen) or PCR purification (Qiagen).

For in-fusion cloning, reactions were incubated with commercially available dry-down components according to the manufacturer's instructions (Clontech).

Classical ligation was performed in a total reaction volume of 20 µl with 1 µl T4 ligase (NEB) in the supplied buffer with 75 ng of digested vector and 5-10 fold molar excess of insert. Reactions were incubated at RT for 1 hour or 16 °C over night and transformed into chemically competent *E. coli* XL1-Blue.

2.2.5 Preparation of competent yeast cells and DNA transformation

This protocol was used for all *S. cerevisiae* as well as *S. pombe* transformations. A 20 ml YPD culture was inoculated with a single yeast colony from a YPD plate and grown over night at 30°C. On the next day, OD₆₀₀ was determined and a new 100 ml culture started with an OD₆₀₀ of 0.25. After 5-6 hours, OD₆₀₀ was at 1.0 and cells were harvested in 250 ml conical tubes (2500 rpm, 5 min). The medium was discarded, cells were resuspended in 25 ml

sterile water by vortexing and centrifuged again. Water was discarded and the cells resuspended in 1 ml of sterile 100 mM Li₂Ac solution (freshly diluted from 1 M stock). The suspension was then transferred into a 1.5 ml reaction tube and centrifuged for 15 sec (table top centrifuge, full speed). Supernatant was removed and the pellet resuspended in 400 µl of fresh 100 mM Li₂Ac. In parallel, 500 µl of salmon sperm DNA (2 mg/ml) were boiled at 95°C for 5 min and quickly chilled on ice. The cells were then split into 100 µl aliquots, pelleted and the supernatant removed. To each pellet, the following transformation mix was added in the following order: (1) 240 µl sterile PEG3350 (50% w/v), (2) 36 µl 1 M Li₂Ac, (3) 50 µl salmon sperm DNA (2 mg/ml), and (4) 34 µl PCR product of the insertion construct (or 2 µl plasmid DNA plus 32 µl water). Tubes were vigorously vortexed for more than 1 min and incubated at 30°C for 30 min under shaking. Subsequently, reactions were transferred to a 42 °C heating block and incubated under shaking for 25 min. Cells were then pelleted (table top centrifuge at 8000 rpm for 15 s), the supernatant removed and cells were resuspended in 1 ml YPD medium. Cells were transferred into 15 ml conical tubes and shaken at 30 °C for 3 h. After centrifugation at 2500 rpm for 5 min, the pellet was resuspended in 500 µl sterile water and plated on YPD plates with the respective marker in two fractions (one plate with 100 µl and one with 400 µl). The plates were incubated at 30 °C for 3-4 days, single colonies picked and re-plated on fresh plates. For verification of correct genomic insertion, the respective genes were amplified by PCR and sequenced.

2.3 Biochemical Methods

2.3.1 Fermentation of *S. cerevisiae*

In order to obtain large amounts of cell mass for Pol I purification from yeast, large scale fermentation in 200 l scale was performed essentially as described⁸ with specific changes. A sample from the respectively used *S. cerevisiae* cryo stock was plated on YPD and grown for 48 hours at 30°C. Precultures of 50 ml were inoculated from those plates and grown overnight. From those, 2 l cultures were started and grown over 8-12 h at 30 °C. Meanwhile, YPD medium was prepared, pH was adjusted to 7.0 with NaOH and the medium was autoclaved in a 200 l fermenter. The 2 l cultures were inspected via light microscopy, combined and transferred into the fermenter to reach a final optical density at 600 nm (OD₆₀₀) of 0.20 – 0.25. Ampicillin and Tetracylin were added (100 µg/µl and 50 µg/µl final concentration, respectively) to avoid bacterial contamination. Antifoam reagent was added to reduce foaming during the fermentation. Cells were grown at 30 °C, 82 NI/min (normal litres per minute) air influx and 250 rpm stirring for ~10 hours until an OD₆₀₀ of 1.8 - 2.2 was reached. Cells were harvested with a continuous-flow centrifuge, resuspended in freezing buffer (Buffer A; 50% slurry) and flash frozen in liquid nitrogen for storage at -80°C.

2.3.2 Fermentation of *S. pombe*

The fermentation of *S. pombe* in large scale was subject to trial-and-error based optimization which finally yielded a reproducible protocol: *S. pombe* cells were plated on YPD from a cryo stock and grown at 30°C for 48-72 h. A preculture of 500 ml was started and grown over night in YPD at 30°C under shaking. Cells were inspected for contaminations via light microscopy and secondary cultures of 2 l each were inoculated at a starting OD₆₀₀ of 0.3 - 0.5. After 10-12 h, cells were inspected and transferred into the 200 l fermenter at a starting OD₆₀₀ of 0.30-0.35. YPD medium was prepared in the fermenter, but pH was not adjusted and was at ~6.0 initially. The medium was autoclaved and Ampicillin and Tetracyline were added to final concentrations of 100 µg/µl and 50 µg/µl, respectively. Antifoam reagent was added to reduce foaming during the fermentation. The fermenter was operated at 22 NI/min (normal litres per minute) air influx and with 250 rpm stirring at 30°C. After 11-13 h, an OD₆₀₀ of 6.0 to 7.5 was reached and cells were harvested with a continuous-flow centrifuge, resuspended in freezing buffer (Buffer A; 50% slurry) and flash frozen in liquid nitrogen for storage at -80°C.

2.3.3 Pol I purification

Pol I enzyme used for crystallization was essentially obtained as described⁸, using a protocol that was based on a procedure originally established by the Tschochner laboratory⁷⁶, but with several changes. Pol I was purified from the expression-optimized strain CB010 expressing a C-terminal Flag/10×histidine-tagged subunit A190. For purification, 500 g of yeast cells were lysed by bead beating in buffer A after the addition of ammonium sulphate to 400 mM from a 3 M stock at 4 °C. The lysate was cleared by centrifugation (30 min at 10,000 xg) and ultracentrifugation (90 min at 30,000 xg) and dialysed overnight against buffer B (50 mM potassium acetate, 20 mM HEPES, pH 7.8, 1 mM MgCl₂, 10% (v/v) glycerol, 10 mM β-mercaptoethanol, 1 mM PMSF and 1 mM benzamidine). After centrifugation (60 min at 18,500 xg) the pellet was re-suspended in buffer C (1.5 M potassium acetate, 20 mM HEPES, pH 7.8, 1 mM MgCl₂, 10 mM imidazole, 10% (v/v) glycerol, 10 mM β-mercaptoethanol, 1 mM PMSF and 1 mM benzamidine) and incubated with 8 ml Ni-NTA beads (Qiagen) for 4 h. Bound protein was washed with five column volumes (CV) buffer C, followed by 5 CV buffer D (300 mM potassium acetate, 20 mM HEPES, pH 7.8, 1 mM MgCl₂, 25 mM imidazole, 10% (v/v) glycerol, 10 mM β-mercaptoethanol) and eluted in 5 CV buffer E (buffer D but containing 200 mM imidazole). The eluate was loaded on a 10/100 MonoQ anion exchange column (GE Healthcare) and eluted with a gradient from 0.3 to 2.0 M potassium acetate in buffer F (20 mM HEPES, pH 7.8, 1 mM MgCl₂, 10% (v/v) glycerol and 5 mM DTT). Eluted Pol I was diluted from 1.1 to 0.2 M potassium acetate, loaded on a 5/50 MonoS cation exchange column (GE Healthcare) and eluted with a gradient from 0.2 to 1.0 M potassium acetate in buffer F including a plateau at 350 mM potassium acetate. Pol I eluted at 490 mM, was concentrated to 500 μl and applied to a Superose 6 10/300 size exclusion column (GE Healthcare) in buffer G (60 mM ammonium sulphate, 5 mM HEPES, pH 7.8, 1 mM MgCl₂, 10 μM ZnCl₂, 5 mM DTT). A single peak contained up to 1.8 mg of homogenous and pure Pol I.

2.3.4 Expression and purification of recombinant proteins

The protocols for recombinant expression and purification of proteins that were used in this work have been previously described. The initiation factor Rrn3 was obtained from *S. cerevisiae*⁴⁴ and from *S. pombe* (this study) with the same protocol. Core Factor consisting of Rrn6, Rrn7 and Rrn11 was prepared similar to the strategy developed in David Schneiders lab²⁶ with several modifications developed together with T. Gubbey during his master thesis⁷⁷. Single domains from Core Factor were designed, expressed and purified during this work as well⁷⁷. The work on elongator complex protein 1 (Elp1) from *S. pombe* was a part of this work and has been partially documented during internships by S. Bussemer⁷⁸ and S. Neyer⁷⁹. A strategy for the recombinant expression and purification of Elp1 and its subdomains has been developed and yielded functional protein in sizable quantities for the first^{78,79}. However, results obtained on Elp1 will not be topic of this thesis. Recombinant Pol I subunit complexes A14/A43 and A49/A34.5 were expressed and purified as developed by S. Geiger^{8,11}.

2.3.5 Protein analysis

Sodium dodecyl sulphate - polyacrylamide gel electrophoresis (SDS-PAGE) was performed with the commercially available NuPAGE system (Invitrogen) using 12% acrylamide gels for polymerase samples and 4-12% gels for other proteins. Protein samples were incubated with 5x SDS-loading dye (25 % Glycerol, 7.5% (w/v) SDS, 250 mM Tris-HCl pH 6.8, 0.5 % Bromphenol blue, 12.5% β -Mercatoethanol) to achieve a final concentration of 1x. Gels were run in 1x MOPS buffer (Invitrogen) at 150-200 V using a prestained protein marker (Invitrogen) as molecular weight standard. Gels were stained with instant blue (Expedeon). At low protein concentrations, TCA-precipitation was performed in order to enrich the sample or gels were silver stained.

For silver staining, gels were soaked in 50% ethanol for 20 min and 5% ethanol (also 20 min). Gels were then incubated 5 min in 35 μ M DTT solution and transferred to silver nitrate solution (1 mg/ml AgNO₃, 1.3 mM formaldehyde) for 10 min. Gels were rinsed twice with 50 ml Millipore water and subsequently washed twice with 25 ml chilled developing solution (30 mg/ml Na₂CO₃, 6.6 mM formaldehyde). Developing was performed for 3-8 min in developing solution and stopped with solid citric acid monohydrate.

Trichloroacetic acid (TCA) precipitation was performed by adding TCA to a final concentration of 10%. Samples were incubated on ice for at least 30 min, centrifuged (table top) at full speed for 15 min and the supernatant was removed. The pellet was washed with 1 ml of acetone (-20°C) and again centrifuged 15 min at full speed. Supernatant was removed and the residual acetone evaporated for 10 min at RT or 3 min at 95 °C. The final protein pellet was then dissolved in 15 µl water and 5 µl 5x SDS loading dye. If required, pH was adjusted by the addition of ammonia vapour in trace amounts.

Protein concentration was determined by absorption measurement at 280 nm using a Nanodrop spectrometer (Thermo Scientific).

Dynamic light scattering (DLS) was performed and evaluated with a Wyatt instrument at the MPI for Biochemistry (Martinsried, Germany) core facility.

2.3.6 Transcription assays

All elongation and cleavage assays were performed exactly as described^{8,80}. Unspecific initiation assays were performed as described⁸¹.

2.4 Crystallization and structure solution

2.4.1 Pol I crystallization and microseeding

Freshly purified Pol I was subjected to commercial screens and to crystallization conditions that had previously produced RNA polymerase crystals from different organisms. MRC-2 microplates (96-well format; SWISSCI) were set up with 100 nl sitting drops using the Phoenix pipetting device (Art Robbins). Initial crystals were obtained in 10% PEG 4000, 300 mM ammonium acetate, 50 mM HEPES, pH 7.5, and 5 mM TCEP at 20 °C. These crystals formed thin plates that poorly diffracted X-rays.

For microseeding, a complete drop containing Pol I crystals was transferred into a seed bead aliquot (Hampton Research) and 60 µl of reservoir solution was added. After vortexing (2x 90 s) and sonication (2x 90 s) 50 nl of seed solution was added to each drop of either 200 nl + 200 nl fresh protein + reservoir solution after they were set up with the Phoenix pipetting device (Art Robbins). Optimization and micro-seeding yielded brick-like crystals with a size of up to 300 × 60 × 40 µm using as reservoir solution 8% PEG 4000, 300 mM ammonium acetate, 50 mM imidazole, pH 7.0, and 5 mM TCEP. After a two-step transfer (30 min each

step) to the same buffer containing an additional 20% PEG 400, crystals were harvested, flash-frozen and stored in liquid nitrogen.

2.4.2 Data collection and processing

Diffraction data were collected at the Swiss Light Source in Villigen, Switzerland, on beamlines PX1 and PX2 as well as at the European Synchrotron Radiation Facility in Grenoble, France, on beamlines ID23-1 and ID29 using Pilatus 6M detectors. Wavelengths, increment, flux and total rotation were adapted to the respective crystal and are given in (Table 13 and 14). Data were processed with XDS⁸² and showed P1 symmetry (Table 13 and 14). An exemplary XDS script is presented in Appendix 6.2.1. A two-fold non-crystallographic symmetry (NCS) axis was detected by calculation of a self-rotation function using program MOLREP and the CCP4 suite⁸³. Analysis of the Matthews coefficient was performed via a web server as well as the program matthews in the CCP4 suite and suggested the presence of two molecules per asymmetric unit as well as the self-rotation function.

2.4.3 Phasing

Molecular replacement using as search models Pol II⁵⁸, a Pol I homology model⁶² or a Pol I electron microscopic envelope⁸ failed. For this, the programs Molrep⁸³ and Phaser⁸⁴ were applied. Soaking with heavy metals as well as cluster derivatives was attempted but either destroyed the crystal or could not be detected. We could, however, use anomalous diffraction from intrinsically bound zinc ions for phasing. After performing a fluorescence scan, three data sets were collected from a single crystal at the peak, inflection, and low-energy remote wavelengths (Table 14). From the peak data set, the positions of 14 zinc ions (7 in each Pol I complex) were determined with SHELX C and D⁸⁵. The occupancies calculated by SHELX were between 100% and 58% for the first 14 sites, followed by a drop to ~25% for additional peaks that were not considered. Zinc positions were refined using autoSHARP⁸⁶ in a multiwavelength anomalous diffraction experiment using four wavelengths (Table 13 and 14). Two Pol II-based homology models of the Pol I core were fitted to match the experimental zinc positions using the program MOLOC. Initial phases at 3.5 Å resolution were obtained with autoSHARP⁸⁶ and yielded a first electron density map. Following solvent flattening with SOLOMON⁸⁶ using the positioned homology models as an initial mask, the program PARROT⁸⁷ performed automated NCS averaging and extended phases to 2.8 Å resolution.

2.4.4 Model building and refinement

An atomic model of Pol I was built with COOT⁸⁸ starting from the positioned homology models. The PHENIX suite⁸⁴ was used to refine the structure with manually assigned rigid body groups considering domain boundaries, and independent TLS parameterization for a total of 24 TLS groups. NCS restraints with groups defined according to the rigid bodies and individual atomic displacement parameters were applied during refinement. In the later stages of refinement, prominent water molecules and two bound sulphate ions were placed and validated by visual inspection. The final refinement script and parameterization files are displayed in Appendix 6.3. The final model has an R_{free} factor of 21.0% at 2.8 Å resolution and excellent stereochemistry (Table 13). For visualization, secondary structure was assigned with DSSP⁸⁹ and by inspection. The model has been deposited in the Protein Data Bank (PDB) under the accession code 4C2M.

3. Results and Discussion

3.1 Purification of *S. cerevisiae* Pol I

In order to optimize purity, homogeneity and yield of Pol I, several parameters in fermentation, tag-type and -location as well as purification were probed and fine-tuned (see Methods). Finally, the strain CB010 with a C-terminal Flag/10xHistidine tag on the largest Pol I subunit A190 was used. The strain carries a triple protease knockout and was used for purification of a 10-subunit variant of Pol II, from which its structure was solved in the first place⁵⁷. Cells were grown to an optical density at 600 nm of 2.0 which corresponds to mid logarithmic growth phase. In principle, the previously used purification technique was maintained⁸. In brief, cells are broken and debris removed. After precipitation, Pol I is re-solubilized and Ni-NTA affinity chromatography performed, followed by anion- as well as cation-exchange chromatography and a final size exclusion step. Due to the higher number of histidines in the affinity tag it was possible to include imidazole in the loading and washing buffers for the Ni-NTA affinity chromatography step. Figure 6 displays anion- and cation-exchange as well as size exclusion (SEC) chromatograms and the corresponding SDS-PAGE gels. Purified Pol I was active in DNA-templated RNA extension and in RNA cleavage (Figure 7).

3.2 *S. cerevisiae* Pol I crystallizes in three different forms, of which one is suitable for structure determination

With the Pol I obtained using the adapted fermentation and purification protocol, it was first attempted to reproduce the initial Pol I crystals⁷⁵. Initial crystalline precipitate was obtained in the original PEG 6000 condition and could be optimized by micro-seeding (streak seed) to yield crystal form A as shown in Figure 8. Crystals of form A diffracted as poorly and displayed the same unit cell as previously observed. The best dataset did not exceed 7 Å resolution and sustained extreme radiation damage which resulted in a fluctuation of 10 Å in length of the longest crystallographic axis during data collection (data not shown). Measures to minimize radiation damage such as manual translation or helical wheel data collection did not resolve the issue. Optimization of crystals by dehydration and or additive screening as well as alternative seeding strategies did not improve diffraction as previously described⁸⁰.

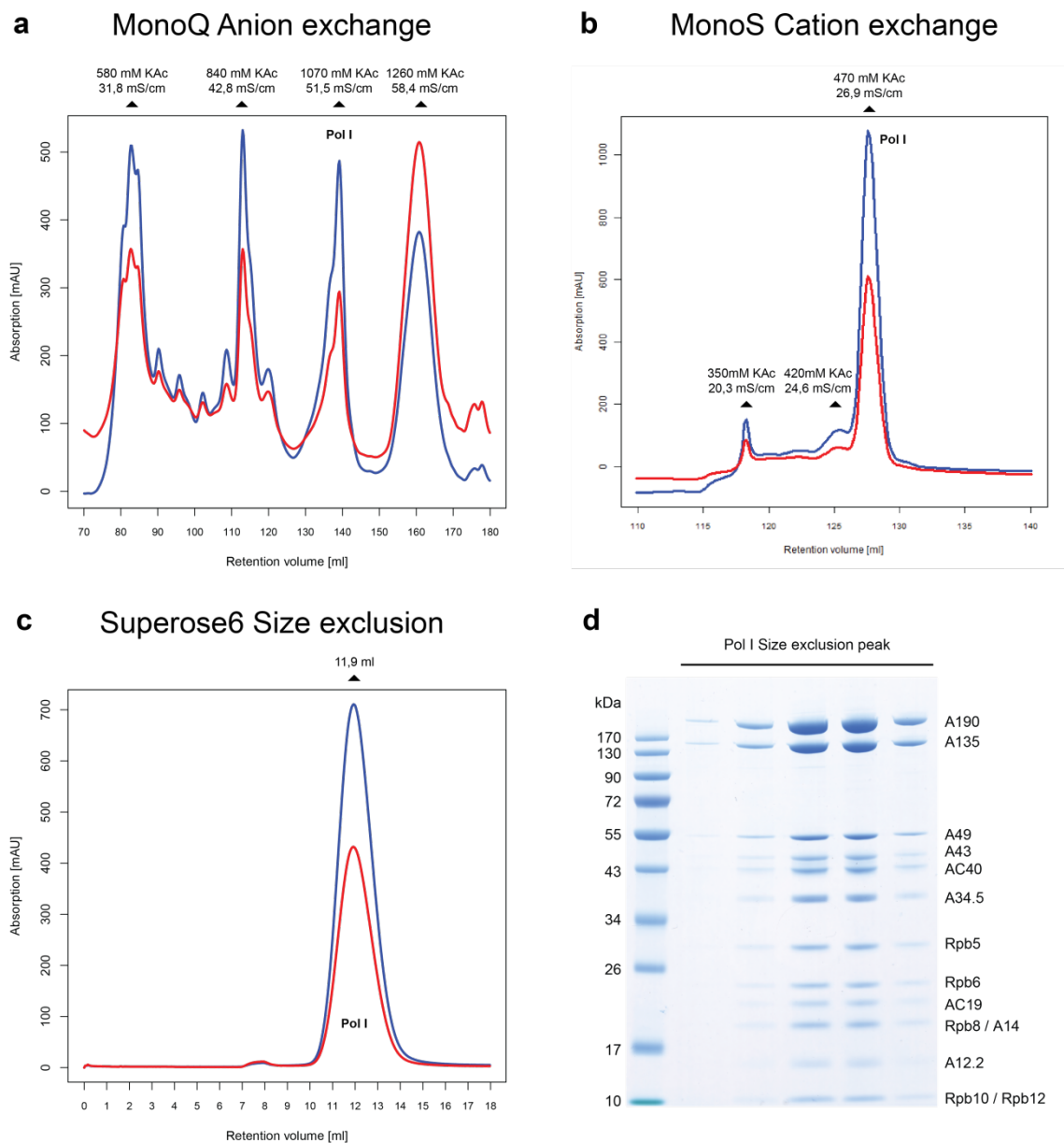


Figure 6. Purification of Pol I.

a-c The three last steps of Pol I purification are MonoQ anion exchange, MonoS cation exchange and Superose6 size exclusion chromatography in that sequence (see Methods). All chromatograms are displayed with absorption at 280 nm (A280) in blue and absorption at 260 nm (A260) in red. Elution parameters are indicated above the respective peaks: Potassium acetate concentration and conductivity for ion exchange and elution volume for SEC. **d** A Coomassie-stained SDS-PAGE of the final SEC peak displays all 14 subunits of Pol I.

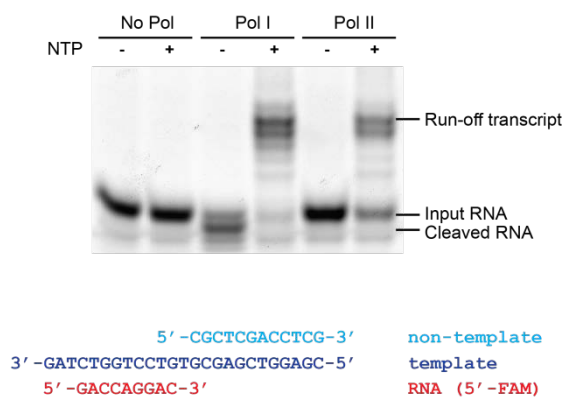


Figure 7. Purified Pol I is active in elongation and cleavage of a preannealed elongation scaffold.

Purified *S. cerevisiae* Pol I and Pol II can extend RNA in a DNA-RNA scaffold in the presence of nucleoside triphosphate substrates (NTPs). In the absence of nucleoside triphosphate substrates, Pol I cleaves RNA. Transcription assays were performed⁸ using the DNA-RNA scaffold shown. After running a 20% acrylamide urea gel, RNA was detected by fluorescence.

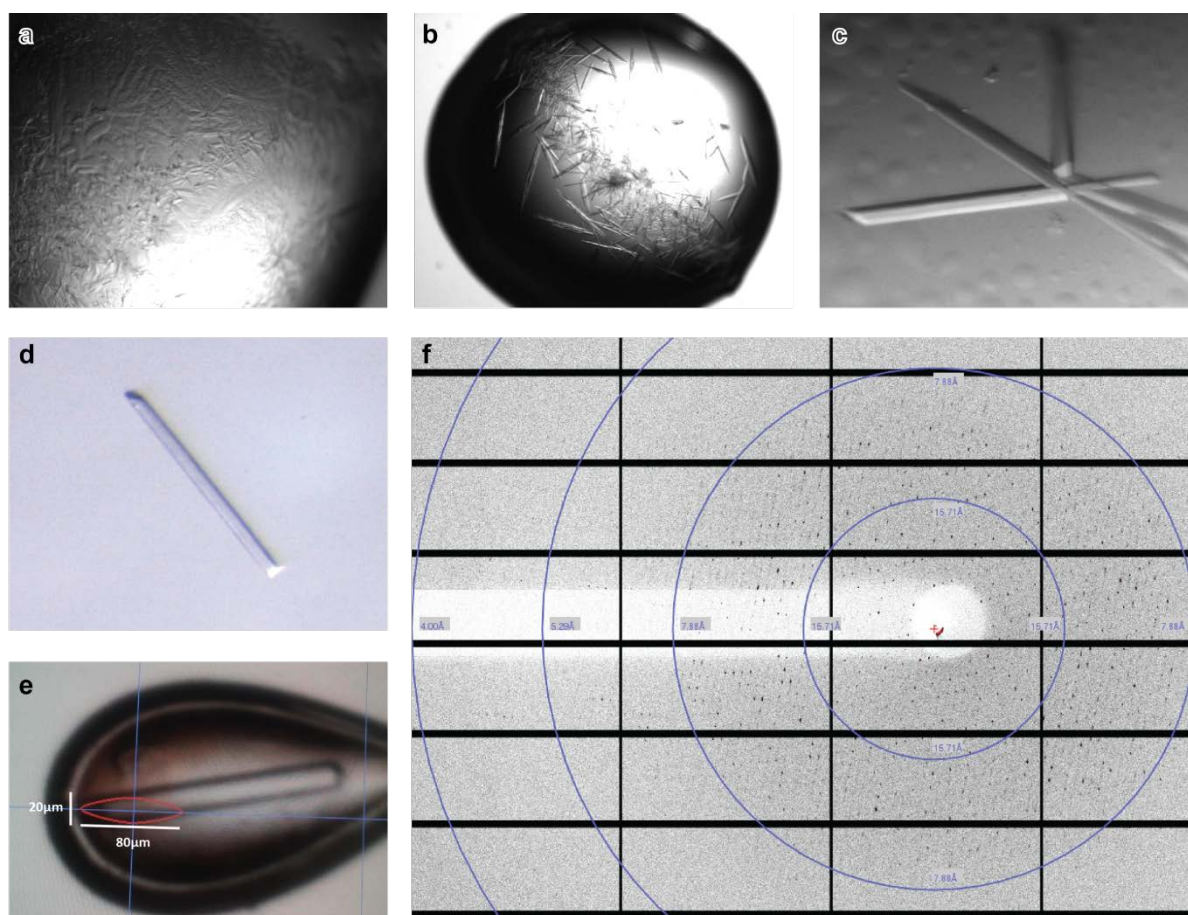
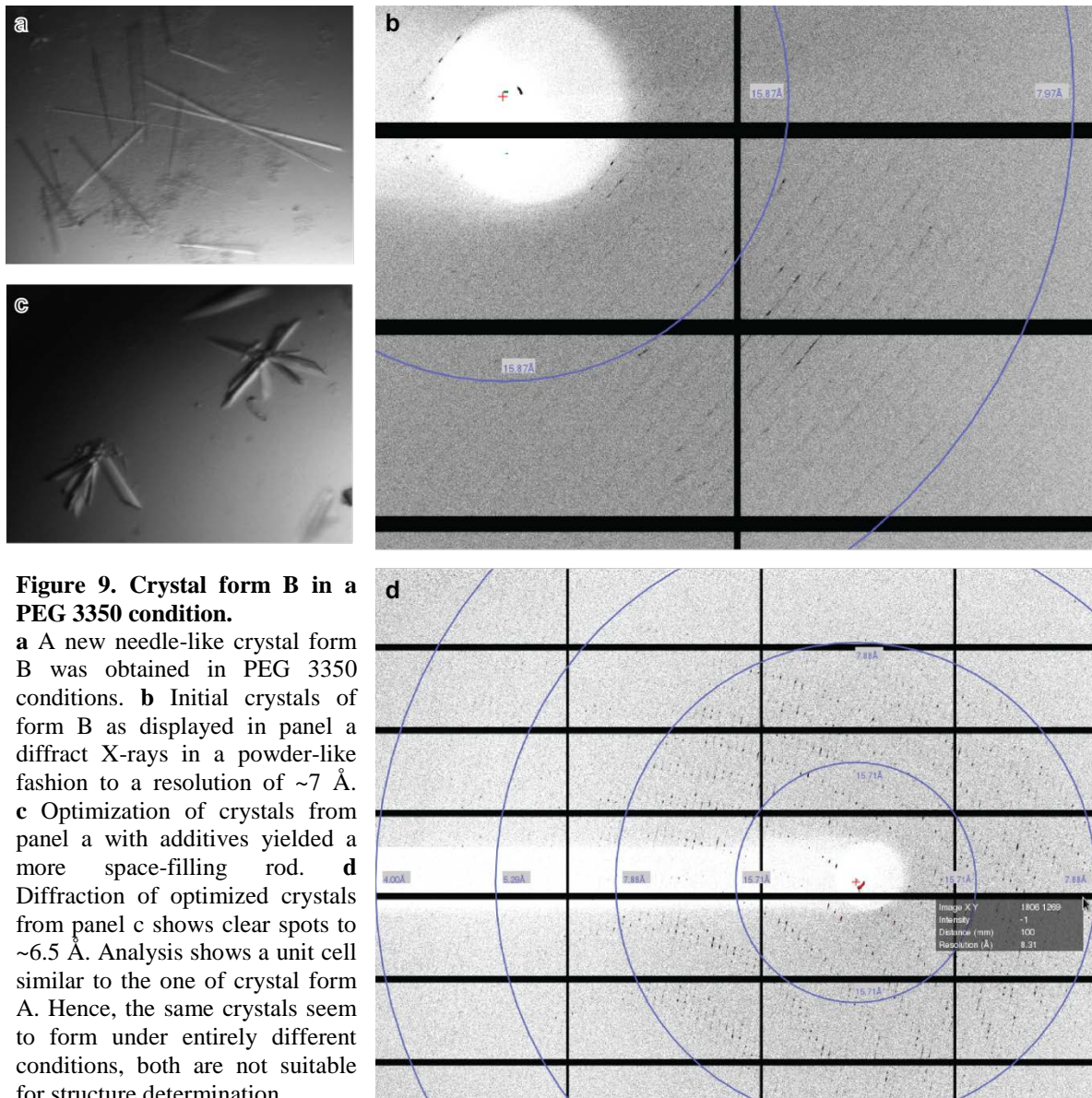


Figure 8. Initial Pol I crystals of form A in the PEG 6000 condition⁷⁵.

a Crystals of form A obtained from initial drop setups as described. **b** Crystals of form A obtained from streak seeding of **a**. **c** Crystals of form A obtained from streak seeding of **b**. **d** and **e** Crystals of form A as displayed in **c** after manipulation with micro-tools and fishing in cryo-protectant solution, respectively. **f** Diffraction pattern of **e**: Diffraction is visible to $\sim 7 \text{ \AA}$ with anisotropic spots to $\sim 4.5 \text{ \AA}$. Spots display a “comet-like” appearance and decay rapidly upon radiation damage.

An alternative crystal form B was obtained by screening in a PEG 3350 condition (Figure 9). While the initial needles only diffracted powder-like, optimization with the additive NDSB-201 (a non-s detergent sulfobetaine) yielded improved rods. Improved rods diffracted X-rays but displayed a unit cell of $\sim 575 \times 286 \times 237 \text{ \AA}^3$ and angles of 90° , 95° and 90° in the C2 space group. It was thus concluded that form B is the same crystal form as form A, even though it grows in a different condition and is obtained with an additive and not from micro seeding. Hence, crystal form B was found not to be suitable for structure determination as well.



On the hunt for a new Pol I crystal form, all conditions that were previously found to crystallize multi-subunit polymerases were screened. In the PEG4000 condition, in which the structure of *S. pombe* Pol II was solved, I obtained a novel Pol I crystal form C of very small rods that grew from a single nucleation point and oriented in a star-shape (Figure 10). Initial X-ray diffraction from a tiny crystal was to low resolution and highly anisotropic. Nevertheless, spots were strong but could hardly be indexed. From the relatively high distance of spots on one axis, however, it could be speculated that this crystal form lacks the extraordinarily long crystallographic axis that is characteristic for crystal forms A and B. Optimization of crystal form C proved challenging, since it turned out to be poorly reproducible in larger drops. Therefore, optimization was carried out in screening drops as

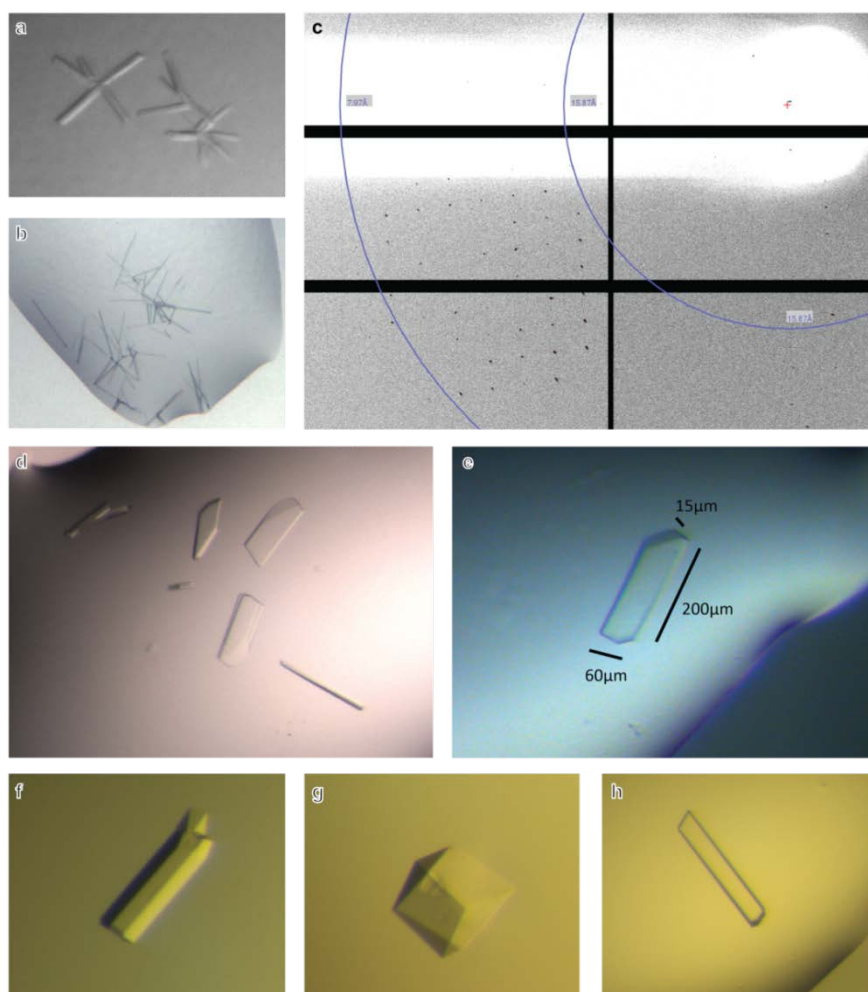


Figure 10. Crystal form C, initial diffraction and crystal optimization.

a and b Initial crystals of the novel form C in a PEG4000 condition (see Methods). **c** Initial diffraction of the crystal in panel a. Despite a strong anisotropic diffraction, spots are clearly defined and display a relatively large spacing, hinting for smaller axes compared to crystal from A and B. **c and d** The first round of optimization in screening drops improved the crystals to 3-dimensional plates. **f-h** Final crystals of form C after several rounds of optimization. Crystals are either plates or bricks. Thick plates as shown in panel f diffracted to the highest resolution.

described (Methods). Whereas additives and drop ratio variations hardly influenced crystallization, micro-seeding by using crushed crystals as a third drop component resulted in a striking improvement of crystal quality. Crystals of the novel form C now grew to sizes of up to 350 μm on the long axis and turned out to actually be plates, not rods (Figure 10e-h).

3.3 Data collection and processing

Optimized crystals of form C diffracted X-rays well to a resolution of 2.8 \AA in the best case. Figure 11a displays a diffraction image of the crystal CE188 (panel b). Processing (see Methods) revealed a triclinic unit cell with axes of 122.8 \AA x 139.1 \AA x 209.6 \AA and angles of 108.0 $^\circ$, 95.4 $^\circ$ and 93.8 $^\circ$. Completeness and redundancy of the data were high and data from different crystals and/or datasets scaled together very well. Matthew coefficient analysis as well as a self-rotation function both suggested the presence of two molecules in the asymmetric unit (AU). The best datasets from four different crystals were merged in order to obtain the best possible results (see Table 13).

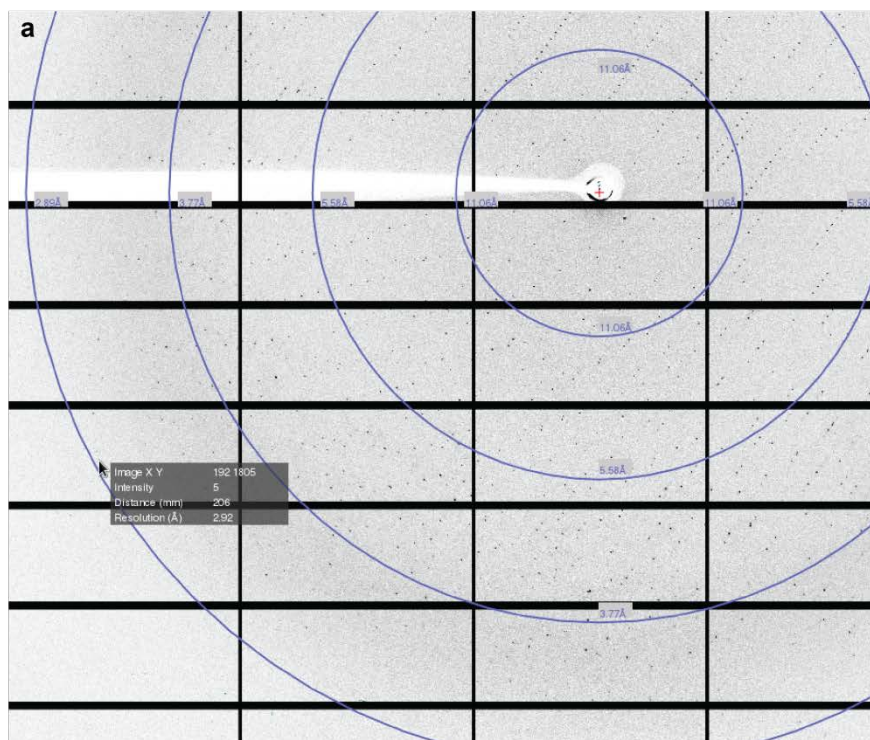


Figure 11. X-ray diffraction of crystal form C.

a Diffraction image of crystal CE188 (shown in **b**). Clear data and well-defined spots to a resolution of $\sim 2.8\text{\AA}$ are visible. **c** Initial indexing shows the triclinic unit cell (see text). **d** Data collection statistics for one dataset from the crystal CE188. Note the low R_{merge} in low resolution shells and the high redundancy as well as completeness and intensity of the data.



c

LATTICE-CHARACTER	BRAVAIS-LATTICE	QUALITY OF FIT	UNIT CELL CONSTANTS (ANGSTROMS & DEGREES)					
			a	b	c	alpha	beta	gamma
* 44	aP	0.0	122.8	139.1	209.6	108.0	95.4	93.8
* 31	aP	38.0	122.8	139.1	209.6	72.0	84.6	93.8
41	mC	59.2	398.7	139.1	122.8	93.8	97.0	88.7
35	mP	118.5	139.1	122.8	209.6	95.4	108.0	93.8
40	oC	139.7	139.1	398.7	122.8	83.0	93.8	91.3
30	mC	150.7	139.1	398.7	122.8	83.0	96.2	88.7
37	mC	207.4	425.6	122.8	139.1	93.8	108.9	78.7
42	oI	228.7	122.8	139.1	402.6	90.1	100.6	93.8

d

SUBSET OF INTENSITY DATA WITH SIGNAL/NOISE ≥ -3.0 AS FUNCTION OF RESOLUTION													
RESOLUTION LIMIT	NUMBER OF REFLECTIONS OBSERVED	UNIQUE POSSIBLE	COMPLETENESS OF DATA	R-FACTOR observed	R-FACTOR expected	COMPARED	I/SIGMA	R-meas	CC(1/2)	Anomalous Corr	SigAno	Nano	
12.97	20778	3162	3040	97.6%	3.7%	4.6%	20751	44.29	4.0%	99.9*	7	0.796	2608
9.17	41254	5886	5921	99.4%	3.7%	4.8%	41206	42.28	4.0%	99.8*	6	0.758	5085
7.49	52415	7621	7661	99.5%	4.5%	5.4%	52402	33.98	4.9%	99.8*	6	0.822	6357
6.48	62317	9013	9062	99.5%	6.4%	7.0%	62271	25.28	6.9%	99.6*	-1	0.811	7526
5.80	75358	10212	10269	99.4%	7.7%	8.4%	75336	22.64	8.3%	99.6*	1	0.804	9199
5.29	80297	11324	11394	99.4%	8.3%	8.8%	80291	21.17	9.0%	99.5*	-1	0.791	9700
4.90	85112	12287	12378	99.3%	8.4%	9.0%	85084	20.40	9.1%	99.5*	-3	0.779	10309
4.59	95366	13208	13307	99.3%	8.6%	9.2%	95328	20.51	9.3%	99.6*	-5	0.770	11583
4.32	103094	14009	14121	99.2%	10.2%	10.9%	103072	19.69	11.0%	99.4*	-4	0.774	12485
4.10	106360	14800	14929	99.1%	13.3%	13.6%	106338	15.84	14.3%	99.2*	-4	0.785	12837
3.91	111198	15601	15761	99.0%	17.5%	18.0%	111164	13.27	18.9%	98.9*	-2	0.787	13409
3.74	114071	16261	16434	98.9%	23.9%	24.3%	114042	10.94	25.8%	98.3*	-2	0.785	13688
3.60	124245	16950	17147	98.9%	33.4%	34.0%	124232	9.08	36.0%	97.4*	-2	0.785	15002
3.47	131065	17620	17835	98.8%	44.0%	44.7%	131052	7.50	47.4%	96.2*	0	0.783	15849
3.35	134617	18277	18523	98.7%	55.4%	55.8%	134602	5.95	59.6%	93.5*	-1	0.772	16479
3.24	131464	18699	18973	98.6%	71.5%	71.2%	131438	4.43	77.3%	87.8*	-1	0.767	15993
3.15	134208	19403	19721	98.4%	88.4%	88.7%	134189	3.51	95.7%	81.7*	-2	0.751	16356
3.06	144021	20058	20408	98.3%	113.7%	114.2%	143994	2.83	122.6%	74.0*	-3	0.731	17571
2.98	150586	20496	20839	98.4%	138.5%	139.2%	150577	2.33	149.0%	67.1*	-3	0.714	18373
2.90	156042	21004	21390	98.2%	172.7%	174.6%	156038	1.90	185.7%	58.1*	-2	0.704	19038
total	2053668	285891	289313	98.8%	17.3%	17.9%	2053407	12.03	18.6%	99.6*	-2	0.766	249447

3.4 Solving the structure of Pol I

For phasing, molecular replacement was attempted but did not yield a conclusive solution (see Methods). Hence, experimental phasing was performed. In our laboratory, Pol II crystals have been phased solely from anomalous diffraction of intrinsically bound zinc atoms beforehand (A.C. Cheung, personal communication). Therefore, the same strategy was applied to solve crystal form C of Pol I. A fluorescence scan on Pol I crystals failed to detect a signal on the zinc absorption edge of the original crystals, but succeeded on the optimized, thick crystals of form C. Datasets were collected from a single crystal (CE175) in a multi wavelength

anomalous diffraction (MAD) scenario on the peak, inflection and low energy remote wavelengths (Table 14). The positions of 14 zinc atoms were determined from the peak dataset in a single wavelength anomalous diffraction (SAD) experiment (Methods; Figure 12). With a manual fit, two models of the 10-subunit Pol II core could be placed on the initial zinc positions. With those positions, a three dimensional fit in the unit cell of crystal form C was obtained (Figure 12c). The phase information of the positioned homology models and the intrinsic zinc atoms in a four-wavelength MAD scenario (together with the data shown in

Table 13. Diffraction data and refinement statistics.

Crystal I - IV	
Data collection^a	
Space group	P1
Cell dimensions	
<i>a, b, c</i> (Å)	122.7, 139.0, 209.6
α, β, γ (°)	108.1, 95.4, 93.8
Resolution (Å)	40-2.8 (2.87-2.80) ^b
<i>R</i> _{sym}	24.0 (201.8)
<i>I</i> / σ <i>I</i>	9.61 (1.52)
Completeness (%)	99.9 (99.8)
Redundancy	13.1 (11.5)
CC _(1/2) ^c (%)	99.6 (54.1)
Refinement	
Resolution (Å)	40-2.80
No. of reflections	320,814
<i>R</i> _{work} / <i>R</i> _{free}	16.8/21.0
No. amino acid residues	8,681
No. of atoms	
Protein	68,820
Ligand/ion	24
Water	214
B-factors (Å ²)	
Protein	81.1
Ligand/ion	130.4
Water	53.8
R.m.s deviations	
Bond lengths (Å)	0.010
Bond angles (°)	1.26
Ramachandran ^d	
Preferred/allowed/disallowed (%)	94.5/4.6/0.9

^aDiffraction data were collected at beamline X10SA of the Swiss Light Source, Switzerland, and ID23-1 as well as ID29 of the European Synchrotron Radiation Facility ESRF in Grenoble, France, and processed with XDS⁸². Data were collected at 0.25° or 0.1° increments (180° or 360° in total, respectively) at a wavelength of 1.0 Å. Datasets of four crystals were merged. The *R*_{pim} values were 0.072 (overall, 40-2.8 Å), 0.026 (40-15.3 Å); 0.659 (2.85-2.80 Å).

^bNumbers in parenthesis refer to the highest resolution shell.

^cCC_{1/2} = percentage of correlation between intensities from random half-datasets⁹⁰.

^dCalculated with MolProbity⁹¹.

Table 13 as a high energy remote) sufficed to generate an initial map. This map already clearly displayed secondary structure features that could be correlated to their Pol II counterparts (Figure 12d). The positioned polymerases were subsequently used as masks for automatic solvent flattening and phase extension (see Methods). The program PARROT was used and yielded an electron density map that was suitable for building the structure of Pol I at atomic resolution. All scripts used for structure determination are given in the appendix of this work. The structure of both molecules in the AU was built manually and refined at 2.8 Å resolution to an R_{free} factor of 21.0%. It comprises a Pol I dimer containing 8,681 amino acid residues, and lacks only the mobile A49 tWH domain and several surface loops.

Table 14. MAD diffraction data collection statistics.

	Peak	Inflection	Remote
Data collection^a			
Wavelength (Å)	1.28288	1.28382	1.29639
Cell dimensions			
<i>a</i> , <i>b</i> , <i>c</i> (Å)	122.0, 139.2, 209.1		
α , β , γ (°)	108.3, 95.1, 94.2		
Resolution (Å)	40-3.5 (3.59-3.50) ^b	40-3.5 (3.59-3.50)	40-3.5 (3.59-3.50)
R_{sym}	15.1 (54.3)	17.0 (74.1)	21.3 (99.8)
$I/\sigma I$	16.54 (6.0)	8.14 (2.0)	6.53 (1.4)
Completeness (%)	98.0 (97.9)	97.2 (95.5)	97.1 (95.5)
Redundancy	9.8 (9.9)	5.0 (5.0)	5.0 (4.9)
$CC_{(1/2)}$ ^c (%)	99.7 (94.5)	99.0 (67.9)	98.5 (47.3)

^aDiffraction data were collected on a Pilatus 6M detector at beamline X06SA of the Swiss Light Source, Villigen, Switzerland and processed with XDS⁸². Data were collected in 0.1° increments (1080° in total). As a high-energy remote dataset, the data given in Table 13 were used.

^bNumbers in parenthesis refer to the highest resolution shell.

^c $CC_{1/2}$ = percentage of correlation between intensities from random half datasets⁹⁰.

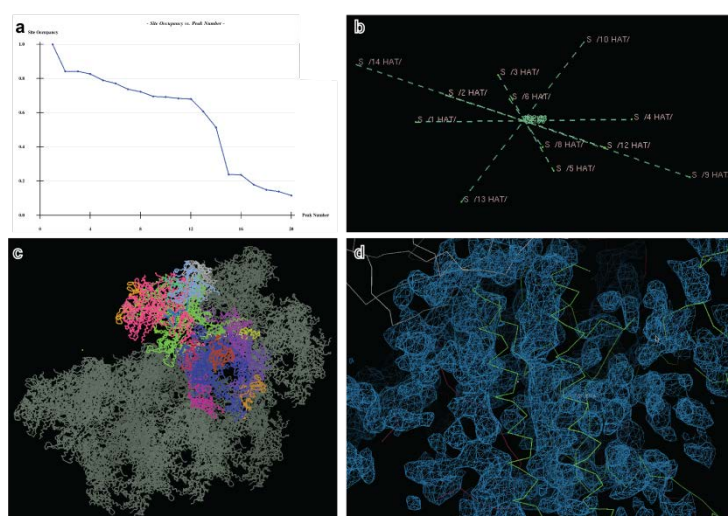


Figure 12. Phasing Pol I with intrinsically bound zincs.

a The occupancy of 14 zinc sites that were determined by SHELX in a SAD scenario is shown. All sites above 50% were considered; <30% sites were discarded as noise or bound solvent molecules. **b** The sites from panel a can be related to each other by rotation around a two-fold axis. This agrees with the presence of two molecules in the asymmetric unit. **c** Two Pol II core models positioned according to zinc positions (coloured chains) can pack in three dimensions in crystal form C. **d** Initial density shows secondary structure elements at positions corresponding to their Pol II counterparts. Here, the funnel helices of Rpb1/A190 are shown.

3.5 Pol I structure

The structure of Pol I in crystal form C reveals the 10-subunit Pol I core and the subcomplexes A49/A34.5 and A14/A43 on opposite sides (Figure 13). Compared with the largest Pol II subunit Rpb1, subunit A190 contains insertions in its domains clamp, dock, cleft, pore and funnel, and lacks parts of the clamp head, foot, jaw and cleft domains (Figure 13c, Figure 14a and c, Figure 32 and Figure 35a). The jaw domain contains a long insertion that we name ‘expander’. The clamp head contains a helical insertion at the position of the archaeal polymerase subunit Rpo13⁷³. Compared to the Pol II subunit Rpb2, subunit A135 contains a truncated external 1 domain, an extended protrusion, and a clamp insertion (Figure 13c and Figure 14 b and d, Figure 33 and Figure 35b).

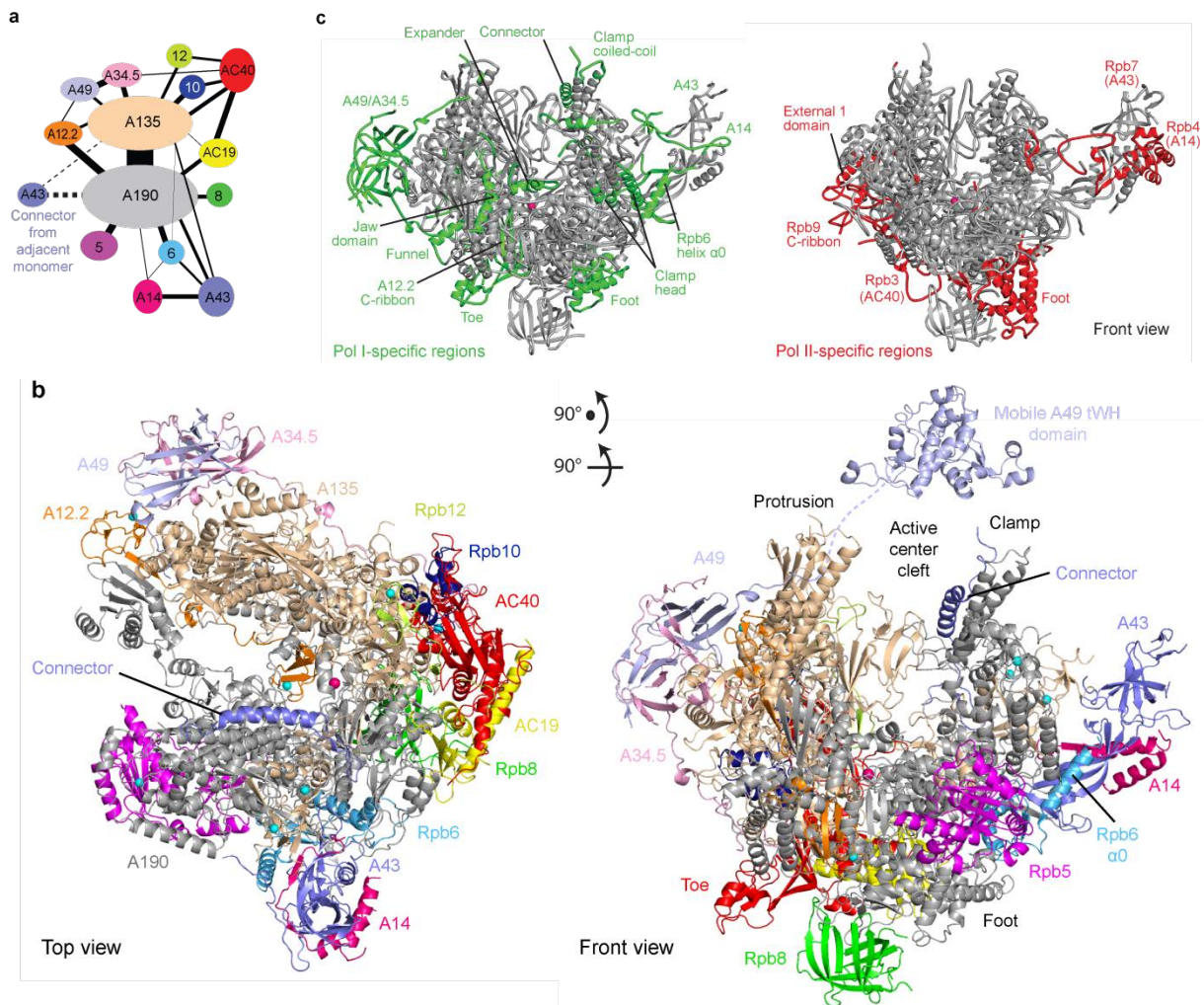


Figure 13. Crystal structure of Pol I.

a Subunit interactions and colour key. The thickness of the connecting lines corresponds to the surface area buried in the corresponding interfaces. Subunits A190, A135, AC40, A14, Rpb5, Rpb6, A43, Rpb8, A12.2, Rpb10, AC19, Rpb12, A49, A34.5 and the A43 connector from the adjacent Pol I enzyme in the dimer correspond to chains A, B, C, D, E, F, G, H, I, J, K, L, M, N and O, respectively, in the PDB coordinate file. **b** Top and side views⁵⁸ of a ribbon representation of the Pol I structure. The mobile A49 tWH domain¹¹ was positioned according to crosslinking information⁶². **c** Regions that differ in fold between Pol I (left) and Pol II (right). Regions with Pol-I- and Pol-II-specific folds are in green and red, respectively.

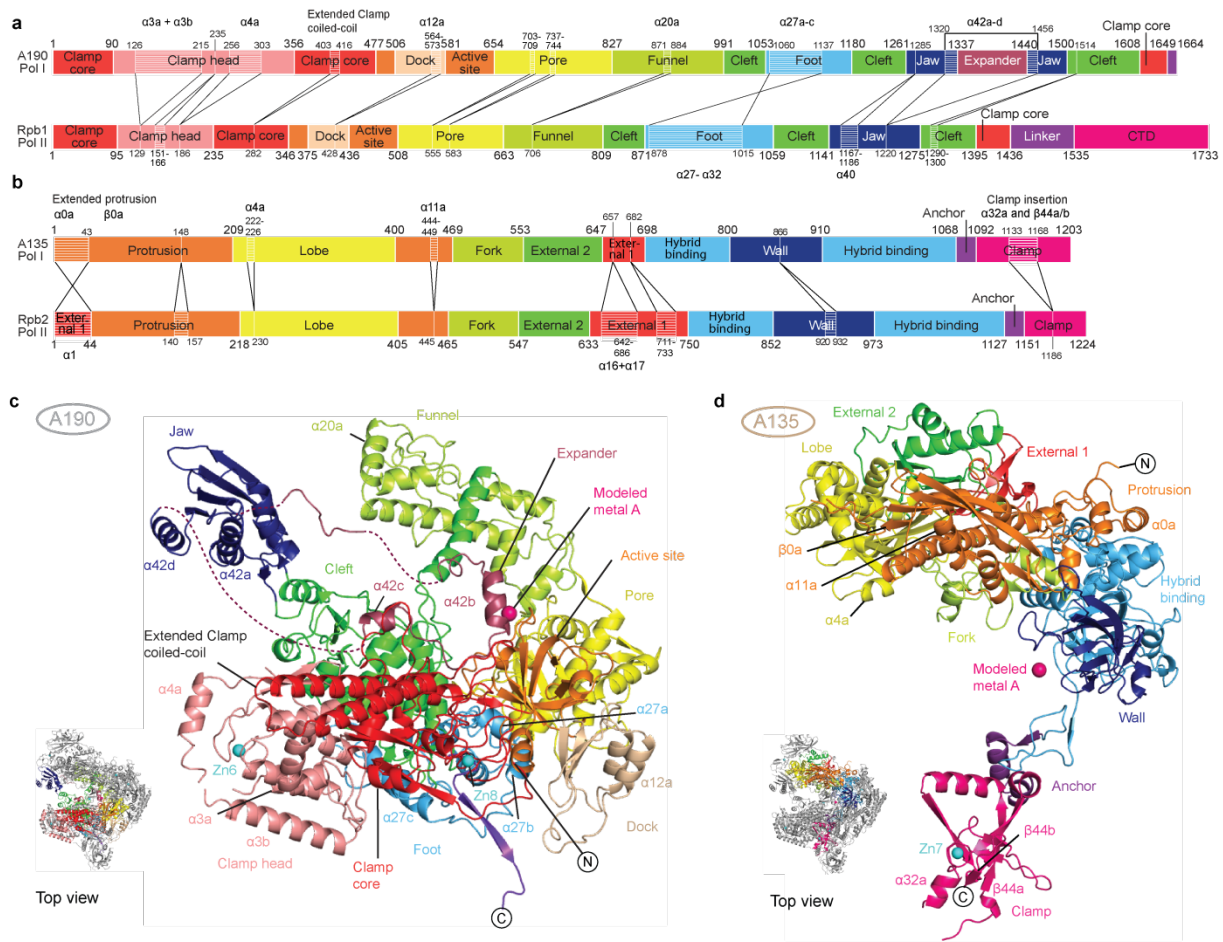


Figure 14. Structure of the two largest Pol I subunits.

a Schematic of domains and domain-like regions of the largest subunit A190, based on the Pol II nomenclature⁵⁸. The amino acid residue numbers at the domain boundaries are indicated. Apparent amino acid insertions and deletions compared with Rpb1 are marked. **b** Schematic of domains and domain-like regions of the second largest Pol I subunit A135, based on the Pol II nomenclature⁵⁸ as in a. **c** Ribbon diagram of A190. The thumbnail shows the location of A190 within Pol I. Locations of N and C termini are indicated. Colour-coding as in a. Top view as in Figure 13. Labelling of corresponding secondary structure elements is as for Pol II⁵⁸. New or lacking secondary structure elements are labelled. New elements were named according to the preceding Pol II element, with lower-case letters added alphabetically for subsequent elements. **d** Ribbon diagram of A135 as in c. The thumbnail shows the location of A135 within Pol I.

A heterodimer of AC40 and AC19 resembles Rpb3/Rpb11 in Pol II, but AC40 contains an additional ‘toe’ domain where the archaeal subunit D contains a domain with an iron-sulphur cluster³ (Figure 13c and Figure 15). Subunit A12.2 binds with its N-terminal zinc ribbon domain (N-ribbon) where the homologous Rpb9 domain binds Pol II⁵⁸, but its C-ribbon binds in the pore like transcription elongation factor IIS (TFIIS)⁹² (Figure 16), consistent with crosslinking⁶². A detailed structural alignment of the two large subunits A190 and A135 as well as of AC40 and AC19 with their respective Pol II counterparts is displayed in Appendix 6.6 (Figure 34).

3.6 Composite active centre and the A49/A34.5 subcomplex

Whereas Pol II contains a ‘tunable’ active site that is transiently complemented by the C-ribbon in TFIIIS⁹², Pol I contains a ‘composite’ active site that comprises the A12.2 C-ribbon. The C-ribbon occludes the binding site for α -amanitin, explaining why Pol I is less sensitive to this toxin than Pol II⁹³. The A12.2 C-ribbon contains a hairpin that reaches the active site like the catalytic hairpin of TFIIIS, explaining the strong RNA cleavage activity of Pol I⁸. Pol III contains a corresponding C-ribbon in its subunit C11⁹⁴. The composite active site of Pol I and III enables efficient proofreading^{8,95} and termination^{96,97}.

The A49/A34.5 subcomplex stabilizes A12.2 (Figure 17a), explaining why it stimulates A12.2-dependent⁸ RNA cleavage¹¹, and why it dissociates after A12.2 deletion⁹⁸. A49/A34.5 stretches over the polymerase surface, to reach the AC40 toe domain with its positively charged A34.5 C-terminal tail (Figure 17). The mobile A49 tWH domain (Figure 13) may close over nucleic acids in the cleft⁶² to increase transcription processivity⁸. The A49/A34.5 subcomplex is related to the Pol II initiation factor TFIIF and to the Pol III subcomplex C37/C53, which contain similar dimerization domains located at corresponding positions⁹⁹⁻¹⁰¹.

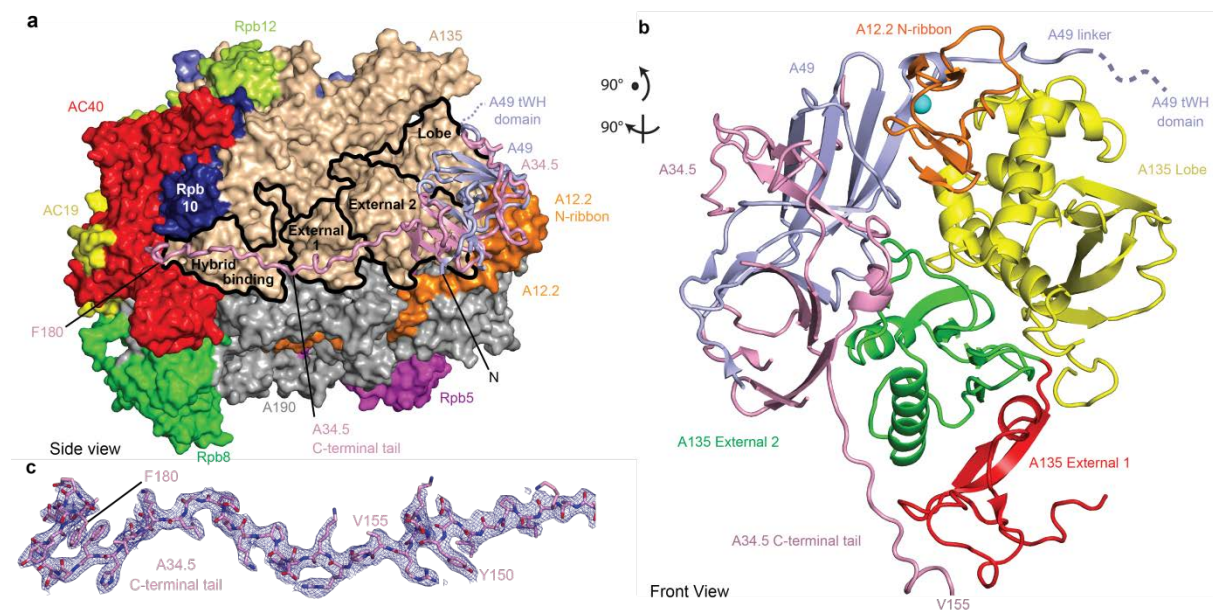


Figure 17. Structure and location of the TFIIF-like subcomplex A49/A34.5.

a Ribbon model of A49/A34.5 on the Pol I core surface viewed from the side⁵⁸. On the basis of a comparison with the Pol-II-TFIIF complex^{99,100}, A49 and A34.5 correspond to TFIIF subunits Tfg1 and Tfg2, respectively. The jaw-lobe module is stabilized by the A49/A34.5 subcomplex in a position close to the protrusion. **b** Interaction of A49/A34.5 with Pol I core domains. The view is from the front of the enzyme⁵⁸. Different Pol I subunit domains are coloured as in Figure 14. **c** 2Fo-Fc electron density (blue mesh, contoured at 1σ) for the positively charged A34.5 C-terminal tail that contributes to A49/A34.5 binding⁶¹.

3.7 Expander and cleft expansion

Compared to Pol II, the active centre cleft of Pol I is expanded by 8 Å (Figure 18). This results from an apparent movement of the two major polymerase modules⁵⁸, ‘core’ and ‘shelf’, which mainly comprise subunits A135 and A190, respectively (Figure 18 and Figure 19). Cleft expansion differs from cleft opening by swinging of the clamp⁵⁸, and includes a relative rotation of the core and shelf modules around an axis through the active site, similar to the ratcheting observed for bacterial RNA polymerase bound by an inhibitor protein¹⁰² and in a paused state¹⁰³. The expanded cleft is stabilized by the expander, which forms two α -helices in the active centre (Figure 18c). The expander binds the bridge helix, which is unwound in its central region (Figure 18d). Expander residues Asp 1385 and Asp 1388 sandwich the Pol I-specific residue Arg 1015 in the unwound bridge helix (Figure 18e). The expander residue Tyr 1384 inserts between the core and shelf modules, whereas Lys 1377 reaches the aspartate loop (Figure 18e).

Cleft expansion changes the active centre that lies at the core-shelf interface (Figure 20a). A tilting between the A190 active site domain and the A135 hybrid-binding domain alters the conformation of the catalytic aspartate loop and loop β 26– β 27 that emanate from these domains (Figure 20b and c). In the tilted conformation, binding of catalytic metal ions and the RNA 3' end as in Pol II^{58,104,105} is impossible. Cleft contraction may rearrange the active site such that the aspartate loop can bind metal ions with its residues Asp 627, Asp 629 and Asp 631, and the A135 loop β 26– β 27 can bind the RNA 3' end with its residues Lys 916 and Lys 924. Binding of the substrate triphosphate may differ in Pol I because the A12.2 hairpin shields the A135 residues Arg 714 and Arg 957, the counterparts of triphosphate-binding Pol II residues. The A12.2 hairpin apparently interferes with closure of the triphosphate-binding trigger loop^{104,105}, but may bind the triphosphate and position metal ion B, as suggested for the TFIIS hairpin during RNA cleavage⁹².

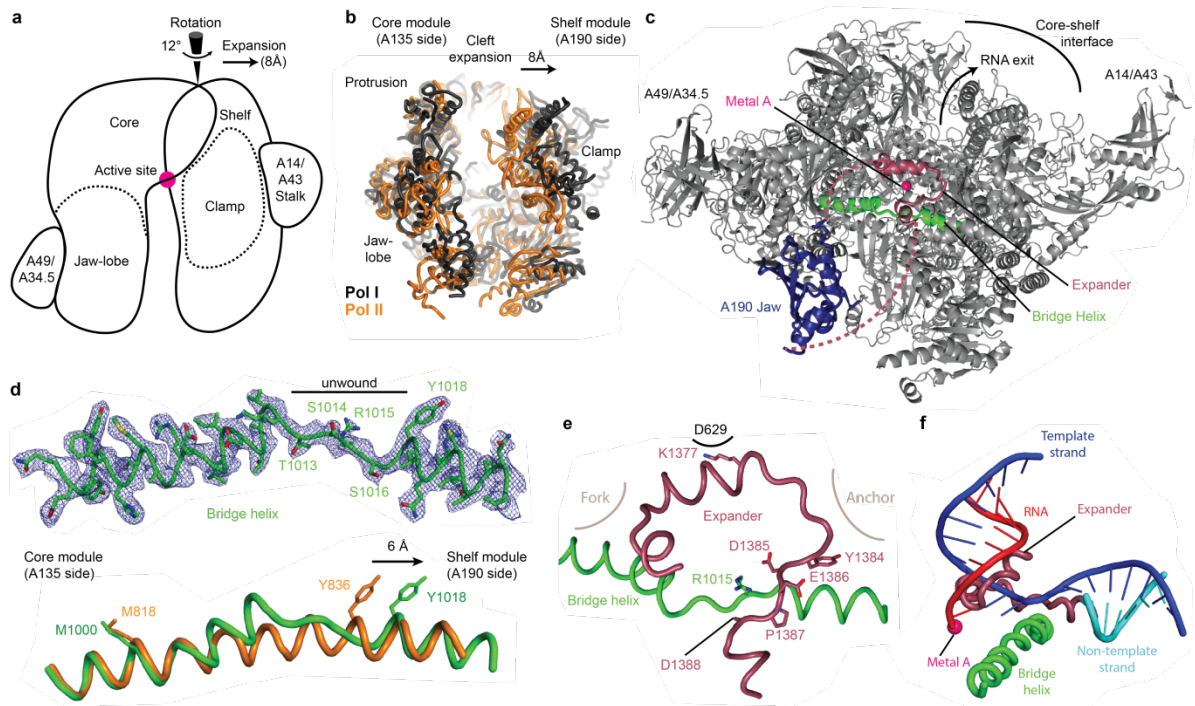


Figure 18. Expanded cleft, expander and unwound bridge helix.

a Schematic of Pol I structure indicating the four mobile modules (core, shelf, clamp and jaw-lobe) and the two peripheral subcomplexes. The view is from the top as in Figure 13, but rotated counter clockwise by 90° . The direction of cleft expansion by movement of the shelf module away from the core module is indicated by an arrow, and goes along with a 12° rotation between the two modules around the indicated axis through the active site. **b** Expansion of the Pol I active centre cleft. Pol I (black) and Pol II (orange) were superimposed with their subunits A135 and Rpb2. The view is as in **a**. **c** A novel expander element (raspberry) that is inserted into the A190 jaw domain (blue) stabilizes the expanded Pol I cleft and a stretched and unwound bridge helix (green). View is from the top⁵⁸, but rotated by 30° towards the front view. **d** 2Fo-Fc electron density (blue mesh, contoured at 1.3σ) for the bridge helix (green) reveals a central, unwound region. At the bottom, a comparison of the bridge helix in Pol II (orange), aligned on the core module side, reveals an expansion by 6 \AA (arrow). View from the front as in Figure 13. **e** The expander (raspberry) stabilizes the unwound central bridge helix (green). View as in **c**. **f** Binding of the expander and the DNA-RNA hybrid in the active centre are mutually exclusive. Superposition of the Pol I structure with the Pol II elongation complex structure (PDB code 1Y1W) reveals clashes between the expander (raspberry) and the DNA template strand (blue) and the RNA transcript (red).

RMSD Ca (Å)		Domain superpositions between Pol I and pseudo-Pol II (Pol I domains organised into a Pol II arrangement)																											RMSD Ca (Å)
Active site	Anchor	Dock	Rpb5	Foot	Cleft	Rpb5	Clamp Core	Clamp A135	Clamp Head	A43	A14	A12.2 N-rib	Jaw Upper	Lobe	Ext2	Ext1	Rpb8	Pore1	Funnel	Fork	Hybrid Binding	AC40	Rpb10	AC19	Protrusion	Rpb12	Wall		
Active site	0.0	1.3	1.3	1.1	1.2	1.0	1.8	2.6	3.1	5.4	8.2	8.5	60.5	19.4	7.7	21.1	7.3	2.4	1.5	2.1	3.2	4.1	3.4	3.6	3.8	4.8	6.2	6.3	
Anchor	0.5	0.0	1.8	1.0	1.1	0.9	1.0	0.6	2.1	5.2	4.5	4.7	65.8	12.5	5.5	24.6	9.6	1.7	2.6	3.3	5.1	6.3	5.3	5.7	6.2	5.5	7.8	6.9	
Dock	0.7	2.0	0.0	1.2	0.8	1.8	3.3	3.9	4.1	5.2	7.7	7.7	51.9	21.3	9.8	31.3	13.3	5.2	4.5	6.2	8.1	9.0	7.7	8.0	7.7	4.6	8.2	9.4	
Rpb5	1.4	0.9	1.7	0.0	1.4	0.7	1.7	1.7	3.3	5.0	5.2	78.6	10.1	10.2	36.2	15.4	6.2	5.6	5.8	8.2	10.0	9.0	8.4	10.6	5.2	12.3	12.6		
Foot	1.7	1.8	1.5	2.0	0.0	1.6	1.7	2.3	4.6	7.4	10.5	10.8	55.1	14.5	13.2	32.0	13.5	4.0	2.8	2.5	3.4	4.6	4.4	4.1	6.7	6.6	12.4	14.4	
Cleft	1.5	1.6	2.3	1.3	0.3	0.8	3.2	6.4	7.4	12.2	12.2	40.5	10.3	8.8	19.6	7.2	6.7	4.0	4.0	4.8	7.9	8.5	7.3	9.2	8.5	9.1	8.6	9.6	
Rpb5	3.5	1.9	2.5	1.7	2.3	1.4	0.0	3.5	7.8	7.1	14.6	14.6	33.4	17.2	18.5	27.8	11.1	11.4	9.5	9.2	11.4	12.8	11.6	13.1	13.8	11.6	12.3	11.3	
Clamp Core	2.3	1.1	2.1	2.4	1.9	2.9	1.6	0.0	1.9	3.9	2.9	2.9	34.5	27.9	18.4	31.6	16.6	6.5	8.6	11.1	13.4	14.6	12.5	14.4	13.2	10.3	8.8	6.7	
Clamp A135	4.4	2.5	3.0	3.5	3.0	3.7	2.4	1.4	0.0	4.1	2.4	2.4	9.6	21.6	15.8	36.7	18.2	9.0	10.0	11.9	14.5	15.9	14.0	15.4	14.5	10.4	10.8	8.8	
Clamp Head	2.5	2.7	3.9	3.1	2.1	3.6	2.5	4.1	7.3	0.0	10.4	10.2	42.0	25.1	20.5	32.4	16.5	9.5	10.1	11.7	14.5	16.2	14.1	16.0	15.9	11.3	11.5	7.4	
A43	10.6	7.8	8.7	9.1	9.3	8.8	6.1	5.2	2.7	10.1	0.0	0.8	56.4	11.4	13.8	47.6	23.7	19.1	17.4	18.1	21.2	23.0	21.2	22.1	21.9	14.5	15.4	14.9	
A14	11.1	8.5	9.2	10.2	9.6	10.0	7.3	6.0	3.8	11.7	0.8	0.0	19.7	16.1	14.9	46.7	23.4	18.9	17.7	18.9	21.8	23.4	21.4	22.9	21.7	15.8	14.6	14.2	
A12.2 N-rib	14.2	20.7	11.9	18.4	14.4	19.8	18.5	14.6	13.5	14.8	17.7	5.7	0.0	19.9	14.1	10.4	26.8	17.6	27.8	16.6	31.1	18.7	17.3	32.0	20.9	21.8	13.9	18.0	
Jaw Upper	9.8	12.0	12.6	11.5	9.8	12.5	12.6	14.7	20.6	9.0	26.7	26.1	44.2	0.0	8.1	8.5	8.8	11.4	12.5	16.0	16.8	16.6	14.3	18.7	13.0	15.5	14.1	13.1	
Lobe	14.0	16.7	17.7	17.0	13.3	16.8	16.3	18.7	22.8	15.8	26.0	25.3	28.1	14.6	0.0	6.1	6.4	7.1	8.0	11.0	10.4	9.9	8.5	11.8	6.0	10.0	15.1	18.1	
External2	15.7	17.9	18.6	18.6	14.0	17.0	16.3	19.4	21.1	22.3	25.5	24.9	64.0	18.3	4.1	0.0	2.9	12.5	7.7	4.8	4.5	4.9	5.4	4.5	7.8	5.9	14.1	13.3	
External1	11.0	12.8	13.4	13.6	9.2	12.2	11.5	14.5	16.4	18.5	22.5	22.2	78.6	23.0	8.0	3.7	0.0	9.5	4.9	2.0	2.5	2.9	2.8	2.7	5.2	3.5	11.0	10.8	
Rpb8	5.4	8.0	6.8	7.0	4.0	5.5	6.4	10.2	9.3	11.5	20.7	21.4	54.1	36.3	23.5	29.3	10.9	0.0	1.2	3.6	3.3	3.2	2.9	2.9	4.3	5.6	12.3	13.6	
Pore1	3.2	5.0	4.2	4.4	2.3	3.5	4.3	6.7	6.5	8.7	14.6	15.1	70.2	24.5	13.9	22.6	7.1	1.2	0.0	1.4	1.2	1.8	2.0	1.2	2.9	5.2	8.8	9.6	
Funnel	8.7	11.0	11.4	10.7	7.5	9.5	9.6	13.3	15.2	14.2	23.4	23.4	88.0	19.9	12.3	12.9	4.3	5.8	2.8	0.0	1.4	2.1	2.2	2.4	3.9	3.6	13.2	12.5	
Fork	8.6	9.4	10.7	10.4	7.8	9.6	8.3	10.0	11.8	14.5	15.1	14.8	75.8	23.1	9.1	9.2	3.6	7.4	3.6	1.7	0.0	1.0	1.2	1.4	3.7	1.4	9.3	8.7	
Hybrid Binding	5.4	6.6	6.9	7.1	4.6	6.4	6.1	8.2	9.8	15.9	16.8	16.8	27.7	39.9	15.0	11.5	3.5	5.8	2.6	1.4	0.0	0.9	1.0	1.7	3.7	7.4	6.9		
AC40	5.4	6.3	7.0	7.8	4.5	7.4	8.6	11.3	13.0	12.4	22.5	22.6	55.4	44.7	29.9	12.3	4.9	5.7	1.9	1.9	1.8	1.0	0.0	1.5	1.9	5.6	6.5	5.5	
Rpb10	5.1	6.9	6.8	7.8	3.4	7.4	9.1	9.3	12.1	18.8	20.3	20.3	74.2	42.3	22.1	6.0	3.7	7.1	2.6	1.0	0.9	0.6	0.9	0.0	2.5	3.4	6.3	5.7	
AC19	6.6	9.4	7.4	8.5	6.0	8.1	9.8	11.8	11.5	11.2	18.9	19.2	60.2	36.0	19.4	18.7	4.8	3.5	2.7	3.6	2.9	1.7	1.1	2.3	0.0	8.1	3.5	5.5	
Protrusion	9.9	10.5	11.7	12.2	8.6	10.8	8.9	10.4	11.0	17.3	11.8	11.4	78.5	37.2	18.2	16.2	8.2	9.2	3.7	1.7	2.8	3.8	2.6	3.5	6.2	0.0	5.9	5.3	
Rpb12	6.0	4.4	5.8	6.6	5.5	5.8	3.1	3.4	5.8	13.7	12.2	12.2	83.7	45.6	23.8	16.4	5.6	10.5	4.8	2.9	2.7	2.4	2.5	3.1	3.8	1.9	0.0	3.1	
Wall	7.2	6.1	7.5	7.8	6.7	6.8	4.5	4.7	4.5	13.2	8.8	8.8	85.7	38.9	19.4	18.1	5.6	9.6	4.9	3.7	3.7	3.5	3.2	4.4	2.9	3.2	2.9	0.0	
Module		Shelf					Clamp			Stalk	Jaw-Lobe				Core														

Figure 19. Shift in domain positions between Pol I and Pol II.

Individual domain fragments of Pol I were isolated, superposed onto their counterparts in Pol II and recombined to form a ‘pseudo-Pol II’ model. This pseudo-Pol II model was then superposed onto the complete Pol I structure over a single common domain (indicated by column headings). The resulting root mean squared deviation (r.m.s.d.) Ca (Å) value for every individual domain (indicated by row headings) was calculated using PyMol and coloured according to value.

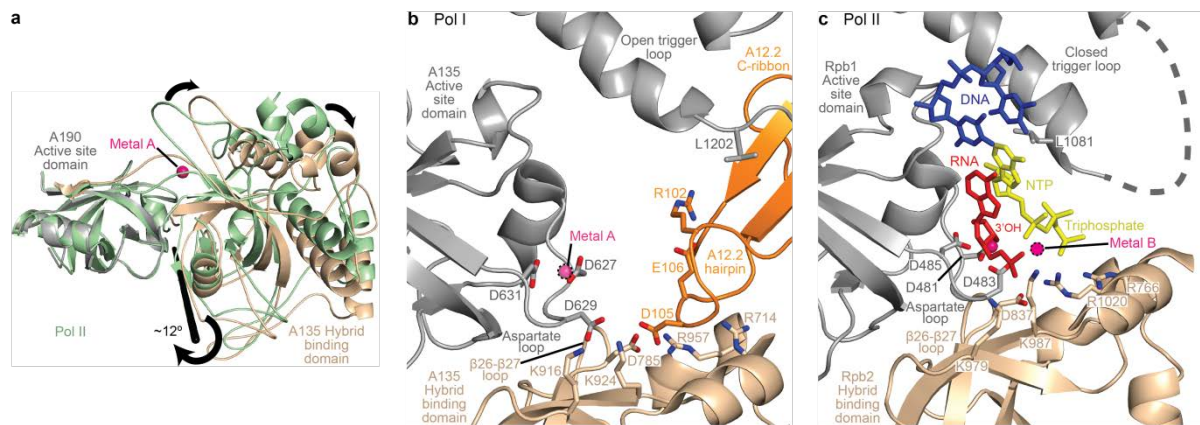


Figure 20. Composite active site and A12.2 hairpin.

a Tilting between the A190 active site domain and the A135 hybrid binding domain. The active site domains of Pol I and Pol II were superposed, and the axis of rotation is indicated. The view is approximately from the side⁵⁸. **b** View of the Pol I active centre from the A135 side towards the clamp. The A12.2 hairpin (orange) forms an integral part of the active site. The backbone carbonyl of Asp 627 is flipped compared to its counterpart Asp 481 in Pol II, and the side chain of Asp 629 is rotated and interacts with Lys 916 and Lys 924 in A135. To catalyse nucleotide addition, the aspartate loop must re-establish a metal-binding conformation and move closer to the A135 loop b26–b27, which may contribute to binding of metal ion B. **c** For comparison, the active site in Pol II with DNA template (blue), RNA (red), and nucleoside triphosphate substrate analogue (yellow) and the closed trigger loop are shown¹⁰⁴.

3.8 Connector and polymerase dimerization

The observed dimeric form of Pol I is established by mutual interactions of the expanded cleft of one polymerase with the stalk subcomplex A14/A43^{8,27} of the other polymerase, resulting in a handshake (Figure 21). A14/A43 binds to the core enzyme similar to its counterparts Rpb4/Rpb7 in Pol II⁷⁰ and C17/C25 in Pol III^{10,101}. A43 also binds a previously unobserved N-terminal α -helix in Rpb6 (Figure 13), explaining the known interaction between A43 and Rpb6²⁷, and loss of A43 and Rpb6 from Pol I after A14 deletion¹⁰⁶. Stalk-mediated Pol I dimerization was also observed by electron microscopy⁶⁰, suggesting that the dimer observed in the crystal corresponds to that formed in solution.

The flexibly linked C-terminal region of A43 folds into a ‘connector’ that invades the cleft of the adjacent polymerase (Figure 21). The connector forms a helix (K5) that binds along the clamp coiled-coil, a β -hairpin (D1–D2) that binds the RNA exit path and the lid, and an acidic C-terminal tail that binds the polymerase switch regions 2 and 3. The connector buries 2,350 \AA^2 of surface area between the two polymerases, consistent with a role in dimer stabilization. The defined structure of the connector and its specific interactions with the polymerase cleft argue that connector-mediated polymerase dimerization is functionally significant. Consistent with this, the connector cannot be accommodated in a modelled contracted state of Pol I, and a C-terminal truncation of A43 that deletes the connector results in thermosensitivity *in vivo*²⁷, and is lethal when combined with other Pol I mutations¹⁰⁷.

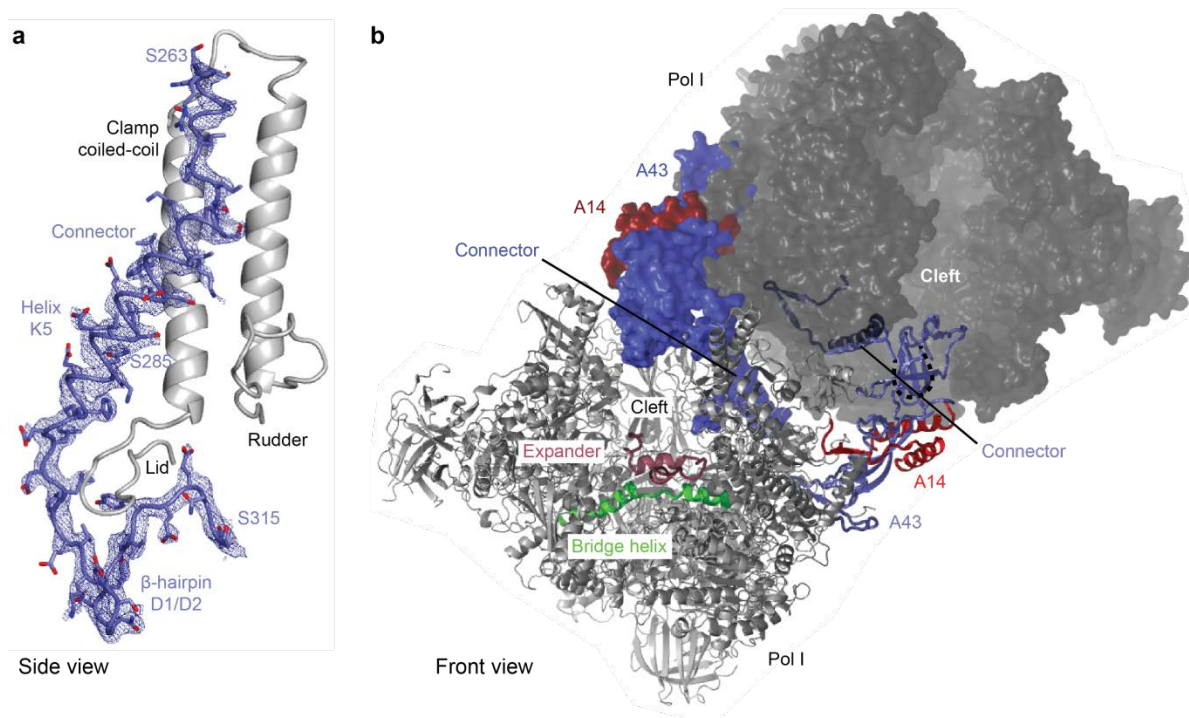


Figure 21. Connector and Pol I dimerization.

a Structure of the A43 connector and corresponding 2Fo-Fc electron density (blue mesh, contoured at 1σ) and its binding to the coiled-coil at the inner side of the clamp (silver). **b** Structure of the Pol I dimer and its stabilization by the A14/A43 subcomplex. One polymerase is shown as a cartoon model, the other in surface representation. The connector (blue) invades the cleft of a neighbouring polymerase.

3.9 Transcription regulation

Pol I dimerization inhibits assembly of the transcription initiation complex because it occludes the binding sites for the Pol I initiation factors Rrn3^{27,44} and Rrn7^{44,68,69} (Figure 21). Pol I dimers and monomers are in a concentration-dependent equilibrium *in vitro* (Figure 22a), but also monomers are predicted to be inactive because the expander overlaps with the binding sites for the DNA template strand and RNA (Figure 18f). The expander binds the cleft of Pol I in solution, as shown by extensive crosslinking⁶² (Figure 22c). The expander interferes with DNA loading in the active centre, because Pol I shows only weak *de novo* RNA synthesis from a tailed DNA template, in contrast to Pol II, which is much more active (Figure 22b). Consistent with a regulatory role of the expander, its deletion does not lead to a growth defect *in vivo* (see Appendix 6.10; Figure 37).

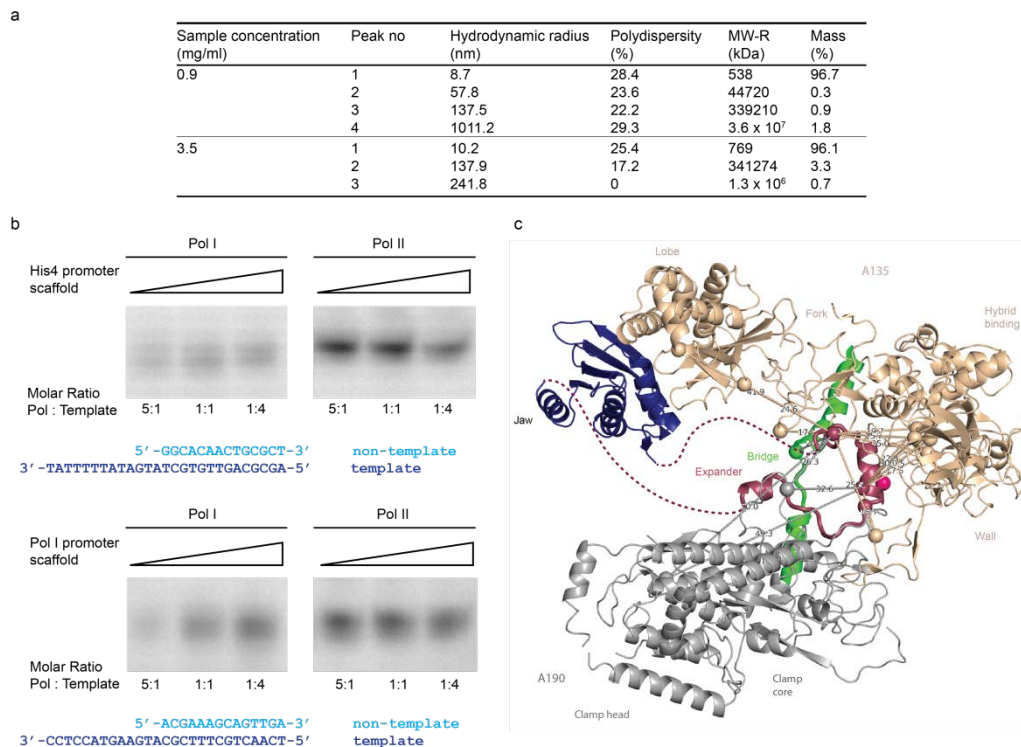


Figure 22. Activity of Pol I and re-evaluation of expander crosslinking data.

a Dynamic light scattering is consistent with a concentration-dependent Pol I dimer-monomer equilibrium in solution. Note that the sample with the higher Pol I concentration shows an increased hydrodynamic radius and apparent (estimated) molecular mass for the predominant peak by mass that accounts for over 96%. The method cannot distinguish monomeric and dimeric species. Thus, the estimated molecular mass observed at 3.5 mg/ml Pol I concentration (769 kDa) arises from a mixture of monomers (590 kDa) and dimers (1,180 kDa). **b** *De novo* RNA synthesis activity on tailed DNA template. Assays were performed as described⁸¹ using the DNA template shown. After running a 20% acrylamide urea gel, *de novo* synthesized, radioactive RNA was detected by phosphorimaging. **c** Previously obtained crosslinks⁶² of the expander element map to the Pol I cleft. Crosslinks to A190 and A135 are indicated in grey and wheat respectively.

Pol I initiation thus requires (1) release of the connector, to generate monomers and enable Rrn3 and Rrn7 binding, (2) release of the expander, to enable DNA loading, and (3) cleft contraction, to induce a catalytically competent conformation of the active centre and enable RNA synthesis. The resulting mature DNA–RNA hybrid excludes the expander from the active centre during elongation, because Pol I is as active as Pol II when provided with a mature hybrid (Figure 7).

This model for regulated Pol I (as illustrated in Figure 23) initiation agrees with known functional data. First, Pol I dimers from yeast extracts are inactive in transcription^{43,51}. Second, when the connector is unavailable for Pol I dimerization, owing to a fusion with Rrn3, Pol I regulation is impaired *in vivo*¹⁶. Third, A43 phosphorylation apparently counteracts Pol I dimerization and promotes Rrn3 binding, because (1) A43 binds Rrn3²⁷ and is phosphorylated in Pol I–Rrn3 complexes⁴⁵, (2) A43 phosphorylation sites⁴⁶ at Ser 208, Ser 220, Ser 262/263 and Ser 285 are exposed in our structure and face Rrn3⁴⁴, and (3) Pol I

dephosphorylation prevents Rrn3 binding and results in low transcription activity⁴⁵, and extracts from non-growing cells lack active Pol-I–Rrn3 complexes⁴³. The same regulatory mechanism apparently exists in multicellular eukaryotes, because the expander is well conserved, and the connector is partially conserved (Appendix 6.9; Figure 36). Consistent with this, inactive human Pol I may be dimeric, whereas human Pol I complexes containing the Rrn3 homologue transcription initiation factor-IA (TIF-IA) are active⁵². Like Rrn3, human TIF-IA binds A43¹⁰⁸, which may be dephosphorylated during the cell cycle by the Cdc14 phosphatase that inhibits Pol I¹⁰⁹.

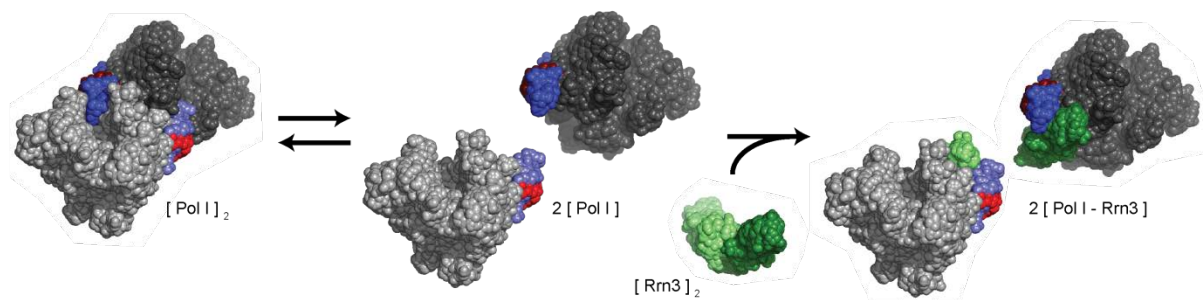


Figure 23. Model for Pol I initiation regulation.

The binding site for the initiation factor Rrn3 (green) is occluded in the inactive Pol I dimer (silver; A14 and A43 highlighted in red and blue, respectively). Rrn3 is released from inactive Rrn3 dimers⁴⁴, resulting in active Pol-I-Rrn3 complexes. For details compare text.

4. Conclusion and Outlook

4.1 Conclusions

The Pol I structure enables a detailed structure–function analysis of rRNA production, the first step in ribosome biogenesis. It also elucidates the evolution of related cellular RNA polymerases. Pol I and III apparently acquired a composite active site for intrinsic RNA proofreading, 3' processing, and chain termination, to enable accurate, high-level production of stable RNA products. The composite active site probably impairs extensive RNA backtracking because the binding site for backtracked RNA¹¹⁰ is occupied by A12.2. Further backtracking may occur during termination and enable cleft expansion and hybrid release, as suggested for the bacterial enzyme¹¹¹ and for Pol III¹¹². By contrast, the tuneable active site of Pol II allows for accommodation of backtracked RNA in the pore, Pol-II-specific regulation during the elongation phase, and 3' RNA processing on the polymerase surface by the machinery for pre-mRNA cleavage and polyadenylation.

The most intriguing finding from this work, however, relates to a possible general mechanism of transcription regulation. We observe an expanded, inhibited conformation of a eukaryotic RNA polymerase that resembles a conformation of bacterial RNA polymerase associated with inactive states^{102,103}. Because the polymerase core is highly conserved, all cellular RNA polymerases can probably interconvert between an expanded inactive state and a contracted active state. State conversion will change the catalytic properties of the enzyme, because the active site is formed at the interface between the mobile core and shelf modules. Only the contracted state contains the active site in a catalytically competent conformation and binds the hybrid tightly. The conversion between polymerase states may be regulated allosterically by factors that bind at the interface of the core and shelf modules. Factors may bind in the pore, as observed for TFIIS⁹² and Gfh1¹⁰², or near the RNA exit channel, as observed for Rrn3^{27,44}, the Pol II initiation factor TFIIB that stimulates RNA chain initiation allosterically⁸¹, and the Pol II coactivator Mediator¹¹³. The bacterial regulator catabolite activator protein¹¹⁴ and the growth regulator ppGpp also bind at the RNA exit channel, and the latter was suggested to influence polymerase activity by modulating the core–shelf interface¹¹⁵.

4.2 Evaluation of previously obtained structural information on Pol I

At the beginning of this work, structural information on Pol I included a negative stain reconstruction⁶⁰, a cryo EM structure⁸, crystal structures of Pol-I-specific subunits^{8,11} and structures of general polymerase subunits within Pol II⁵⁸. During the work on this thesis, crosslinking/MS data that were published from our lab allowed the positioning of Pol-I-specific subunits on a Pol-II-based homology model⁶². With the availability of a complete Pol I crystal structure, it is now possible to compare the results of the other methods and evaluate them.

Crystal structures of the A49/A34.5 dimerization module and the A14/A43 stalk were most helpful during building of the Pol I structure. The overall fold is identical in Sebastian Geiger's great structures that could be positioned by simply placing them roughly inside the respective densities and rigid-body-fitting them. Some regions in the respective subunits, however, differ from their in-solution structures when bound to Pol I. Firstly, the C-terminal tail of A34.5 becomes structured without adopting any secondary structure (Figure 17). This explains why the A49/A34.5 subcomplex dissociates upon an A34.5 C-terminal deletion¹¹. Secondly, the tWH domain solved in the same study¹¹ is not visible in Pol I. Most likely, it becomes structured upon binding of DNA and/or interaction with transcription factors. Furthermore, the C-terminal region of the stalk subunit A43 was suspected to be flexible and unstructured in solution⁶¹. As we found here, it forms the connector element that mediates dimerization of two polymerases. Hence, crystal structures of single subunits were correct and most helpful but information inferred from them turned out to be incomplete.

The negative stain EM reconstruction from Patrick Schulz's group provided a nice envelope of the polymerase (Figure 5b)⁶⁰. Positioning of subunits and general interpretation in this study were most accurate despite the rather low resolution and the early publication date. Notably, a dimeric state of Pol I was described and is similar to the one observed in the crystal structure presented in this work. The comparison of results from both techniques was a great control for the results obtained in this study. Of course, detailed description of novel elements, such as the expander and the connector and a quantification of cleft opening or its underlying core/shelf rotation was impossible from EM data.

Cryo EM results are somewhat harder to evaluate. Dimers have not been observed in this case⁸. Positions of Pol-I-specific subunits turned out to not entirely correspond to the crystal structure. The stalk is positioned in the same spot, but more closely attached to the polymerase in the crystal structure. Density of the truncated foot domain is rather strong in the

EM envelope and the AC40 toe domain was not visible. The position of the dimerization module was interpreted differently in the EM density compared to the crystal structure. In cryo EM it was placed on the bottom side of the core module (Figure 5). The massive density at this part around the position of AC40/AC19 and the N-terminal region of A135 in the crystal structure could result from either a different state of the polymerase under cryo conditions, a bound impurity (rather unlikely since not observed in SDS-PAGE), or a partial misinterpretation of the polymerase position inside the density since Pol II was used as a reference. The same is the case for the density observed for the C-terminal domain of A12.2 on the outside of the polymerase. Another possible speculation concerning the identity of the additional density on the core module that was interpreted as dimerization module and A12.2 C-terminus could be the following: We discussed the detachment of the expander element during transcription since it would otherwise clash with nucleic acids inside the active centre cleft. If the cryo EM density resembles an active, contracted, state of the polymerase, the expander must be detached from the inside of the cleft but still needs to be close to the jaw. It is therefore possible that the expander is observed in a storage position on the outside of the polymerase while not being bound inside the cleft, explaining the additional densities in cryo EM.

In contrast to partial disagreements between the cryo EM interpretation and the crystal structure, results from crosslinking/mass spectrometry⁶² agree with the crystal structure very well. The position of the dimerization domain and the A12.2 C-terminal domain were similar. Even a prediction of the A190 Jaw-insertion being situated inside the cleft was indeed true and turned out to be the expander element.

The general polymerase subunits Rpb5, Rpb6, Rpb8, Rpb10 and Rpb12 are mostly identical in Pol II and Pol I. Rpb6 forms an additional N-terminal helix $\alpha 0$ which was discussed earlier. Additionally, some further density is visible at the N-terminus of Rpb12 which binds to “Domain 2” of AC40. Rpb5, Rpb8 and Rpb10 are otherwise identical in Pol I and Pol II despite the occasional visibility of a residue more or less and minor differences in side-chain positions. Zinc binding sites of the general subunits are conserved and have Zinc atoms bound in all cases. Hence, it can be concluded that the general polymerase subunits carry out the same functions and occupy the same position. Nevertheless, some degrees of freedom are present which make room for polymerase-specific interactions, such as the Rpb6 helix $\alpha 0$.

For the above mentioned reasons it can be concluded that a combination of negative stain EM and crosslinking/MS data gave rise to the most correct information agreeing with the state observed in the crystal structure. This might be helpful for future projects, in case different

methods provide alternative results. It was even possible to infer information about a different, monomeric, state of the polymerase from crosslinking results and hence extended the space available for interpretations. In cryo EM, either sample preparation and freezing resulted in the adaptation of an alternate conformation, or technical problems led to alterations of the density that do not agree with the crystal structure very well. This also explains the impossibility to use a Pol I cryo EM envelope as a model for molecular replacement to solve the crystal form A. It might indeed be useful to reprocess EM data using the open conformation presented in this study. If technical difficulties played a role during initial processing, this would come to light and might be helpful for future EM processing. If no differences in the density arise from re-processing, functional conclusions for conformational rearrangements could be drawn.

4.3 RNA polymerase I from an evolutionary point of view

With the availability of a detailed atomic model for a second eukaryotic multi-subunit RNA polymerase, it now becomes possible to inspect evolutionary relationships in a new light. Firstly, it was confirmed that additional Pol I subunits indeed are built-in transcription factors. The A49/A34.5 dimerization module resembles the fold of the Tfg1/Tfg2 domains in TFIIF as described¹¹. Furthermore, the C-terminal ribbon of A12.2 adopts the fold of its TFIIIS counterpart as suggested⁶².

Most unexpectedly, the AC40 toe domain adopts the fold of the archaeal subunit RpoD that binds an iron-sulphur-cluster. Despite displaying a similar fold, the toe is likely not capable of binding an iron-sulphur-cluster itself since 3 of the 4 coordinating cysteine residues of RpoD are not present in AC40 and a bulky Phenylalanine (F251) occupies the binding pocket. Another archaeal feature can be observed in the clamp head region. The first large clamp head insertion (A190 helices α 3a and α 3b; residues 126 – 215; see Figure 14) is situated in the same place at which the residues 38 – 82 of the archaeal subunit Rpo13 bind to the polymerase (PDB entry 2WAQ)⁷³. Although the double-helical fold is similar in both parts, they bind in a $\sim 180^\circ$ flipped manner. Functional relevance, however, remains unclear. The second clamp head insertion displays partial density close to the clamp coiled-coil but cannot be built continuously which is why no homologues could be identified. The clamp coiled-coil itself is elongated in Pol I when compared to any other polymerase. This might improve connector binding due to the enlarged interaction surface available which, however, remains speculative. The existence of an enlarged coiled-coil disagrees with the described binding of

Spt4/5 to Pol I²⁹, since the Spt4/5 structure bound to a recombinant clamp¹¹⁶ would clash in this case. Further *in vitro* experiments with purified components may be in place to resolve this conflict in the Pol I system.

The absence of large parts of the foot domain in A190 compared to Rpb1 was mentioned earlier (Figure 13). Again, it is not clear if there is functional relevance. Potentially, the foot domain is used as a binding site for a Pol-II-specific factor which does not need to interact with Pol I leading to a degeneration of the element. The mediator complex could be such a factor. It would be interesting to mutate the foot domain of Pol II in a Rpb1 shuffle strain in a way that resembles the Pol I foot. This might lead to differences in transcription factor binding by Pol II.

The most interesting novel elements in Pol I, however, are the expander and the connector. Both are specific to Pol I and can, in a way, also be regarded as built-in transcription factors, similar to the dimerization module, the tWH or the C-terminal ribbon of A12.2. Functional or structural equivalents might be present in the Pol II or Pol III transcription systems. Modulation of the Core/Shelf interface by different factors has already been speculated about (see above). Hence, connector binding might be nothing but a Pol-I-specific, built-in inactivation factor that has functional homologues in other systems. Similarly, the expander-like elements could be present in Pol II transcription factors that contribute to cleft-opening or that prevent unspecific DNA interaction inside the cleft. The fact that both elements have not been identified in Pol I previously and that they are hardly predictable from amino acid sequence information argues that the same could be the case in the Pol II system.

In general, it seems like Pol I resembles a minimalistic system for transcription that carries features from both other eukaryotic polymerases as well as the archaeal polymerase. Homologues of factors that only transiently interact with other polymerases are permanently built into Pol I. This makes a lot of sense, since a much lower degree of regulation is required for Pol I. Pol II transcribes thousands of genes and thus needs to be regulated at a number of different levels for which, most likely, different possibilities have emerged throughout eukaryotic evolution. In contrast, Pol I just needs to perform one single task: the production of rRNA. For this it only needs to be switched on or off, dependent on the cell cycle phase or on the availability of nutrients. The permanently bound TFIIIS homologue in A12.2 enables rapid resolving of problems arising from mis-incorporation of nucleotides or backtracking. It also ensures that no sequence mistakes can be made which would otherwise have catastrophic effects during ribosome assembly.

Furthermore, the same minimalistic tendencies can be observed in the Pol I initiation system. The Pol II initiation system is extremely complicated and includes factors like TFIIF, TFIIE, TFIIA, TFIIB, TFIID, TFIIH and mediator with a total of almost 100 subunits⁴. The Pol III initiation system is somewhat more compact but still contains numerous factors including the 7-subunit factor TFIIC and the trimeric TFIIB that interact with polymerase as well as DNA⁴. Directly Pol-I-associated initiation factors solely comprise Rrn3 and the core factor as the main components in addition to the ubiquitously present TBP and the indirectly interacting UBF⁴. Now, if the core factor is more closely examined, it becomes clear that it contains three central elements: the TFIIB-like factor Rrn7⁶⁸, the TPR domain-containing Rrn11 and Rrn6 with its large WD40 beta-propeller (inferred from sequence homology and domain prediction). Most interestingly, a central part of TFIIC (τ 91) also contains a large WD40 beta-propeller¹¹⁷ and interacts with τ 131 which itself is a TPR domain protein. Last, the central TFIIB component Brf1 is homologue to Rrn7^{68,69}. To summarize: If the Pol III initiation machinery is condensed to its most basic parts, one ends up with the homologues of the Pol-I-specific core factor of Rrn6, Rrn7 and Rrn11, of which Rrn6 and Rrn7 also have distant homologues in the Pol II factors TFIID and TFIIB, respectively. This agrees with the Pol I system indeed being the evolutionary most compacted and specialized initiation system and thus most ideally suited for structural investigation.

4.4 Future perspectives

Solving the high resolution structure of Pol I in an inactive, dimeric state with an expanded active centre cleft mainly accomplished three things: Firstly, it answered a lot of open questions that were discussed throughout this thesis. Secondly, it raised the same number of new, more detailed questions that arise from interpretation of the novel data. And finally, it opened up the possibility to extend structural studies to polymerase complexes.

A large number of follow-up projects come to mind. Having the structure firstly allows for new attempts on solving the structure of the old crystal form A that C. Kuhn discovered and S. Jennebach worked on^{75,80}. Despite low resolution of the data ($\sim 5.5\text{\AA}$), conformational flexibilities might be visible. Especially the behaviour of connector and expander elements as well as the general state of cleft extension (or contraction) will allow for further speculation on functional significance. It may also explain why all past attempts to solve the Pol I structure from crystal form A were not successful. Initial results look promising but naturally,

re-processing of the data takes time and interpretation of low-resolution maps is not straight forward.

In the crystal form C, which has been obtained and solved in this work, soaking of factors is hardly possible due to the dimeric state and the very tight packing (solvent content 57%). Nevertheless, single or di-nucleotides could be soaked into the crystal to examine very early initiation states. They could be accommodated despite the presence of the expander inside the active centre cleft. Additionally, the toxin α -amanitin could be soaked at high concentrations in order to see if it replaces the A12.2 C-terminal domain or binds differently in Pol I compared to Pol II¹¹⁸.

A second paper describing the structure of Pol I was published by the Müller lab alongside this work¹¹⁹. The resolution and data quality was slightly below the work described here. Nevertheless, similar elements are observed and similar conclusions drawn, thereby providing an unbiased validation for our work and vice versa. Interestingly, their work describes the expander element solely as an inhibitor of unspecific DNA binding¹¹⁹ since they present a different crystal form that does not have the expander resolved but otherwise is similar to ours, i.e. it exhibits the expanded cleft conformation. The authors therefore conclude that the expander does not contribute to stabilization of an expanded cleft¹¹⁹. In contrast to that, our map quality allowed for residue-specific analysis of expander interactions with the inside of the cleft (see Figure 18e, Figure 36 and Appendix 6.9). This suggests a contribution of the expander to open-cleft-stabilization. In terms of data interpretation, the absence of an element in a low-resolution structure might be a hint, but is somewhat speculative to be used as a sole argument for functional significance. Meaning that the expanded-cleft dimer could still be formed due to an influence of the expander, but expander detachment follows due to buffer conditions or as a crystallization artefact. In order to clarify the role of the expander element, additional experiments have hence to be conducted: Firstly, a Pol I version with the complete expander knockout needs to be purified and subjected to functional assays, in order to see if polymerase function (initiation, elongation and cleavage) are influenced. This version might also be subjected to crystallization trials. If the expander stabilizes an expanded cleft, a deletion might lead to crystallization in a contracted form. Secondly, a recombinant expander could be purified and added to the polymerase in excess. This could lead to an increased occurrence of dimers that could be addressed in DLS experiments. Gradual addition of recombinant expander to transcription assays could furthermore display its influence on DNA binding specificity.

Similar to the expander, the connector element should be further investigated. A novel knockout of the element starting from A43 residue 251 to the C-terminus should be remade. Previous knockouts²⁷ lack a small part of the A43 OB-fold⁶¹ in addition to the connector. Purified Pol I from a connector deletion strain might show a reduced tendency for dimerization, as might be the case for expander knockouts. In general, crystallization of Pol I with a contracted cleft should be aimed at, since a number of questions could be answered: What happens to the A12.2 C-terminal domain upon cleft contraction? How does the active centre actually get rearranged into its active state and becomes capable of performing catalysis? What are the dynamics of nucleic acid binding and elongation? Is the dimerization module attached identically in the expanded and the contracted state? For this purpose, deletion of the expander and the connector are two possible strategies. Furthermore, an expander/connector double knockout could be useful. Additionally, dissociation of the stalk, eg. by A14 deletion as described¹⁰⁷, could drive crystallization in a different form since the stalk is not available for crystal contacts and/or dimer formation. Independently, A34.5 could be deleted which is accompanied by A49 dissociation from the polymerase¹¹ could give rise to a different crystal form. These experiments are under way and might, if successful, lead to a number of interesting follow-up results. It is furthermore worthwhile to construct the mentioned strains in *S. pombe* as well as in *S. cerevisiae*. The respective changes might indeed result in the minimal changes that are required for consistent and reproducible crystallization of the *S. pombe* enzyme (see Appendix 6.1).

Independently of the projects that aim at obtaining the structure of Pol I in an active, contracted state, it is now possible to attempt the crystallization of Pol I in complex with transcription factors and/or nucleic acids. Considering elongation factors, binding of the Spt4/5 complex should be examined, a potential complex checked by EM and probed for crystallization. Additionally, recombinant Paf1 complex became available in the lab (Xu et al. unpublished). This complex could be bound to Pol I, potentially in the presence of Spt4/5 similarly to a recent study in Pol II^{32,33}. This large elongation factor complex could be subjected to EM and crosslinking/MS studies to examine its general architecture.

But most interestingly, the initiation complex can now be targeted. Crystallization of a Pol I / Rrn3 complex can be attempted since tight binding was established⁴⁴ and phase information can now be obtained by molecular replacement with the Pol I structure. An extension to the minimal pre-initiation complex by addition of recombinant CF is the next step. CF expression and purification has been established together with T. Gubbey throughout this work⁷⁷. We also managed to form this complex and subject it to negative stain EM (M. Kock) and

crosslinking/MS analysis in collaboration with F. Herzog. Results will enable the positioning of CF elements that can be modelled and the A49 tWH domain in relation to CF. This hybrid approach allows for a high confidence positioning and combines the methods that were proven to be most reliable in the Pol I field (see above). The complex itself can be further extended by a DNA/RNA hybrid scaffold and TBP to form the complete Pol I PIC. The strong stability of this complex also makes it a prime target for crystallization, since it resembles the minimal, evolutionary conserved polymerase initiation machinery. This project can furthermore be complemented by the *S. pombe* Pol I system, that became available during the course of this study (see Appendix 6.1).

In terms of the initiation complex, it might also be worth to break it down into its minimal domains. A minimal Rrn7 construct could be bound to the polymerase. The Rrn7-N210 constructs (see Materials Table 10) comprises the TFIIB-like elements and the N-terminal cyclin fold, as far as can be inferred from homology analysis⁶⁸. It thus resembles the TFIIB construct that has been successfully crystallized together with Pol II⁸¹ and might be able to bind to Pol I on its own. Other CF domains, such as the WD40 beta propeller of Rrn6 of the TPR domain of Rrn11 can be examined by crystallography, especially considering that Rrn11 in *S. pombe* is enormously truncated and contains only the minimally conserved TPR part. In any case, partial structures would be helpful to later solve the initiation complex.

In a different line of investigation, the cleft expansion and contraction demonstrated on the dimeric structure of Pol I presented in this work should be addressed. Does Pol II indeed perform a similar movement under specific circumstances? Does the same hold true for archaeal polymerase and for Pol III? Or might there be an evolutionary relationship between bacterial polymerase and Pol I that restricts the explained core-shelf-movement to the two of them? To answer these questions, it is constantly aimed at solving novel structures of polymerases in different states and with different transcription factors bound.

To summarize, the structure of Pol I presented here is the conclusion of an almost 10-year long quest for the right crystal form. The description of novel elements and a dimeric state with an extended active centre cleft furthermore elaborated a novel theory of the regulation of Pol I in specific and of all polymerases in general.

5. References

- 1 Roeder, R. G. & Rutter, W. J. Multiple forms of DNA-dependent RNA polymerase in eukaryotic organisms. *Nature* **224**, 234-237 (1969).
- 2 Zhang, G. *et al.* Crystal structure of *Thermus aquaticus* core RNA polymerase at 3.3 Å resolution. *Cell* **98**, 811-824 (1999).
- 3 Hirata, A., Klein, B. J. & Murakami, K. S. The X-ray crystal structure of RNA polymerase from Archaea. *Nature* **451**, 851-854, doi:10.1038/nature06530 (2008).
- 4 Vannini, A. & Cramer, P. Conservation between the RNA polymerase I, II, and III transcription initiation machineries. *Molecular cell* **45**, 439-446, doi:10.1016/j.molcel.2012.01.023 (2012).
- 5 Herr, A. J., Jensen, M. B., Dalmay, T. & Baulcombe, D. C. RNA polymerase IV directs silencing of endogenous DNA. *Science* **308**, 118-120, doi:10.1126/science.1106910 (2005).
- 6 Wierzbicki, A. T. *et al.* Spatial and functional relationships among Pol V-associated loci, Pol IV-dependent siRNAs, and cytosine methylation in the Arabidopsis epigenome. *Genes & development* **26**, 1825-1836, doi:10.1101/gad.197772.112 (2012).
- 7 Cramer, P. *et al.* Structure of eukaryotic RNA polymerases. *Annual review of biophysics* **37**, 337-352, doi:10.1146/annurev.biophys.37.032807.130008 (2008).
- 8 Kuhn, C. D. *et al.* Functional architecture of RNA polymerase I. *Cell* **131**, 1260-1272, doi:10.1016/j.cell.2007.10.051 (2007).
- 9 Armache, K. J., Kettenberger, H. & Cramer, P. Architecture of initiation-competent 12-subunit RNA polymerase II. *Proceedings of the National Academy of Sciences of the United States of America* **100**, 6964-6968, doi:10.1073/pnas.1030608100 (2003).
- 10 Jasiak, A. J., Armache, K. J., Martens, B., Jansen, R. P. & Cramer, P. Structural biology of RNA polymerase III: subcomplex C17/25 X-ray structure and 11 subunit enzyme model. *Molecular cell* **23**, 71-81, doi:10.1016/j.molcel.2006.05.013 (2006).
- 11 Geiger, S. R. *et al.* RNA polymerase I contains a TFIIF-related DNA-binding subcomplex. *Molecular cell* **39**, 583-594, doi:10.1016/j.molcel.2010.07.028 (2010).
- 12 Fernandez-Tornero, C. *et al.* Insights into transcription initiation and termination from the electron microscopy structure of yeast RNA polymerase III. *Molecular cell* **25**, 813-823, doi:10.1016/j.molcel.2007.02.016 (2007).
- 13 Ben-Shem, A., Jenner, L., Yusupova, G. & Yusupov, M. Crystal structure of the eukaryotic ribosome. *Science* **330**, 1203-1209, doi:10.1126/science.1194294 (2010).
- 14 Kressler, D., Hurt, E. & Bassler, J. Driving ribosome assembly. *Biochimica et biophysica acta* **1803**, 673-683, doi:10.1016/j.bbamcr.2009.10.009 (2010).
- 15 Warner, J. R. The economics of ribosome biosynthesis in yeast. *Trends in biochemical sciences* **24**, 437-440 (1999).
- 16 Laferte, A. *et al.* The transcriptional activity of RNA polymerase I is a key determinant for the level of all ribosome components. *Genes & development* **20**, 2030-2040, doi:10.1101/gad.386106 (2006).

-
- 17 Miller, O. L., Jr. & Beatty, B. R. Visualization of nucleolar genes. *Science* **164**, 955-957 (1969).
 - 18 Trumtel, S., Leger-Silvestre, I., Gleizes, P. E., Teulieres, F. & Gas, N. Assembly and functional organization of the nucleolus: ultrastructural analysis of *Saccharomyces cerevisiae* mutants. *Molecular biology of the cell* **11**, 2175-2189 (2000).
 - 19 Venema, J. & Tollervey, D. Ribosome synthesis in *Saccharomyces cerevisiae*. *Annual review of genetics* **33**, 261-311, doi:10.1146/annurev.genet.33.1.261 (1999).
 - 20 McStay, B. & Grummt, I. The epigenetics of rRNA genes: from molecular to chromosome biology. *Annual review of cell and developmental biology* **24**, 131-157, doi:10.1146/annurev.cellbio.24.110707.175259 (2008).
 - 21 Nomura, M. Ribosomal RNA genes, RNA polymerases, nucleolar structures, and synthesis of rRNA in the yeast *Saccharomyces cerevisiae*. *Cold Spring Harbor symposia on quantitative biology* **66**, 555-565 (2001).
 - 22 Merz, K. *et al.* Actively transcribed rRNA genes in *S. cerevisiae* are organized in a specialized chromatin associated with the high-mobility group protein Hmo1 and are largely devoid of histone molecules. *Genes & development* **22**, 1190-1204, doi:10.1101/gad.466908 (2008).
 - 23 Moss, T., Langlois, F., Gagnon-Kugler, T. & Stefanovsky, V. A housekeeper with power of attorney: the rRNA genes in ribosome biogenesis. *Cellular and molecular life sciences : CMLS* **64**, 29-49, doi:10.1007/s00018-006-6278-1 (2007).
 - 24 Aprikian, P., Moorefield, B. & Reeder, R. H. New model for the yeast RNA polymerase I transcription cycle. *Molecular and cellular biology* **21**, 4847-4855, doi:10.1128/MCB.21.15.4847-4855.2001 (2001).
 - 25 Lin, C. W. *et al.* A novel 66-kilodalton protein complexes with Rrn6, Rrn7, and TATA-binding protein to promote polymerase I transcription initiation in *Saccharomyces cerevisiae*. *Molecular and cellular biology* **16**, 6436-6443 (1996).
 - 26 Bedwell, G. J., Appling, F. D., Anderson, S. J. & Schneider, D. A. Efficient transcription by RNA polymerase I using recombinant core factor. *Gene* **492**, 94-99, doi:10.1016/j.gene.2011.10.049 (2012).
 - 27 Peyroche, G. *et al.* The recruitment of RNA polymerase I on rDNA is mediated by the interaction of the A43 subunit with Rrn3. *The EMBO journal* **19**, 5473-5482, doi:10.1093/emboj/19.20.5473 (2000).
 - 28 Anderson, S. J. *et al.* The transcription elongation factor Spt5 influences transcription by RNA polymerase I positively and negatively. *The Journal of biological chemistry* **286**, 18816-18824, doi:10.1074/jbc.M110.202101 (2011).
 - 29 Viktorovskaya, O. V., Appling, F. D. & Schneider, D. A. Yeast transcription elongation factor Spt5 associates with RNA polymerase I and RNA polymerase II directly. *The Journal of biological chemistry* **286**, 18825-18833, doi:10.1074/jbc.M110.202119 (2011).
 - 30 Zhang, Y., Sikes, M. L., Beyer, A. L. & Schneider, D. A. The Paf1 complex is required for efficient transcription elongation by RNA polymerase I. *Proceedings of the National Academy of Sciences of the United States of America* **106**, 2153-2158, doi:10.1073/pnas.0812939106 (2009).

-
- 31 Tomson, B. N. & Arndt, K. M. The many roles of the conserved eukaryotic Paf1 complex in regulating transcription, histone modifications, and disease states. *Biochimica et biophysica acta* **1829**, 116-126, doi:10.1016/j.bbagr.2012.08.011 (2013).
- 32 Wier, A. D., Mayekar, M. K., Heroux, A., Arndt, K. M. & Vandemark, A. P. Structural basis for Spt5-mediated recruitment of the Paf1 complex to chromatin. *Proceedings of the National Academy of Sciences of the United States of America* **110**, 17290-17295, doi:10.1073/pnas.1314754110 (2013).
- 33 Mayekar, M. K., Gardner, R. G. & Arndt, K. M. The recruitment of the *Saccharomyces cerevisiae* Paf1 complex to active genes requires a domain of Rtf1 that directly interacts with the Spt4-Spt5 complex. *Molecular and cellular biology* **33**, 3259-3273, doi:10.1128/MCB.00270-13 (2013).
- 34 Albert, B. *et al.* RNA polymerase I-specific subunits promote polymerase clustering to enhance the rRNA gene transcription cycle. *The Journal of cell biology* **192**, 277-293, doi:10.1083/jcb.201006040 (2011).
- 35 Kufel, J., Dichtl, B. & Tollervey, D. Yeast Rnt1p is required for cleavage of the pre-ribosomal RNA in the 3' ETS but not the 5' ETS. *Rna* **5**, 909-917 (1999).
- 36 Petfalski, E., Dandekar, T., Henry, Y. & Tollervey, D. Processing of the precursors to small nucleolar RNAs and rRNAs requires common components. *Molecular and cellular biology* **18**, 1181-1189 (1998).
- 37 Ursic, D., Himmel, K. L., Gurley, K. A., Webb, F. & Culbertson, M. R. The yeast SEN1 gene is required for the processing of diverse RNA classes. *Nucleic acids research* **25**, 4778-4785 (1997).
- 38 Dengl, S. & Cramer, P. Torpedo nuclease Rat1 is insufficient to terminate RNA polymerase II in vitro. *The Journal of biological chemistry* **284**, 21270-21279, doi:10.1074/jbc.M109.013847 (2009).
- 39 Reiter, A. *et al.* The Reb1-homologue Ydr026c/Nsi1 is required for efficient RNA polymerase I termination in yeast. *The EMBO journal* **31**, 3480-3493, doi:10.1038/emboj.2012.185 (2012).
- 40 French, S. L., Osheim, Y. N., Cioci, F., Nomura, M. & Beyer, A. L. In exponentially growing *Saccharomyces cerevisiae* cells, rRNA synthesis is determined by the summed RNA polymerase I loading rate rather than by the number of active genes. *Molecular and cellular biology* **23**, 1558-1568 (2003).
- 41 Lawrence, R. J. *et al.* A concerted DNA methylation/histone methylation switch regulates rRNA gene dosage control and nucleolar dominance. *Molecular cell* **13**, 599-609 (2004).
- 42 Grummt, I. Different epigenetic layers engage in complex crosstalk to define the epigenetic state of mammalian rRNA genes. *Human molecular genetics* **16 Spec No 1**, R21-27, doi:10.1093/hmg/ddm020 (2007).
- 43 Milkereit, P. & Tschochner, H. A specialized form of RNA polymerase I, essential for initiation and growth-dependent regulation of rRNA synthesis, is disrupted during transcription. *The EMBO journal* **17**, 3692-3703, doi:10.1093/emboj/17.13.3692 (1998).

-
- 44 Blattner, C. *et al.* Molecular basis of Rrn3-regulated RNA polymerase I initiation and cell growth. *Genes & development* **25**, 2093-2105, doi:10.1101/gad.17363311 (2011).
- 45 Fath, S. *et al.* Differential roles of phosphorylation in the formation of transcriptional active RNA polymerase I. *Proceedings of the National Academy of Sciences of the United States of America* **98**, 14334-14339, doi:10.1073/pnas.231181398 (2001).
- 46 Gerber, J. *et al.* Site specific phosphorylation of yeast RNA polymerase I. *Nucleic acids research* **36**, 793-802, doi:10.1093/nar/gkm1093 (2008).
- 47 Ficarro, S. B. *et al.* Phosphoproteome analysis by mass spectrometry and its application to *Saccharomyces cerevisiae*. *Nature biotechnology* **20**, 301-305, doi:10.1038/nbt0302-301 (2002).
- 48 Claypool, J. A. *et al.* Tor pathway regulates Rrn3p-dependent recruitment of yeast RNA polymerase I to the promoter but does not participate in alteration of the number of active genes. *Molecular biology of the cell* **15**, 946-956, doi:10.1091/mbc.E03-08-0594 (2004).
- 49 Mayer, C. & Grummt, I. Ribosome biogenesis and cell growth: mTOR coordinates transcription by all three classes of nuclear RNA polymerases. *Oncogene* **25**, 6384-6391, doi:10.1038/sj.onc.1209883 (2006).
- 50 Philippi, A. *et al.* TOR-dependent reduction in the expression level of Rrn3p lowers the activity of the yeast RNA Pol I machinery, but does not account for the strong inhibition of rRNA production. *Nucleic acids research* **38**, 5315-5326, doi:10.1093/nar/gkq264 (2010).
- 51 Milkereit, P., Schultz, P. & Tschochner, H. Resolution of RNA polymerase I into dimers and monomers and their function in transcription. *Biological chemistry* **378**, 1433-1443 (1997).
- 52 Miller, G. *et al.* hRRN3 is essential in the SL1-mediated recruitment of RNA Polymerase I to rRNA gene promoters. *The EMBO journal* **20**, 1373-1382, doi:10.1093/emboj/20.6.1373 (2001).
- 53 Drygin, D., Rice, W. G. & Grummt, I. The RNA polymerase I transcription machinery: an emerging target for the treatment of cancer. *Annual review of pharmacology and toxicology* **50**, 131-156, doi:10.1146/annurev.pharmtox.010909.105844 (2010).
- 54 Hein, N., Hannan, K. M., George, A. J., Sanij, E. & Hannan, R. D. The nucleolus: an emerging target for cancer therapy. *Trends in molecular medicine*, doi:10.1016/j.molmed.2013.07.005 (2013).
- 55 Temiakov, D. *et al.* Structural basis of transcription inhibition by antibiotic streptolydigin. *Molecular cell* **19**, 655-666 (2005).
- 56 Belogurov, G. A. *et al.* Transcription inactivation through local refolding of the RNA polymerase structure. *Nature* **457**, 332-335, doi:10.1038/nature07510 (2009).
- 57 Cramer, P. *et al.* Architecture of RNA polymerase II and implications for the transcription mechanism. *Science* **288**, 640-649 (2000).
- 58 Cramer, P., Bushnell, D. A. & Kornberg, R. D. Structural basis of transcription: RNA polymerase II at 2.8 angstrom resolution. *Science* **292**, 1863-1876, doi:10.1126/science.1059493 (2001).

-
- 59 Bushnell, D. A. & Kornberg, R. D. Complete, 12-subunit RNA polymerase II at 4.1-Å resolution: implications for the initiation of transcription. *Proceedings of the National Academy of Sciences of the United States of America* **100**, 6969-6973, doi:10.1073/pnas.1130601100 (2003).
- 60 Bischler, N. *et al.* Localization of the yeast RNA polymerase I-specific subunits. *The EMBO journal* **21**, 4136-4144 (2002).
- 61 Geiger, S. R., Kuhn, C. D., Leidig, C., Renkawitz, J. & Cramer, P. Crystallization of RNA polymerase I subcomplex A14/A43 by iterative prediction, probing and removal of flexible regions. *Acta crystallographica. Section F, Structural biology and crystallization communications* **64**, 413-418, doi:10.1107/S174430910800972X (2008).
- 62 Jennebach, S., Herzog, F., Aebersold, R. & Cramer, P. Crosslinking-MS analysis reveals RNA polymerase I domain architecture and basis of rRNA cleavage. *Nucleic acids research* **40**, 5591-5601, doi:10.1093/nar/gks220 (2012).
- 63 Gaiser, F., Tan, S. & Richmond, T. J. Novel dimerization fold of RAP30/RAP74 in human TFIIF at 1.7 Å resolution. *Journal of molecular biology* **302**, 1119-1127, doi:10.1006/jmbi.2000.4110 (2000).
- 64 Lefevre, S. *et al.* Structure-function analysis of hRPC62 provides insights into RNA polymerase III transcription initiation. *Nature structural & molecular biology* **18**, 352-358, doi:10.1038/nsmb.1996 (2011).
- 65 Wang, Z. & Roeder, R. G. Three human RNA polymerase III-specific subunits form a subcomplex with a selective function in specific transcription initiation. *Genes & development* **11**, 1315-1326 (1997).
- 66 Wu, C. C. *et al.* RNA polymerase III subunit architecture and implications for open promoter complex formation. *Proceedings of the National Academy of Sciences of the United States of America* **109**, 19232-19237, doi:10.1073/pnas.1211665109 (2012).
- 67 Soding, J., Biegert, A. & Lupas, A. N. The HHpred interactive server for protein homology detection and structure prediction. *Nucleic acids research* **33**, W244-248, doi:10.1093/nar/gki408 (2005).
- 68 Knutson, B. A. & Hahn, S. Yeast Rrn7 and human TAF1B are TFIIB-related RNA polymerase I general transcription factors. *Science* **333**, 1637-1640, doi:10.1126/science.1207699 (2011).
- 69 Naidu, S., Friedrich, J. K., Russell, J. & Zomerdijk, J. C. TAF1B is a TFIIB-like component of the basal transcription machinery for RNA polymerase I. *Science* **333**, 1640-1642, doi:10.1126/science.1207656 (2011).
- 70 Armache, K. J., Mitterweger, S., Meinhart, A. & Cramer, P. Structures of complete RNA polymerase II and its subcomplex, Rpb4/7. *The Journal of biological chemistry* **280**, 7131-7134, doi:10.1074/jbc.M413038200 (2005).
- 71 Spahr, H., Calero, G., Bushnell, D. A. & Kornberg, R. D. Schizosaccharomyces pombe RNA polymerase II at 3.6-Å resolution. *Proceedings of the National Academy of Sciences of the United States of America* **106**, 9185-9190, doi:10.1073/pnas.0903361106 (2009).
- 72 Campbell, E. A. *et al.* Structural mechanism for rifampicin inhibition of bacterial rna polymerase. *Cell* **104**, 901-912 (2001).

-
- 73 Korkhin, Y. *et al.* Evolution of complex RNA polymerases: the complete archaeal RNA polymerase structure. *PLoS biology* **7**, e1000102, doi:10.1371/journal.pbio.1000102 (2009).
- 74 Werner, F. & Grohmann, D. Evolution of multisubunit RNA polymerases in the three domains of life. *Nature reviews. Microbiology* **9**, 85-98, doi:10.1038/nrmicro2507 (2011).
- 75 Kuhn, C. D. *Functional Architecture of RNA Polymerase I* Ph.D. thesis, Ludwig-Maximilians-Universität München, (2008).
- 76 Tschochner, H. A novel RNA polymerase I-dependent RNase activity that shortens nascent transcripts from the 3' end. *Proceedings of the National Academy of Sciences of the United States of America* **93**, 12914-12919 (1996).
- 77 Gubbey, T. *The essential Core Factor complex is recruited to RNA Polymerase I by the specific transcription initiator Rrn3*, Ludwig-Maximilians-Universität München, (2012).
- 78 Bussemer, S. Cloning, recombinant expression and purification of a *Schizosaccharomyces pombe* Elp1 variant for its structural and functional characterization. (Ludwig-Maximilians Universität München, 2010).
- 79 Neyer, S. Cloning, recombinant expression and purification of *Schizosaccharomyces pombe* Elp1 for its structural and functional characterization. (Ludwig-Maximilians Universität München, 2011).
- 80 Jennebach, S. *RNA polymerase I domain architecture and basis of rRNA cleavage* Ph.D. thesis, Ludwig-Maximilians-Universität München, (2011).
- 81 Sainsbury, S., Niesser, J. & Cramer, P. Structure and function of the initially transcribing RNA polymerase II-TFIIB complex. *Nature* **493**, 437-440, doi:10.1038/nature11715 (2013).
- 82 Kabsch, W. Xds. *Acta crystallographica. Section D, Biological crystallography* **66**, 125-132, doi:10.1107/S09074444909047337 (2010).
- 83 4, C. C. P. N. The CCP4 suite: programs for protein crystallography. *Acta Crystallographica Section D: Biological Crystallography* **50**, 760-763, doi:10.1107/S09074444994003112 (1994).
- 84 Adams, P. D. *et al.* PHENIX: a comprehensive Python-based system for macromolecular structure solution. *Acta crystallographica. Section D, Biological crystallography* **66**, 213-221, doi:10.1107/S09074444909052925 (2010).
- 85 Sheldrick, G. M. Experimental phasing with SHELXC/D/E: combining chain tracing with density modification. *Acta Crystallographica Section D: Biological Crystallography* **66**, 479-485, doi:10.1107/S09074444909038360 (2010).
- 86 Vonrhein, C., Blanc, E., Roversi, P. & Bricogne, G. Automated structure solution with autoSHARP. *Methods in molecular biology* **364**, 215-230, doi:10.1385/1-59745-266-1:215 (2007).
- 87 Cowtan, K. Recent developments in classical density modification. *Acta crystallographica. Section D, Biological crystallography* **66**, 470-478, doi:10.1107/S0907444490903947X (2010).

-
- 88 Emsley, P., Lohkamp, B., Scott, W. G. & Cowtan, K. Features and development of Coot. *Acta crystallographica. Section D, Biological crystallography* **66**, 486-501, doi:10.1107/S0907444910007493 (2010).
- 89 Kabsch, W. & Sander, C. Dictionary of protein secondary structure: pattern recognition of hydrogen-bonded and geometrical features. *Biopolymers* **22**, 2577-2637, doi:10.1002/bip.360221211 (1983).
- 90 Karplus, P. A. & Diederichs, K. Linking crystallographic model and data quality. *Science* **336**, 1030-1033, doi:10.1126/science.1218231 (2012).
- 91 Davis, I. W. *et al.* MolProbity: all-atom contacts and structure validation for proteins and nucleic acids. *Nucleic acids research* **35**, W375-383, doi:10.1093/nar/gkm216 (2007).
- 92 Kettenberger, H., Armache, K. J. & Cramer, P. Architecture of the RNA polymerase II-TFIIS complex and implications for mRNA cleavage. *Cell* **114**, 347-357 (2003).
- 93 Buhler, J. M., Sentenac, A. & Fromageot, P. Isolation, structure, and general properties of yeast ribonucleic acid polymerase A (or I). *The Journal of biological chemistry* **249**, 5963-5970 (1974).
- 94 Ruan, W., Lehmann, E., Thomm, M., Kostrewa, D. & Cramer, P. Evolution of two modes of intrinsic RNA polymerase transcript cleavage. *The Journal of biological chemistry* **286**, 18701-18707, doi:10.1074/jbc.M111.222273 (2011).
- 95 Alic, N. *et al.* Selectivity and proofreading both contribute significantly to the fidelity of RNA polymerase III transcription. *Proceedings of the National Academy of Sciences of the United States of America* **104**, 10400-10405, doi:10.1073/pnas.0704116104 (2007).
- 96 Prescott, E. M. *et al.* Transcriptional termination by RNA polymerase I requires the small subunit Rpa12p. *Proceedings of the National Academy of Sciences of the United States of America* **101**, 6068-6073, doi:10.1073/pnas.0401393101 (2004).
- 97 Arimbasseri, A. G., Rijal, K. & Maraia, R. J. Transcription termination by the eukaryotic RNA polymerase III. *Biochimica et biophysica acta* **1829**, 318-330, doi:10.1016/j.bbagr.2012.10.006 (2013).
- 98 Van Mullem, V., Landrieux, E., Vandenhoute, J. & Thuriaux, P. Rpa12p, a conserved RNA polymerase I subunit with two functional domains. *Molecular microbiology* **43**, 1105-1113 (2002).
- 99 Chen, Z. A. *et al.* Architecture of the RNA polymerase II-TFIIF complex revealed by cross-linking and mass spectrometry. *The EMBO journal* **29**, 717-726, doi:10.1038/emboj.2009.401 (2010).
- 100 Eichner, J., Chen, H. T., Warfield, L. & Hahn, S. Position of the general transcription factor TFIIF within the RNA polymerase II transcription preinitiation complex. *The EMBO journal* **29**, 706-716, doi:10.1038/emboj.2009.386 (2010).
- 101 Fernandez-Tornero, C. *et al.* Conformational flexibility of RNA polymerase III during transcriptional elongation. *The EMBO journal* **29**, 3762-3772, doi:10.1038/emboj.2010.266 (2010).
- 102 Tagami, S. *et al.* Crystal structure of bacterial RNA polymerase bound with a transcription inhibitor protein. *Nature* **468**, 978-982, doi:10.1038/nature09573 (2010).

-
- 103 Weixlbaumer, A., Leon, K., Landick, R. & Darst, S. A. Structural basis of transcriptional pausing in bacteria. *Cell* **152**, 431-441, doi:10.1016/j.cell.2012.12.020 (2013).
- 104 Cheung, A. C., Sainsbury, S. & Cramer, P. Structural basis of initial RNA polymerase II transcription. *The EMBO journal* **30**, 4755-4763, doi:10.1038/emboj.2011.396 (2011).
- 105 Wang, D., Bushnell, D. A., Westover, K. D., Kaplan, C. D. & Kornberg, R. D. Structural basis of transcription: role of the trigger loop in substrate specificity and catalysis. *Cell* **127**, 941-954, doi:10.1016/j.cell.2006.11.023 (2006).
- 106 Smid, A., Riva, M., Bouet, F., Sentenac, A. & Carles, C. The association of three subunits with yeast RNA polymerase is stabilized by A14. *The Journal of biological chemistry* **270**, 13534-13540 (1995).
- 107 Beckouet, F., Mariotte-Labarre, S., Peyroche, G., Nogi, Y. & Thuriaux, P. Rpa43 and its partners in the yeast RNA polymerase I transcription complex. *FEBS letters* **585**, 3355-3359, doi:10.1016/j.febslet.2011.09.011 (2011).
- 108 Yuan, X., Zhao, J., Zentgraf, H., Hoffmann-Rohrer, U. & Grummt, I. Multiple interactions between RNA polymerase I, TIF-IA and TAF(I) subunits regulate preinitiation complex assembly at the ribosomal gene promoter. *EMBO reports* **3**, 1082-1087, doi:10.1093/embo-reports/kvf212 (2002).
- 109 Clemente-Blanco, A. *et al.* Cdc14 phosphatase promotes segregation of telomeres through repression of RNA polymerase II transcription. *Nature cell biology* **13**, 1450-1456, doi:10.1038/ncb2365 (2011).
- 110 Cheung, A. C. & Cramer, P. Structural basis of RNA polymerase II backtracking, arrest and reactivation. *Nature* **471**, 249-253, doi:10.1038/nature09785 (2011).
- 111 Epshtein, V., Cardinale, C. J., Ruckenstein, A. E., Borukhov, S. & Nudler, E. An allosteric path to transcription termination. *Molecular cell* **28**, 991-1001, doi:10.1016/j.molcel.2007.10.011 (2007).
- 112 Nielsen, S., Yuzenkova, Y. & Zenkin, N. Mechanism of eukaryotic RNA polymerase III transcription termination. *Science* **340**, 1577-1580, doi:10.1126/science.1237934 (2013).
- 113 Soutourina, J., Wydau, S., Ambroise, Y., Boschiero, C. & Werner, M. Direct interaction of RNA polymerase II and mediator required for transcription in vivo. *Science* **331**, 1451-1454, doi:10.1126/science.1200188 (2011).
- 114 Lawson, C. L. *et al.* Catabolite activator protein: DNA binding and transcription activation. *Current opinion in structural biology* **14**, 10-20, doi:10.1016/j.sbi.2004.01.012 (2004).
- 115 Zuo, Y., Wang, Y. & Steitz, T. A. The mechanism of E. coli RNA polymerase regulation by ppGpp is suggested by the structure of their complex. *Molecular cell* **50**, 430-436, doi:10.1016/j.molcel.2013.03.020 (2013).
- 116 Martinez-Rucobo, F. W., Sainsbury, S., Cheung, A. C. & Cramer, P. Architecture of the RNA polymerase-Spt4/5 complex and basis of universal transcription processivity. *The EMBO journal* **30**, 1302-1310, doi:10.1038/emboj.2011.64 (2011).
- 117 Mylona, A. *et al.* Structure of the tau60/Delta tau91 subcomplex of yeast transcription factor IIIC: insights into preinitiation complex assembly. *Molecular cell* **24**, 221-232, doi:10.1016/j.molcel.2006.08.013 (2006).

-
- 118 Brueckner, F. & Cramer, P. Structural basis of transcription inhibition by alpha-amanitin and implications for RNA polymerase II translocation. *Nature structural & molecular biology* **15**, 811-818, doi:10.1038/nsmb.1458 (2008).
- 119 Fernandez-Tornero, C. *et al.* Crystal structure of the 14-subunit RNA polymerase I. *Nature* **502**, 644-649, doi:10.1038/nature12636 (2013).
- 120 Ringel, R. *et al.* Structure of human mitochondrial RNA polymerase. *Nature* **478**, 269-273, doi:10.1038/nature10435 (2011).
- 121 Schwinghammer, K. *et al.* Structure of human mitochondrial RNA polymerase elongation complex. *Nature structural & molecular biology* **20**, 1298-1303, doi:10.1038/nsmb.2683 (2013).
- 122 Chen, S. *et al.* Repression of RNA Polymerase I upon Stress Is Caused by Inhibition of RNA-Dependent Deacetylation of PAF53 by SIRT7. *Molecular cell* **52**, 303-313, doi:10.1016/j.molcel.2013.10.010 (2013).
- 123 Lariviere, L. *et al.* Structure of the Mediator head module. *Nature* **492**, 448-451, doi:10.1038/nature11670 (2012).
- 124 Krissinel, E. & Henrick, K. Inference of macromolecular assemblies from crystalline state. *Journal of molecular biology* **372**, 774-797, doi:10.1016/j.jmb.2007.05.022 (2007).

6. Appendix

6.1 *Schizosaccharomyces pombe* RNA polymerase I

6.1.1 Construction and cultivation of *S. pombe* strains with tagged Pol I subunits

At the beginning of this work, several strategies were designed which all aimed at obtaining a novel crystal form for RNA polymerase I. Work on crystal form A by C. Kuhn⁷⁵ and S. Jennebach⁸⁰ showed that the originally obtained crystals of *S. cerevisiae* Pol I were not suitable for solving its structure. Around the same time, a study from the lab of R. Kornberg presented the crystal structure of *S. pombe* Pol II⁷¹. This proved that, in principle, the structure of multi-subunit RNA polymerases can be solved from other organisms, especially *S. pombe*. Therefore, the initial idea for this work was to establish a protocol that enables the purification of Pol I from the fission yeast *S. pombe* and use it for crystallization trials. In detail, this means that *S. pombe* strains with tagged Pol I needed to be constructed, their large scale fermentation established and a purification protocol developed.

All in all, the subunits of Pol I are largely conserved between *S. cerevisiae* and *S. pombe* (see Table 15). The most striking difference is the size of the subunit A43. Its charged C-terminal domain that we term “connector” (see Results) is lacking entirely in *S. pombe*. Thus, the molecular weight of the 14-subunit enzyme in *S. cerevisiae* is roughly 20 kDa larger than in *S. pombe* (589.6 kDa and 568.5 kDa, respectively). Regarding its biochemical features, the *S. pombe* enzyme is predicted to have a slightly higher PI (6.55 compared to 6.25 in *S. cerevisiae*; calculated with the program “Protparam” of the “Expasy” toolkit on www.expasy.org). The sequence identity between Pol I of both organisms is 48,6%. It is therefore likely that the enzyme is similar but could display different surface properties which might influence crystallization.

Table 15. Comparison of Pol I subunit sizes in *S. cerevisiae* and *S. pombe*

Subunit	No. of residues in <i>S. cerevisiae</i>	No. of residues in <i>S. pombe</i>	Sequence identity [%]
A190	1664	1689	50
A135	1203	1227	61
A49	415	425	27
A43	326	173	34
AC40	335	348	56
A34.5	233	251	17
Rpb5	215	210	56
Rpb6	155	142	49
A14	137	147	13
Rpb8	146	125	43
AC19	142	125	48
A12.2	125	119	57
Rpb10	70	71	71
Rpb12	70	63	38

As a strain, the wild-type like 972h- was used, from which Pol II was previously purified and crystallized⁷¹. Taking into account that a bulky tag for purification might hinder crystallization, a rather small tag was chosen: a C-terminal Flag- coupled to a 10xhistidine tag. The Flag-tag (DYKDDDDK) is used linker as well as an epitope tag to follow the polymerase fractions throughout the purification steps. The 10xhistidine tag was chosen to enable a high-affinity Ni-NTA purification. As tag locations, the three Pol-I-specific subunits A14, A49 and AC40 were used. While A14 and A49 are Pol-I-specific, peripheral subunits, AC40 is shared with Pol III. Genomic insertion constructs were designed, containing the following elements (see Figure 24a): 5' – homology to the 3' end of the Pol I subunit – Flag-tag – 10xHis tag – Stop codon – G418 resistance cassette – homology to the terminator sequence of the Pol I subunit – 3'. The respective constructs were ordered (Gene Art) and amplified from the delivered plasmids. Genomic insertion into *S. pombe* was performed as described for *S. cerevisiae* (see Methods). Correct insertion was tested by amplification of the 3' end of modified genes (see Figure 24a). For all three insertion-constructs, positive clones were obtained (Figure 24b). Since it could not be excluded that the inserted tags have an influence on polymerase assembly or function, growth curves of 500 ml cultures were recorded (Figure 24c). All constructed strains were viable and none of the Pol I tags lead to a growth defect. Slight fluctuations are more likely to originate from experimental error than from significant growth defects.

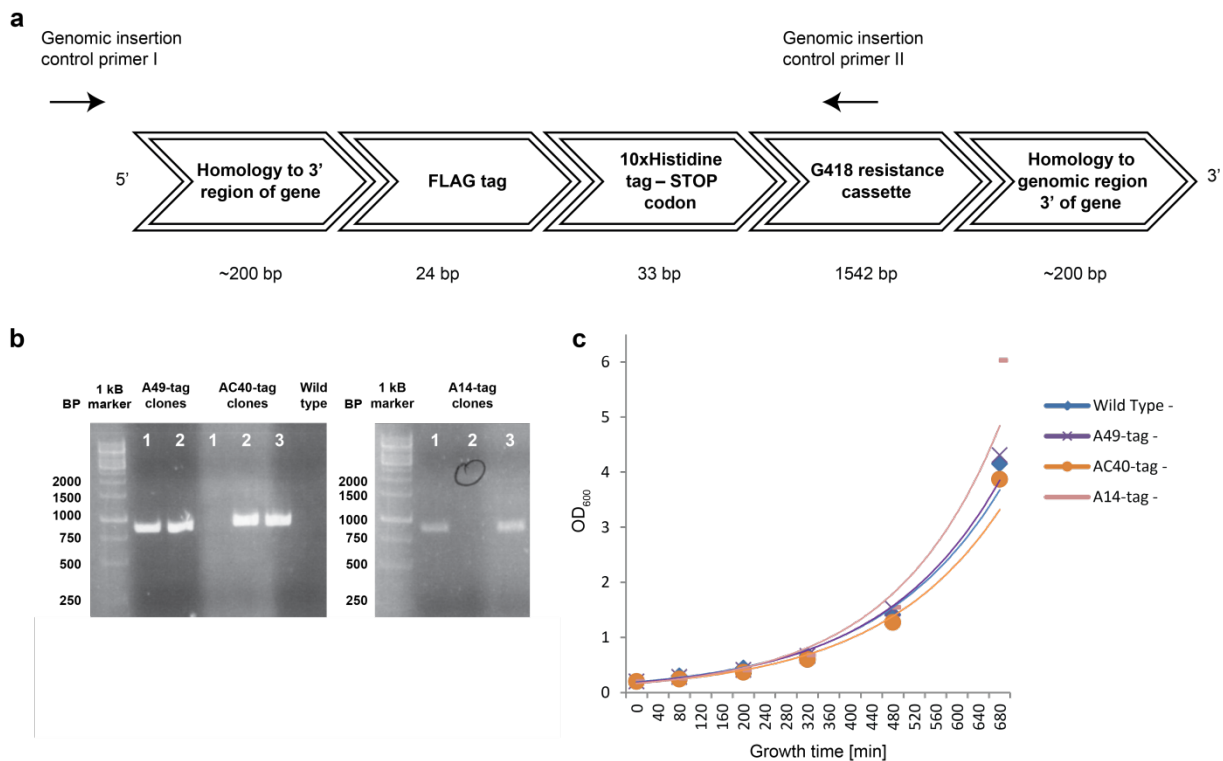


Figure 24. Generation *S. pombe* strains with tagged Pol I subunits.

a Design of constructs for genomic insertion and location of control primers to validate correct insertion. The same strategy was used for construction of all three Pol-I-tag strains. **b** Result of control PCRs from genomic DNA of the established strains shows a product in 2 of 3 clones for each strain. Sybr-safe stained 1% agarose gel with 1kB marker. **c** Growth curves of the constructed strains in comparison to the wild type strain show no growth defect during the first 12 hours.

In order to obtain cell masses that enable the purification of a sufficient amount of Pol I from endogenous expression levels, large scale fermentation of *S. pombe* was inevitable. The establishment of a respective protocol, however, was not straight forward and included trial-and-error based optimization of parameters from classical *S. cerevisiae* fermentation as well as *S. pombe* growth in culture flasks. The protocol that was finally established is detailed in the Methods section of this work.

6.1.2 *S. pombe* Pol I - purification and activity

Resulting from completion of the first stages of this work, *S. pombe* strains with tagged Pol I subunits could be cultivated in large quantities: a 200 litre fermenter yielded up to 2.5 kg of *S. pombe* cells. Even though the handling of *S. pombe* is somewhat different to *S. cerevisiae*, the purification protocol for Pol I could in principle be maintained. As shown in a western blot in Figure 25a, the first steps could be adapted with little to no buffer changes. For anion exchange and cation exchange (MonoQ and MonoS, respectively), gradients were maintained

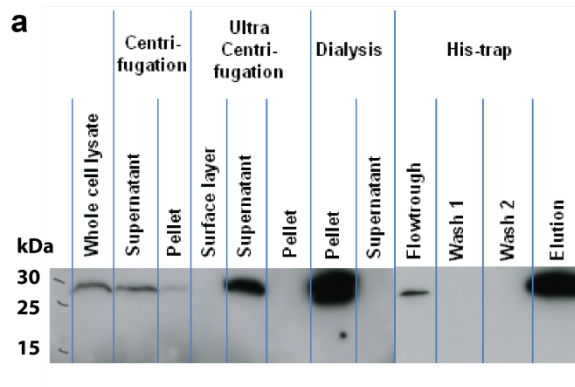
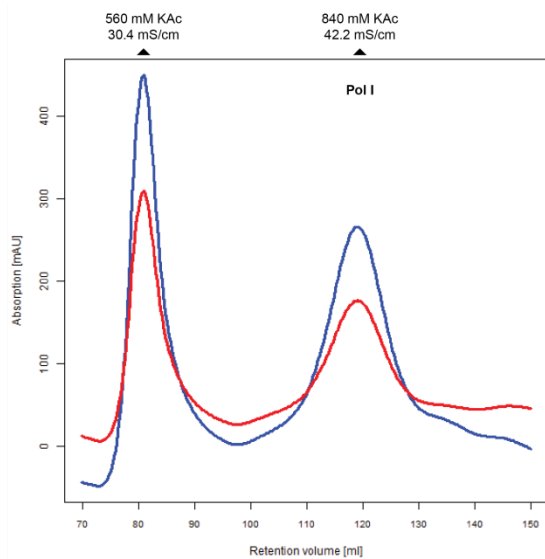


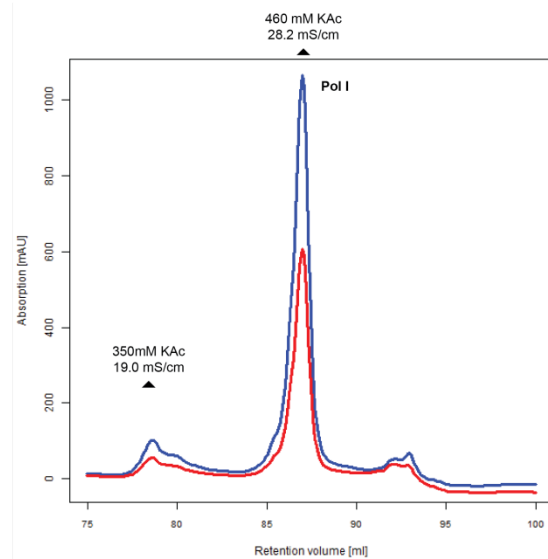
Figure 25. Purification of *S. pombe* Pol I.

a The first steps of the purification are cell lysis, two centrifugation steps, dialysis and Ni-NTA affinity chromatography. The Flag-tag of the A14 subunit is followed during these steps via an anti-flag western blot detected with secondary HRP antibody. **b-d** Elution profiles of the columns run throughout the purification. The respective elution parameters are indicated. **e** Coomassie-stained SDS-PAGE of *S. pombe* Pol I after SEC. Subunit identities are indicated and were confirmed by mass spectrometry.

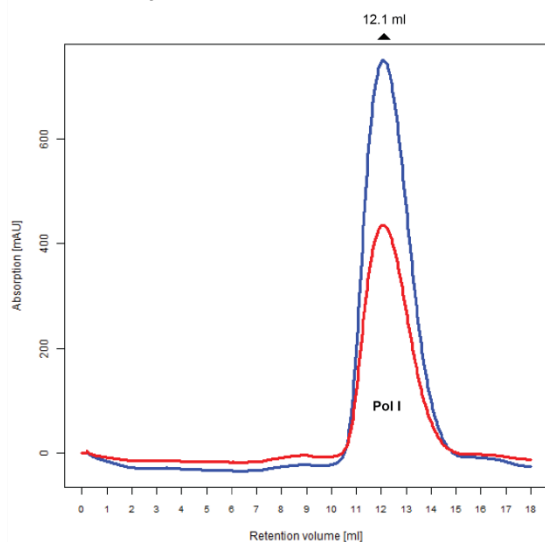
b MonoQ Anion exchange



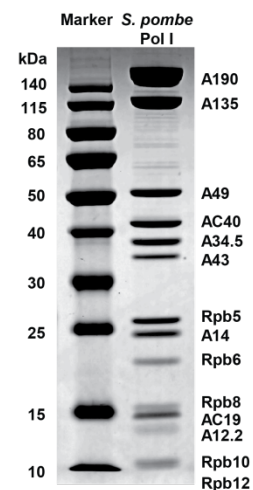
c MonoS Cation exchange



d Superose6 Size exclusion



e



from the *S. cerevisiae* protocol, but elution profiles and contaminant peaks changed as well as the elution properties of the polymerase (see Figure 25b-d). The MonoS cation exchange step was not as important for the *S. pombe* protein as for its *S. cerevisiae* counterpart. The step

rather polishes the purity, comparable to the size exclusion step. However, the overall yield of *S. pombe* Pol I was mostly higher than from *S. cerevisiae*. Therefore, the loss of protein associated with performing the MonoS step could be tolerated and the step was maintained. After the final Superose6 size exclusion step, all Pol I bands are visible on a Coomassie-stained SDS-PAGE (Figure 25e). The presence of all 14 subunits was confirmed by mass spectrometry. A purification from three pellets (about 500 g yeast) yielded up to 2.5 mg protein if the MonoS step was included. For establishment, the A14-tag strain was used. Later, the AC40-tagged strain appeared to have slightly higher yield without increasing Pol III contamination and was thus used from that point on.

Following establishment of a reproducible protocol for large scale Pol I purification from *S. pombe*, the second phase of the project was completed. Nevertheless, before crystallization trials were initiated, it needed to be ensured that the purified complex is stable and can carry out its designated task: transcribing RNA from a DNA template and cleave it, if required. For this reason, elongation and cleavage assays were performed with fluorescently labelled RNA annealed to a tailed template DNA-scaffold (Figure 26).

The assay was carried out exactly as described^{8,80}. It is clearly visible, that upon addition of *S. pombe* Pol I and NTPs elongation as well as cleavage of RNA take place. Thus, it can be concluded that the purified Pol I from *S. pombe* is active and must hence be in its natural state, not being damaged by the purification procedure. Therefore, the protocol can be used to obtain material that is suitable for crystallization trials.

6.1.3 Attempts to crystallize *S. pombe* Pol I

Being able to purify active *S. pombe* Pol I in sizable quantities was a prerequisite for performing large scale crystallization trials. All screens that were available at the crystallization facility of the MPI for Biochemistry (Martinsried, Germany) were tested with the purified *S. pombe* Pol I. Additionally, drop ratios, Pol I concentrations and temperatures

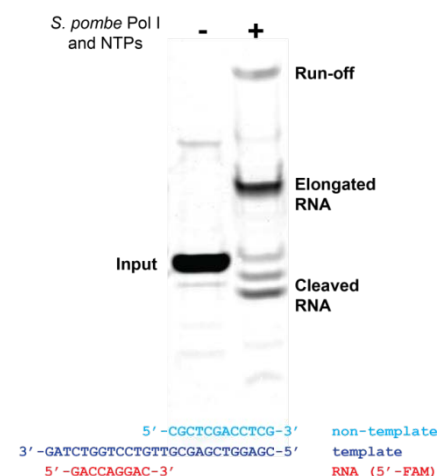


Figure 26. Elongation/cleavage assay of *S. pombe* Pol I.

A standard elongation/cleavage assay was performed with Pol I from *S. pombe* with the displayed scaffold was performed as described^{8,80}. An elongation is clearly visible as is a partial cleavage activity. 20% urea PAGE, fluorescence detection.

were screened. During the first experiments, initial crystals were obtained in two related PEG 3350 conditions (Figure 27a and b) from a number of different preparations. Unfortunately, those could not be reproduced during later stages of the project. It can be speculated, that most likely purification protocols and experience in polymerase handling had improved and advanced the purity of proteins during the course of the experiments. Hence it is likely that either a contaminant crystallized and formed the crystals in Figure 27a and b, or, that the presence of contaminants (such as residual proteases) fostered the crystallization of *S. pombe* Pol I. Regardless, the initial crystals diffracted X-rays to low resolution (Figure 27f). It was, however, not possible to determine space group parameters from that. Other crystals of *S. pombe* Pol I were obtained (Figure 27c-e), but it was either impossible to improve them (d and e) or reproducibility was again an issue (c).

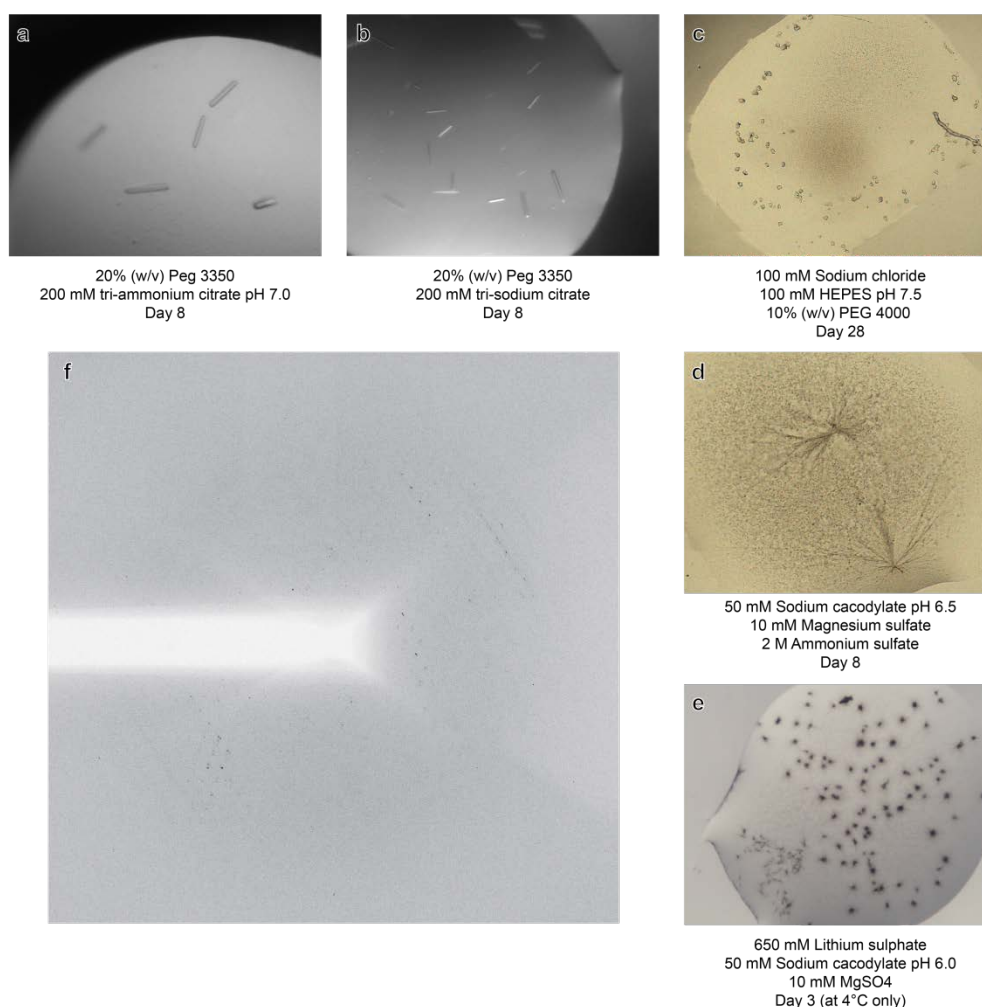


Figure 27. Crystallization of *S. pombe* Pol I.

a and **b** Rod-shaped crystals that were obtained from early Pol I preparations in related conditions. **c – e** Additional crystal forms and their respective conditions. For details see text. **f** Diffraction analysis of the crystals from **a**. The diffraction clearly originated from protein, but it was impossible to conclusively index the data from the obtained frames.

Throughout the project, another crystal form of *S. pombe* Pol I appeared at different stages but always from perfectly pure polymerase samples, thus minimizing the possibility that a contamination played a role in this case. These crystals in the PEG 4000 condition (15% (w/v) PEG 4000, 100 mM Tris pH8.5, 200 mM MgCl₂ in 100 nl drops set up with 8 mg/ml Pol I at 20°C; Figure 28) did not diffract in the PX scanner, which records single frames of the crystals while they are still inside the crystallization drop. Therefore, the crystals cannot consist of salt but must be made of protein. The crystals of this form, however, were extremely fragile and mostly embedded into a protein skin on the top of the drop which tends to build up at high protein concentrations. This made it impossible to fish them from small screening drops and analyse their X-ray diffraction properties. If the project was to be continued at any point in time, the experimentator's recommendation would be to start off from these crystals and try to optimize them.

After the consistent occurrence of reproducibility issues with the discussed *S. pombe* Pol I crystal forms, it became clear that untreated Pol I does not crystallize easily. It was therefore attempted to alter the surface properties of the enzyme and thereby potentially influence its ability to crystallize. For this purpose, several strategies were probed: (1) nucleic acid scaffolds of different sizes and compositions were added, (2) it was attempted to bind the initiation factor Rrn3 from *S. pombe* and thereby stabilize the position of stalk subunits, (3) subunits were dissociated chemically or by genomic deletion, and (4) exposed surface loops of the native enzyme were digested with different proteases. Protein originating from either of these attempts was subsequently subjected to high throughput screens at the crystallization facility of the MPI for Biochemistry (Martinsried, Germany). However, it was impractical to screen all ~20,000 available conditions for each of the experiments, for different concentration and drop ratios etc. Hence, the so-called "Pol-Screens" were designed. They include conditions at which multi-subunit polymerases were crystallized before (*S. cerevisiae* Pol II, *S. pombe* Pol II, bacterial polymerase, etc.). Additionally, conditions for crystallization

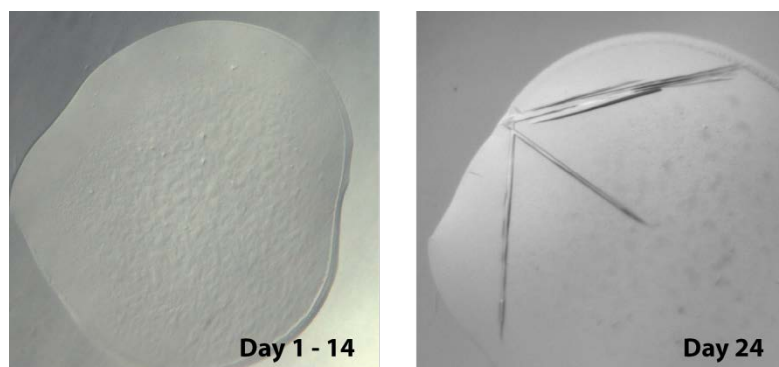


Figure 28. *S. pombe* Pol I crystals in a PEG 4000 condition.

The same drop is displayed 14 and 24 days after setup. After two weeks, relatively large, needle-like crystals grew and did not diffract in a salt-like manner. Handling and reproducibility of those crystals proved challenging.

of Pol II complexes with initiation factors and for the mitochondrial RNA polymerase were added. For all of these, a gradient of precipitant concentration is covered in the screens. This makes it relatively easy to judge if a novel polymerase sample is suitable for crystallization and at the same time covers a range of likely conditions.

The results of the different strategies listed above were as follows:

(1) The *S. pombe* RNA polymerase I bound all nucleic acid scaffolds that were provided to it, as determined by the A280/A260 ratio in analytical size exclusion experiments (data not shown). However, none of the bound scaffolds did influence its tendency to crystallize consistently.

(2) The initiation factor Rrn3 was cloned from *S. pombe*, expressed recombinantly and purified for the first time. Unfortunately, the expressions were highly contaminated with chaperones that migrate identically to Rrn3 in SDS-PAGE. The small amount of protein that could be purified did not interact with Pol I as strongly as it was shown for its *S. cerevisiae* counterpart⁴⁴. Therefore, at the time being it was not possible to form a *S. pombe* Pol I / Rrn3 complex that could be subjected to meaningful crystallization trials. If follow-up studies were to be made, it might be worthwhile to prepare *S. pombe* Pol I in the presence of phosphatase inhibitors. A phosphorylated version of Pol I might bind Rrn3 more easily, as suggested in other studies⁴⁴.

(3) Chemical dissociation of the peripheral Pol I – subunit complex A49/A34.5 was described in the *S. cerevisiae* system⁸. The same protocol was performed on *S. pombe* Pol I. However, two problems made it impossible to transfer the procedure. Firstly, the *S. pombe* enzyme reacted much stronger and dissociated heavily. Secondly, the fraction of polymerase that actually lost A49/A34.5 and remained stable showed a reduced binding to MonoQ anion exchanger. This is most likely due to the absence of the charged C-terminal region of the stalk subunit A43 in *S. pombe*. Thus, a different re-purification method has to be chosen if reattempted. MonoS cation exchange is most likely not applicable, since one of the regions mostly responsible for MonoS resin binding is the lysine-rich C-terminal tail of A34.5, which is removed alongside A49. Size exclusion would remove the urea and might thus lead to partial reattachment of dissociated subunits. If performed under urea conditions, a second size exclusion would be necessary to remove urea independently, since it might influence experiments to follow (such as crystallization trials). A Ni-NTA affinity purification might be of use but would again leave the sample contaminated with imidazole.

Since the chemical dissociation of Pol I subunits in large scale was unsuccessful, purification of Pol I from *S. pombe* strains with mutated subunits was considered. During the course of

this work, a study from the lab of Oliver Gadal reported *S. pombe* strains with deleted A34.5 and A49 subunits³⁴. Those strains were kindly gifted to us and a A190-Flag/10xhistidine tag was introduced to the A34.5 deletion strain. The strain itself shows a slow-growth phenotype and does not reach cell densities of wild type *S. pombe* strain under laboratory conditions. Nevertheless, Pol I could be purified from this strain with the exception of the MonoS cation exchange step (due to the lack of A34.5 lysine-rich tail). The purified Pol I version is termed “Pol I Δ ” and not only entirely lacks A34.5 but also A49 (Figure 29). Thus, genomic construction of a polymerase version with different surface properties was successful in *S. pombe* for the first time. However, Pol I Δ displayed other impurities and a partial contamination with Pol III as identified by mass spectrometry. Additionally, other subunits were substoichiometric in the Pol I Δ variant and the overall yield was extremely low (about 100 μ g Pol I Δ from 350 g yeast). Crystallization screens were carried out nevertheless but did not yield hits in the initial standard screens and the Pol-screens.

(4) For the crystallization of recombinant proteins, it has become a standard procedure to partially digest single proteins or complexes and analyse the dynamics of the reaction to identify stable fragments. These fragments can then expressed separately and subjected to further rounds of digestion and finally might be suitable for crystallization⁶¹. For endogenously purified multi-subunit complexes such as Pol I, however, this strategy is not applicable due to enormous cloning efforts and lethality issues. Thus, an adaptation of the strategy was applied in this case. Firstly, in-drop digest of *S. pombe* Pol I was performed similarly to the procedure that lead to solution of the structure of human mitochondrial RNA polymerase^{120,121}. For Pol I, this did not improve crystallization behaviour. Secondly, a limited digest with different proteases was performed and stopped after one hour by the addition of an excess of protease inhibitor mix. Digested polymerase was subsequently

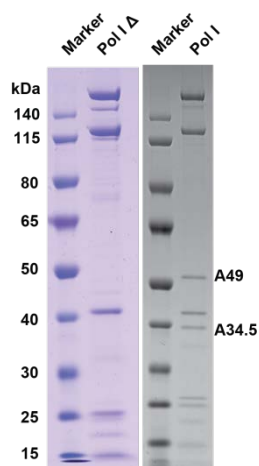


Figure 29. Purification of *S. pombe* Pol I Δ .

Pol I from a *S. pombe* strain with a genomic deletion of A34.5 and an AC40 Flag/His-tag was purified (MonoS cation exchange skipped). The subunit-complex A49/34.5 dissociated completely and is not visible in Coomassie stained SDS-PAGE. Pol I Δ displays an increased amount of contaminating bands

gelfiltered to remove proteases and their inhibitors, and subjected to functionality assays as well as crystallization trials. Figure 30a compares the analytical size exclusion profile of an untreated *S. pombe* Pol I sample with a subtilisin digestion variant (SDS-PAGE of both is displayed in b). The profiles and band patterns show that, following proteolytic digestion, the polymerase stays assembled but loses a large portion of its molecular weight. Hence, the removal of surface parts was likely successful. Similar to subtilisin digestion, the protocol was also successful with the proteases trypsin and chymotrypsin. All proteases gave rise to a distinct band pattern in the digested polymerases (Figure 30c). To test if the stubbed polymerases are still functionally active, standard elongation/cleavage assays were performed. Whereas elongation seemed to be slightly impaired, all digestion variants did elongate the RNA and were capable of product cleavage (Figure 30d).

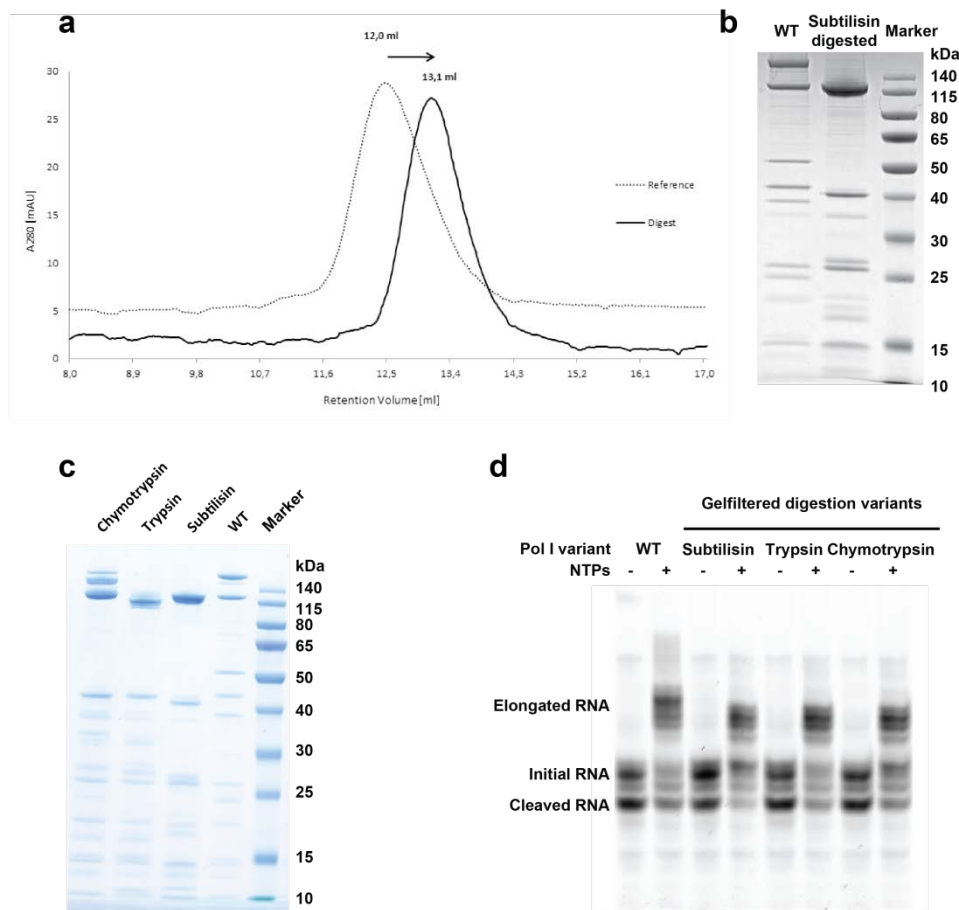


Figure 30. Proteolytic digest of *S. pombe* Pol I.

a Size exclusion chromatograms of undigested and subtilisin digested polymerase. An elution shift of 1.1 ml hints at massive removal of unstructured parts, whereas the polymerase core seems to be stable since the digestion variant still elutes in a single peak. **b** Coomassie-stained SDS-PAGE of the peaks from a. **c** Difference in gel band patterns of Pol I in a Coomassie-stained SDS-PAGE following proteolytic digest and SEC. **d** All digestion variants are still active as shown by an elongation/cleavage assay. Fluorescence detection of 20% urea PAGE.

Subjected to crystallization screens, the subtilisin and trypsin digestion variants did not produce any hits. In contrast, the chymotrypsin digest crystallized after 10-15 days at a Pol I concentration of 5 mg/ml in 30% Jeffamine ED-2001 pH 7.0 and 100 mM Hepes pH 7.0 (Figure 31a-c). Crystals grew at 20°C in 100 nl drops for 5 – 10 days and were very small but seemed to be clean ellipsoids of up to 25 µm length. Reproduction proved successful in every 3rd trial most likely due to sample inhomogeneity resulting from up-scaling issues with the digestion protocol. One successful reproduction of the digestions crystals yielded needle-like crystals (Figure 31d) after over a month. The Jeffamine drops, however, dry out quickly and crystals could not be removed from protein skin to subject them to X-ray diffraction analysis.

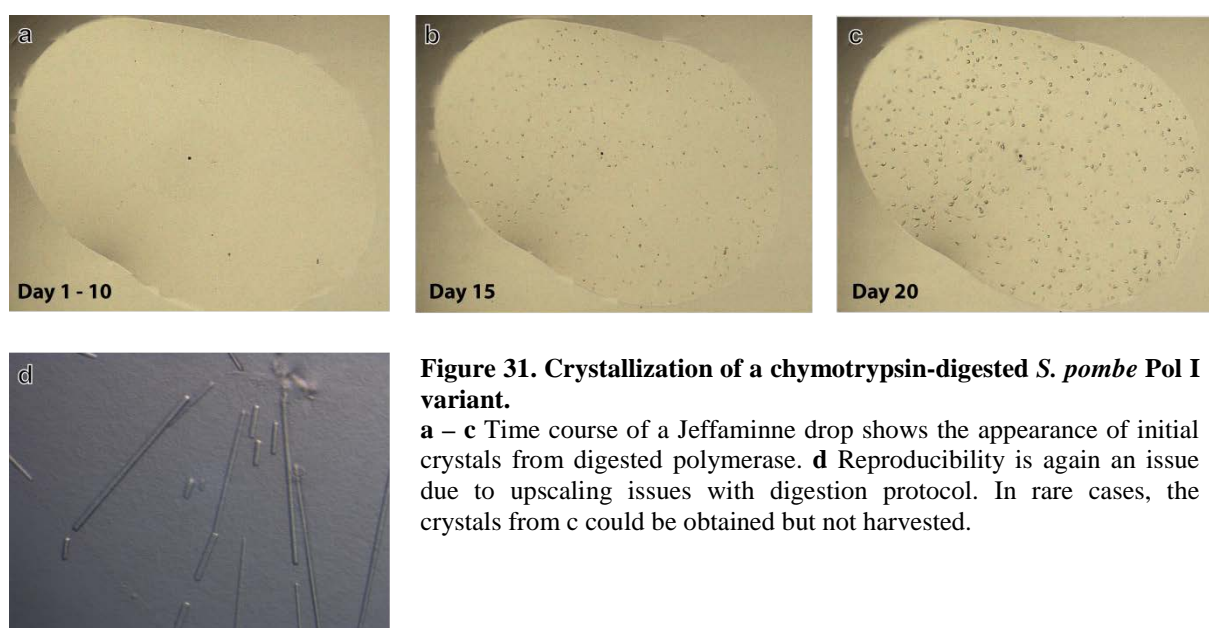


Figure 31. Crystallization of a chymotrypsin-digested *S. pombe* Pol I variant.

a – c Time course of a Jeffamine drop shows the appearance of initial crystals from digested polymerase. **d** Reproducibility is again an issue due to upscaling issues with digestion protocol. In rare cases, the crystals from c could be obtained but not harvested.

6.1.4 Conclusion of the *S. pombe* Pol I project

The goal of this work was to produce a novel crystal form of Pol I from which its structure can be solved. For this purpose, using the *S. pombe* enzyme as an alternative for *S. cerevisiae* was the central strategy. Initial results were positive: a fermentation and purification protocol could be established and first crystals were obtained rapidly. Later on, however, reproducibility became a central issue. Quality of the different fermentations and purifications seems to be an issue that can hardly be quantified. Nevertheless, comparable problems appear to occur also for *S. cerevisiae* Pol II if complex with transcription factors: Some preps produce high quality crystals whereas others don't diffract to high resolution at all. In the case of *S. pombe* Pol I, the difference, however, was whether the protein would crystallize at all.

The subunit A43 was always present in preparations but tended to be substoichiometric. Also, it migrated at much higher apparent molecular weight in SDS-PAGE than its theoretical molecular weight of 21 kDa would suggest. This hints at the occurrence of posttranslational modifications. Beside the known phosphorylation other modifications such as sumoylation, ubiquitinylation or acetylation could take place. In the human system, for example, acetylation of the A49 homologue has been recently reported to play a regulatory role¹²². Similarly, the absence of the connector element in *S. pombe* could result in the need for a different level of A43 regulation by posttranslational modification. By purifying a mixture of modified and unmodified complexes, a heterogeneity would be introduced, which could explain the inconsistency in *S. pombe* Pol I crystallization behaviour.

Nevertheless, despite failure to consistently crystallize Pol I from *S. pombe*, the work on it resulted in a number of benefits:

- (1) This is the first time that RNA polymerase I from an organism other than *S. cerevisiae* could be purified in crystallization grade quality and quantity.
- (2) Pol-Screens to easily probe crystallization behaviour of novel samples have been designed for this project and are now widely used also for Pol-II-related projects and ultimately were an integral part of solving the structure of *S. cerevisiae* Pol I, since they gave rise to the first hit of crystal form C.
- (3) A novel system for functional and structural projects was established. Since crystallization is dependent on small influences, Pol I complexes of *S. pombe* could be superior to their *S. cerevisiae* homologues and thus provide an easily accessible secondary system for further generations of PhD students working on polymerase projects. Similar experiences have been made with the “mediator head” in our lab¹²³. For functional analysis, *in vitro* data from a second organism can be of importance as controls just as well.
- (4) Experience in handling of polymerases seems to be of great importance to ensure consistency. Therefore, establishing a new system was the best possible training and provided all the practical experience necessary for solving the structure of a polymerase and thus laid a solid groundwork for the work carried out in the *S. cerevisiae* system.

With this, the project can be judged as a partial success despite the inability to solve the structure of *S. pombe* Pol I as of now.

6.2 Scripts for crystallographic data processing

6.2.1 XDS script for data integration

```
!*****
! XDS.INP used on crystal CE188 for the PILATUS 6M pixel detector at SLS
!*****
DETECTOR=PILATUS           MINIMUM_VALID_PIXEL_VALUE=0 OVERLOAD=1048500
SENSOR_THICKNESS=0.32
NX=2463 NY=2527 QX=0.172 QY=0.172 !PILATUS 6M

DIRECTION_OF_DETECTOR_X-AXIS= 1.0 0.0 0.0
DIRECTION_OF_DETECTOR_Y-AXIS= 0.0 1.0 0.0
TRUSTED_REGION=0.0 1.41

!===== JOB CONTROL PARAMETERS =====
!JOB= XDCORR INIT COLSPOT IDXREF !THIS JOB WAS USED IN A FIRST RUN FOR INDEXING
JOB= DEFPIX XPLAN INTEGRATE CORRECT

!===== GEOMETRICAL PARAMETERS =====
ORGX=1250.0 ORGY=1238 !Detector origin (pixels)
DETECTOR_DISTANCE= 575 ! (mm)

ROTATION_AXIS= 1.0 0.0 0.0
OSCILLATION_RANGE=0.1

X-RAY_WAVELENGTH= 1.00000
INCIDENT_BEAM_DIRECTION=0.0 0.0 1.0
FRACTION_OF_POLARIZATION=0.99
POLARIZATION_PLANE_NORMAL= 0.0 1.0 0.0

!===== CRYSTAL PARAMETERS =====
SPACE_GROUP_NUMBER=0 !0 is used for unknown crystals
FRIEDEL'S_LAW=TRUE.

!===== SELECTION OF DATA IMAGES =====
NAME_TEMPLATE_OF_DATA_FRAMES=~ /ce188/ce188_1_0?????.cbf
DATA_RANGE=1 5300
BACKGROUND_RANGE=1 20

!===== INDEXING PARAMETERS =====
SEPMIN=4.0
CLUSTER_RADIUS=2

!===== DECISION CONSTANTS FOR FINDING CRYSTAL SYMMETRY =====
MAX_CELL_AXIS_ERROR=0.03 ! Maximum relative error in cell axes tolerated
MAX_CELL_ANGLE_ERROR=2.0 ! Maximum cell angle error tolerated

TEST_RESOLUTION_RANGE=8.0 4.5
MIN_RFL_Rmeas= 50 ! Minimum #reflections needed for calculation of Rmeas
MAX_FAC_Rmeas=2.0 ! Sets an upper limit for acceptable Rmeas

!===== PARAMETERS CONTROLLING REFINEMENTS =====
REFINE(INTEGRATE)= BEAM ORIENTATION CELL
!REFINE(CORRECT)=DISTANCE BEAM ORIENTATION CELL AXIS

!===== CRITERIA FOR ACCEPTING REFLECTIONS =====
VALUE_RANGE_FOR_TRUSTED_DETECTOR_PIXELS= 6000 30000

INCLUDE_RESOLUTION_RANGE=70.0 2.8

MINIMUM_ZETA=0.05

!===== INTEGRATION AND PEAK PROFILE PARAMETERS =====
NUMBER_OF_PROFILE_GRID_POINTS_ALONG_ALPHA/BETA=13

!===== PARAMETERS DEFINING BACKGROUND AND PEAK PIXELS =====
MINIMUM_NUMBER_OF_PIXELS_IN_A_SPOT=3
```

6.2.2 XSCALE script for the combination of five datasets from four crystals

```

0-DOSE_SIGNIFICANCE_LEVEL=0.50
OUTPUT_FILE=merge_zero.hkl
FRIEDEL'S_LAW=TRUE
MERGE=TRUE
STRICT_ABSORPTION_CORRECTION=FALSE

INPUT_FILE= ../ce188/xds_2/XDS_ASCII.HKL
INCLUDE_RESOLUTION_RANGE= 40 2.8
CRYSTAL_NAME=ce188_2

INPUT_FILE= ../ce188/xds/XDS_ASCII.HKL
INCLUDE_RESOLUTION_RANGE= 40 2.8
CRYSTAL_NAME=ce188_1

INPUT_FILE= ../ce201/xds/XDS_ASCII.HKL
INCLUDE_RESOLUTION_RANGE= 40 2.8
CRYSTAL_NAME=ce201

INPUT_FILE= ../ce259/xds_b/XDS_ASCII.HKL
INCLUDE_RESOLUTION_RANGE= 40 2.8
CRYSTAL_NAME=ce259_b

INPUT_FILE= ../ce152/xds/XDS_ASCII.HKL
INCLUDE_RESOLUTION_RANGE= 40 2.8
CRYSTAL_NAME=ce152

```

6.2.3 XSCALE – Selected output parameters

```

THE DATA COLLECTION STATISTICS REPORTED BELOW ASSUMES:
SPACE_GROUP_NUMBER= 1
UNIT_CELL_CONSTANTS= 122.74 139.02 209.55 108.060 95.403 93.848
ALL DATA SETS WILL BE SCALED TO ../ce188/xds_2/XDS_ASCII.HKL

*****
READING INPUT REFLECTION DATA FILES
*****

NUMBER OF UNIQUE REFLECTIONS IN FILE "REMOVE.HKL" 163

DATA MEAN REFLECTIONS INPUT FILE NAME
SET# INTENSITY ACCEPTED REJECTED
1 0.2659E+02 643001 316 ../ce188/xds_2/XDS_ASCII.HKL
2 0.2835E+02 1638774 769 ../ce188/xds/XDS_ASCII.HKL
3 0.8544E+01 765475 479 ../ce201/xds/XDS_ASCII.HKL
4 0.2161E+02 380492 259 ../ce259/xds_b/XDS_ASCII.HKL
5 0.1127E+02 770320 352 ../ce152/xds/XDS_ASCII.HKL

*****
OVERALL SCALING AND CRYSTAL DISORDER CORRECTION
*****

CORRELATIONS BETWEEN INPUT DATA SETS AFTER CORRECTIONS

DATA SETS NUMBER OF COMMON CORRELATION RATIO OF COMMON B-FACTOR
#i #j REFLECTIONS BETWEEN i,j INTENSITIES (i/j) BETWEEN i,j

1 2 137844 0.966 1.0060 -0.1070
1 3 105989 0.955 1.0063 0.0559
2 3 106853 0.944 1.0065 0.0198
1 4 84571 0.918 0.9930 -0.5293
2 4 87131 0.935 1.0109 -0.5341
3 4 76583 0.899 1.0267 -1.1212
1 5 114809 0.929 0.9950 0.2459
2 5 115454 0.943 0.9855 0.2195
3 5 94390 0.915 0.9767 0.4377
4 5 76769 0.959 1.0379 -0.1888

SUBSET OF INTENSITY DATA WITH SIGNAL/NOISE >= -3.0 AS FUNCTION OF RESOLUTION
RESOLUTION NUMBER OF REFLECTIONS COMPLETENESS R-FACTOR R-FACTOR COMPARED I/SIGMA R-meas CC(1/2) Anomal SigAno Nano
LIMIT OBSERVED UNIQUE POSSIBLE OF DATA observed expected

12.52 40590 3478 3597 96.7% 8.3% 10.8% 40590 30.37 8.7% 99.7* -13 0.676 3402
8.85 86692 6567 6577 99.8% 9.3% 11.4% 86692 30.16 9.6% 99.8* -17 0.629 6538
7.23 105359 8480 8494 99.8% 11.0% 12.8% 105359 24.10 11.5% 99.7* -17 0.686 8432
6.26 134659 10110 10123 99.9% 13.5% 14.9% 134659 20.42 14.1% 99.5* -19 0.691 10096
5.60 155578 11348 11354 99.9% 15.0% 16.4% 155578 18.72 15.6% 99.5* -19 0.680 11331
5.11 160339 12647 12666 99.8% 15.6% 16.8% 160339 17.34 16.2% 99.4* -19 0.685 12604
4.73 179718 13775 13785 99.9% 16.1% 17.1% 179718 17.17 16.8% 99.4* -23 0.673 13749
4.43 198177 14751 14759 99.9% 17.1% 18.0% 198177 16.51 17.7% 99.4* -22 0.677 14727
4.17 210053 15700 15712 99.9% 19.1% 20.0% 210053 14.87 19.9% 99.2* -19 0.690 15670
3.96 211043 16572 16583 99.9% 22.7% 23.5% 211043 12.52 23.6% 98.8* -18 0.701 16514
3.78 226004 17508 17527 99.9% 27.7% 28.7% 226004 10.67 28.8% 98.5* -18 0.713 17474
3.61 244122 18170 18183 99.9% 35.4% 36.4% 244122 9.15 36.9% 97.9* -16 0.729 18133
3.47 259891 19069 19093 99.9% 44.4% 45.7% 259891 7.76 46.1% 97.0* -14 0.736 19043
3.35 261803 19820 19837 99.9% 54.5% 56.2% 261803 6.28 56.7% 95.3* -13 0.733 19760
3.23 262055 20421 20441 99.9% 71.0% 72.1% 262055 4.81 73.9% 92.0* -10 0.744 20365
3.13 275504 21262 21300 99.8% 86.9% 88.3% 275504 3.91 90.4% 88.6* -9 0.738 21209
3.04 291152 21807 21828 99.9% 110.2% 112.7% 291152 3.17 114.6% 83.4* -7 0.730 21777
2.95 304614 22508 22545 99.8% 135.3% 136.6% 304614 2.59 140.6% 77.2* -7 0.730 22485
2.87 311277 23188 23214 99.9% 166.9% 169.0% 311277 2.05 173.5% 68.2* -5 0.713 23151
2.80 274084 23763 23801 99.8% 201.8% 205.1% 274081 1.52 211.3% 54.1* -4 0.691 23388
total 4192714 320944 321419 99.9% 24.0% 25.5% 4192711 9.61 25.0% 99.6* -13 0.710 319848

```

6.3 Scripts and parameterization files for structure refinement

6.3.1 Refinement strategy file for phenix.refine

```
phenix.refine \  
~/merge3/merge3.mtz \  
~/poll/build6_5.pdb \  
strategy=rigid_body+individual_sites+individual_adp+tls \  
refinement.input.xray_data.r_free_flags.label=FreeR_flag \  
rigid_bodies.params \  
ncs_groups.params \  
tlsmd.params \  
main.ncs=True ncs.type=cartesian \  
ncs.find_automatically=False \  
check_rotamer_consistency=False \  
disulfide_distance_cutoff=0.5 \  
adp.convert_to_iso=true \  
adp.set_b_iso=60 \  
poli-zinc.restraints \  
solvent.params \  
refinement.ncs.excessive_distance_limit=None \  
main.number_of_macro_cycles=6
```

6.3.2 Definition of bond lengths for one coordinated Zinc atom

```
refinement.geometry_restraints.edits {  
  zn_sg_dist = 2.34  
  sigma_zn_sg_dist = 0.05  
  zn_ne2_dist = 2.00  
  sigma_zn_ne2_dist = 0.02  
  slack = None  
  
  ### Zn A:3001 ###  
  bond {  
    action = *add  
    atom_selection_1 = chain A and resid 3001 and resname ZN and name ZN  
    atom_selection_2 = chain A and resid 62 and resname CYS and name SG  
    distance_ideal = $zn_sg_dist  
    sigma = $sigma_zn_sg_dist  
    slack = $slack  
  }  
  bond {  
    action = *add  
    atom_selection_1 = chain A and resid 3001 and resname ZN and name ZN  
    atom_selection_2 = chain A and resid 65 and resname CYS and name SG  
    distance_ideal = $zn_sg_dist  
    sigma = $sigma_zn_sg_dist  
    slack = $slack  
  }  
  bond {  
    action = *add  
    atom_selection_1 = chain A and resid 3001 and resname ZN and name ZN  
    atom_selection_2 = chain A and resid 72 and resname CYS and name SG  
    distance_ideal = $zn_sg_dist  
    sigma = $sigma_zn_sg_dist  
    slack = $slack  
  }  
  bond {  
    action = *add  
    atom_selection_1 = chain A and resid 3001 and resname ZN and name ZN  
    atom_selection_2 = chain A and resid 75 and resname HIS and name NE2  
    distance_ideal = $zn_ne2_dist  
    sigma = $sigma_zn_ne2_dist  
    slack = $slack  
  }  
}
```

6.3.3 Definition file for NCS refinement

```
refinement.ncs.restraint_group {
  reference = chain A and resseq 1:84
  selection = chain P and resseq 1:84
}
refinement.ncs.restraint_group {
  reference = chain A and resseq 85:139
  selection = chain P and resseq 85:139
}
refinement.ncs.restraint_group {
  reference = chain A and resseq 176:272
  selection = chain P and resseq 176:272
}
refinement.ncs.restraint_group {
  reference = chain A and resseq 296:363
  selection = chain P and resseq 296:363
}
refinement.ncs.restraint_group {
  reference = chain A and resseq 364:380
  selection = chain P and resseq 364:380
}
refinement.ncs.restraint_group {
  reference = chain A and resseq 381:441
  selection = chain P and resseq 381:441
}
refinement.ncs.restraint_group {
  reference = chain A and resseq 442:477
  selection = chain P and resseq 442:477
}
refinement.ncs.restraint_group {
  reference = chain A and resseq 478:652
  selection = chain P and resseq 478:652
}
refinement.ncs.restraint_group {
  reference = chain A and resseq 653:826
  selection = chain P and resseq 653:826
}
refinement.ncs.restraint_group {
  reference = chain A and resseq 827:989
  selection = chain P and resseq 827:989
}
refinement.ncs.restraint_group {
  reference = chain A and resseq 990:1028
  selection = chain P and resseq 990:1028
}
refinement.ncs.restraint_group {
  reference = chain A and resseq 1029:1152
  selection = chain P and resseq 1029:1152
}
refinement.ncs.restraint_group {
  reference = chain A and resseq 1160:1204
  selection = chain P and resseq 1160:1204
}
refinement.ncs.restraint_group {
  reference = chain A and resseq 1213:1337
  selection = chain P and resseq 1213:1337
}
refinement.ncs.restraint_group {
  reference = chain A and resseq 1361:1395
  selection = chain P and resseq 1361:1395
}
refinement.ncs.restraint_group {
  reference = chain A and resseq 1596:1664
  selection = chain P and resseq 1596:1664
}
refinement.ncs.restraint_group {
  reference = chain B and resseq 8:79
  selection = chain Q and resseq 8:79
}
refinement.ncs.restraint_group {
  reference = chain B and resseq 88:204
  selection = chain Q and resseq 88:204
}
refinement.ncs.restraint_group {
  reference = chain B and resseq 205:404
  selection = chain Q and resseq 205:404
}
refinement.ncs.restraint_group {
  reference = chain B and resseq 405:489
  selection = chain Q and resseq 405:489
}
refinement.ncs.restraint_group {
  reference = chain B and resseq 490:697
  selection = chain Q and resseq 490:697
}
refinement.ncs.restraint_group {
  reference = chain B and resseq 698:798
  selection = chain Q and resseq 698:798
}
refinement.ncs.restraint_group {
  reference = chain B and resseq 799:910
  selection = chain Q and resseq 799:910
}
refinement.ncs.restraint_group {
  reference = chain B and resseq 911:1038
  selection = chain Q and resseq 911:1038
}
refinement.ncs.restraint_group {
  reference = chain B and resseq 1039:1203
  selection = chain Q and resseq 1039:1203
}
refinement.ncs.restraint_group {
  reference = chain C and resseq 31:76
  selection = chain R and resseq 31:76
}
refinement.ncs.restraint_group {
  reference = chain C and resseq 77:220
  selection = chain R and resseq 77:220
}
refinement.ncs.restraint_group {
  reference = chain C and resseq 221:334
  selection = chain R and resseq 221:334
}
refinement.ncs.restraint_group {
  reference = chain D
  selection = chain S
}
refinement.ncs.restraint_group {
  reference = chain G and resseq 14:127
  selection = chain V and resseq 14:127
}
refinement.ncs.restraint_group {
  reference = chain G and resseq 128:250
  selection = chain V and resseq 128:250
}
refinement.ncs.restraint_group {
  reference = chain O and resseq 265:315
  selection = chain 4 and resseq 265:315
}
refinement.ncs.restraint_group {
  reference = chain E and resseq 5:147
  selection = chain T and resseq 5:147
}
refinement.ncs.restraint_group {
  reference = chain E and resseq 148:215
  selection = chain T and resseq 148:215
}
refinement.ncs.restraint_group {
  reference = chain F
  selection = chain U
}
refinement.ncs.restraint_group {
  reference = chain H
  selection = chain W
}
refinement.ncs.restraint_group {
  reference = chain I and resseq 2:74
  selection = chain X and resseq 2:74
}
refinement.ncs.restraint_group {
  reference = chain I and resseq 75:125
  selection = chain X and resseq 75:125
}
refinement.ncs.restraint_group {
  reference = chain J
  selection = chain Y
}
refinement.ncs.restraint_group {
  reference = chain K
  selection = chain Z
}
refinement.ncs.restraint_group {
  reference = chain L
  selection = chain 1
}
refinement.ncs.restraint_group {
  reference = chain M
  selection = chain 2
}
refinement.ncs.restraint_group {
  reference = chain N and resseq 22:140
  selection = chain 3 and resseq 22:140
}
refinement.ncs.restraint_group {
  reference = chain N and resseq 141:180
  selection = chain 3 and resseq 141:180
}
```

6.3.4 Definition file for Rigid body refinement

```
refinement.refine.sites {  
  
rigid_body = chain A and resseq 1:84  
rigid_body = chain A and resseq 85:139  
rigid_body = chain A and resseq 176:272  
rigid_body = chain A and resseq 296:363  
rigid_body = chain A and resseq 364:380  
rigid_body = chain A and resseq 381:441  
rigid_body = chain A and resseq 442:477  
rigid_body = chain A and resseq 478:652  
rigid_body = chain A and resseq 653:826  
rigid_body = chain A and resseq 827:989  
rigid_body = chain A and resseq 990:1028  
rigid_body = chain A and resseq 1029:1152  
rigid_body = chain A and resseq 1160:1204  
rigid_body = chain A and resseq 1213:1350  
rigid_body = chain A and resseq 1362:1395  
rigid_body = chain A and resseq 1440:1543  
rigid_body = chain A and resseq 1544:1595  
rigid_body = chain A and resseq 1596:1664  
rigid_body = chain B and resseq 8:79  
rigid_body = chain B and resseq 88:204  
rigid_body = chain B and resseq 205:404  
rigid_body = chain B and resseq 405:489  
rigid_body = chain B and resseq 490:697  
rigid_body = chain B and resseq 698:798  
rigid_body = chain B and resseq 799:910  
rigid_body = chain B and resseq 911:1038  
rigid_body = chain B and resseq 1039:1203  
rigid_body = chain C and resseq 31:76  
rigid_body = chain C and resseq 77:220  
rigid_body = chain C and resseq 221:334  
rigid_body = chain G and resseq 14:127  
rigid_body = chain G and resseq 128:250  
rigid_body = chain E and resseq 5:147  
rigid_body = chain E and resseq 148:215  
rigid_body = chain F  
rigid_body = chain D  
rigid_body = chain H  
rigid_body = chain I and resseq 2:74  
rigid_body = chain I and resseq 75:125  
rigid_body = chain J  
rigid_body = chain K  
rigid_body = chain L  
rigid_body = chain M  
rigid_body = chain N and resseq 22:140  
rigid_body = chain N and resseq 141:180  
rigid_body = chain O  
rigid_body = chain P and resseq 1:84  
rigid_body = chain P and resseq 85:139  
rigid_body = chain P and resseq 176:272  
rigid_body = chain P and resseq 296:363  
rigid_body = chain P and resseq 364:380  
rigid_body = chain P and resseq 381:441  
rigid_body = chain P and resseq 442:477  
rigid_body = chain P and resseq 478:652  
rigid_body = chain P and resseq 653:826  
rigid_body = chain P and resseq 827:989  
rigid_body = chain P and resseq 990:1028  
rigid_body = chain P and resseq 1029:1152  
rigid_body = chain P and resseq 1160:1204  
rigid_body = chain P and resseq 1213:1350  
rigid_body = chain P and resseq 1362:1395  
rigid_body = chain P and resseq 1440:1543  
rigid_body = chain P and resseq 1544:1595  
rigid_body = chain P and resseq 1596:1664  
rigid_body = chain Q and resseq 8:79  
rigid_body = chain Q and resseq 88:204  
rigid_body = chain Q and resseq 205:404  
rigid_body = chain Q and resseq 405:489  
rigid_body = chain Q and resseq 490:697  
rigid_body = chain Q and resseq 698:798  
rigid_body = chain Q and resseq 799:910  
rigid_body = chain Q and resseq 911:1038  
rigid_body = chain Q and resseq 1039:1203  
rigid_body = chain R and resseq 31:76  
rigid_body = chain R and resseq 77:220  
rigid_body = chain R and resseq 221:334  
rigid_body = chain V and resseq 14:127  
rigid_body = chain V and resseq 128:250  
rigid_body = chain T and resseq 5:147  
rigid_body = chain T and resseq 148:215  
rigid_body = chain U  
rigid_body = chain S  
rigid_body = chain W  
rigid_body = chain X and resseq 2:74  
rigid_body = chain X and resseq 75:125  
rigid_body = chain Y  
rigid_body = chain Z  
rigid_body = chain 1  
rigid_body = chain 2  
rigid_body = chain 3 and resseq 22:140  
rigid_body = chain 3 and resseq 141:180  
rigid_body = chain 4  
}
```

6.3.5 Definition file for TLS refinement

```
refinement.refine.adp {  
  tls = chain A and (resid 654:1013 or resid 1361:1367) or \  
    chain B and (resid 8:209 or resid 400:553 or resid 647:1068) or \  
    chain C or \  
    chain J or \  
    chain K or \  
    chain L or \  
    chain N and resid 147:180  
  tls = chain A and (resid 477:653 or resid 1014:1261 or resid 1368:1395 or resid 1500:1608) or \  
    chain B and resid 1069:1092 or \  
    chain E or \  
    chain F and resid 73:154  
  tls = chain A and (resid 1:476 or resid 1609:1649 or resid 3001:3002) or \  
    chain B and (resid 1093-1203 or resid 3001) or \  
    chain O  
  tls = chain A and resid 1650:1664 or \  
    chain D or \  
    chain F and resid 55:72 or \  
    chain G  
  tls = chain M or \  
    chain N and resid 25:146  
  tls = chain I and (resid 2:52 or resid 3001)  
  tls = chain I and resid 53:78  
  tls = chain I and (resid 79:125 or resid 3002)  
  tls = chain A and (resid 1262:1337 or resid 1440:1499)  
  tls = chain B and resid 210:399  
  tls = chain B and resid 554:646  
  tls = chain H  
  tls = chain P and (resid 654:1013 or resid 1361:1367) or \  
    chain Q and (resid 8:209 or resid 400:553 or resid 647:1068) or \  
    chain R or \  
    chain Y or \  
    chain Z or \  
    chain 1 or \  
    chain 3 and resid 147:181  
  tls = chain P and (resid 477:653 or resid 1014:1261 or resid 1368:1395 or resid 1500:1608) or \  
    chain Q and resid 1069:1092 or \  
    chain T or \  
    chain U and resid 73:154  
  tls = chain P and (resid 1:476 or resid 1609:1649 or resid 3001:3002) or \  
    chain Q and (resid 1093-1203 or resid 3001) or \  
    chain 4  
  tls = chain P and resid 1650:1664 or \  
    chain S or \  
    chain U and resid 55:72 or \  
    chain V  
  tls = chain 2 or \  
    chain 3 and resid 25:146  
  tls = chain X and (resid 2:52 or resid 3001)  
  tls = chain X and resid 53:78  
  tls = chain X and (resid 79:125 or resid 3002)  
  tls = chain P and (resid 1262:1337 or resid 1440:1499)  
  tls = chain Q and resid 210:399  
  tls = chain Q and resid 554:646  
  tls = chain W  
}
```

6.3.6 Solvent definition file for refinement

```
refinement {  
  main.ordered_solvent = True  
  
  ordered_solvent {  
    # reduce resolution limit to allow ordered solvent below 2.8 Å  
    low_resolution = 2.9  
    mode = every_macro_cycle  
    output_chain_id = w  
    # more reasonable minimum and maximum hydrogen bond distances  
    h_bond_min_mac = 2.2  
    h_bond_min_sol = 2.2  
    h_bond_max = 3.5  
    b_iso_min = 1.0  
    b_iso_max = 70.0  
    # B-factor for new water molecules; if not set, the mean B-factor is used  
    b_iso = 50.0  
    primary_map_type = mFobs-DFmodel  
    primary_map_cutoff = 3.0  
    secondary_map_and_map_cc_filter {  
      cc_map_2_type = 2mFobs-DFmodel  
      poor_cc_threshold = 0.7  
      poor_map_value_threshold = 1.0  
    }  
  }  
}
```

6.4 Structure-based alignment of A190 and Rpb1

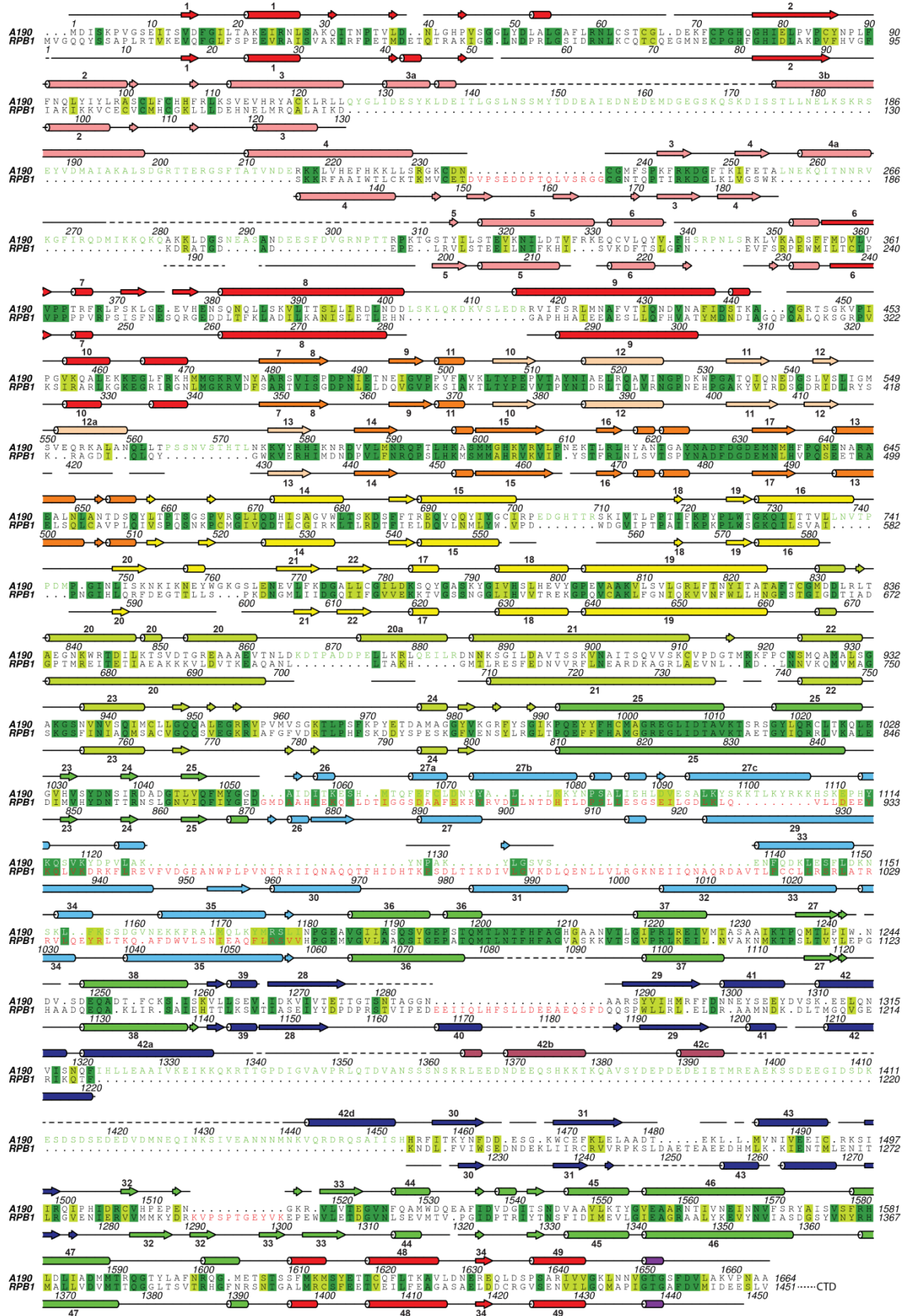


Figure 32. Structure-based alignment of A190 and Rpb1.

Invariant and conserved residues are highlighted in green and light green, respectively. Secondary structure elements are indicated above and below the alignment for A190 and Rpb1, respectively (cylinders, helices; arrows, strands). Residues that form different folds in Pol I or form Pol-II-specific folds are in green or red, respectively (compare Figure 13 and Figure 14).

6.5 Structure-based alignment of A135 and Rpb2



Figure 33. Structure-based alignment of A135 and Rpb2.

Invariant and conserved residues are highlighted in green and light green, respectively. Secondary structure elements are indicated above and below the alignment for A135 and Rpb2, respectively (cylinders, helices; arrows, strands). Residues that form different folds in Pol I or form Pol-II-specific folds are in green or red, respectively (compare Figure 13 and Figure 14).

6.6 Structure-based alignment of AC40/AC19 and the Rpb3/Rpb11 subcomplex

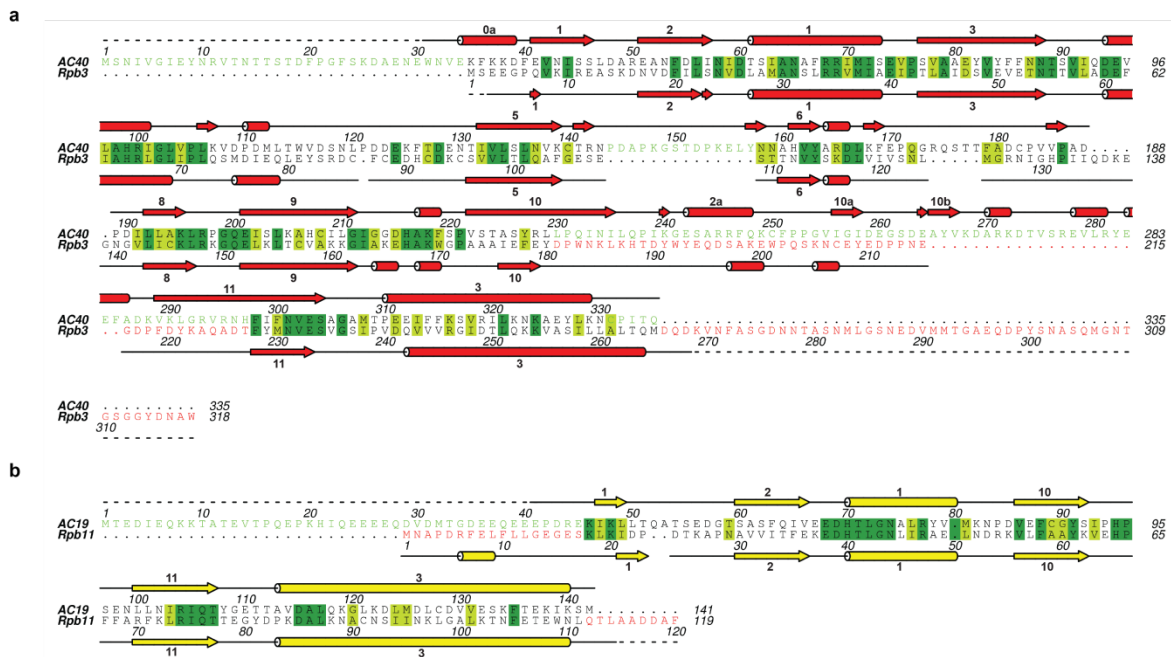


Figure 34. Structure-based sequence alignment of the sub complex AC40/AC19 with Rpb3/Rpb11. Structure-based alignment of AC40 and Rpb3 (a) and of AC19 and Rpb11 (b). Invariant and conserved residues are highlighted in green and light green, respectively. Secondary structure elements are indicated above and below the alignment for AC40 and Rpb3, respectively (cylinders, helices; arrows, strands). Residues that form different folds in Pol I or form Pol-II-specific folds are in green or red, respectively (compare Figure 13 and Figure 15).

6.7 Conservation of Pol I and Pol II subunits

According to the presented structure-based sequence alignments and a previously published one⁸, the identity between subunits of Pol I and Pol II was re-evaluated. A new (and for the first time structurally founded) table of identities was prepared (Table 16).

Table 16. Subunits of the three *S. cerevisiae* RNA polymerases with Sequence identity inferred from structure-based sequence alignments

RNA polymerase	Pol I	Pol II	Pol III [*]
Core enzyme subunits	A190	Rpb1 (22.2%) [†]	C160
	A135	Rpb2 (25.9%) [†]	C128
	AC40	Rpb3 (18.9%) [†]	AC40
	AC19	Rpb11 (20.0%) [†]	AC19
	A12.2 [‡]	Rpb9 [‡] (18.3%) [†]	C11 [‡]
	Rpb5	Rpb5	Rpb5
	Rpb6	Rpb6	Rpb6
	Rpb8	Rpb8	Rpb8
	Rpb10	Rpb10	Rpb10
	Rpb12	Rpb12	Rpb12
Stalk subcomplex A14/A43	A14	Rpb4 (1.8%) [†]	C17
	A43	Rpb7 (12.3%) [†]	C25
TFIIF-like subcomplex	A49	Tfg1 (TFIIF α)	C37
	A34.5	Tfg2 (TFIIF β)	C53

^{*}Pol III additionally contains the trimeric subcomplex C82/C34/C31 that was not included here.

[†]Percentage amino acid residues of the Pol II subunit that are identical in the corresponding Pol I subunit, based on the structure-based alignments and published data.

[‡]The C-terminal zinc-ribbon domain of A12.2 and C11 corresponds to domain III of the Pol II elongation and transcript cleavage stimulatory factor TFIIS.

6.8 Domain differences between the polymerase subunits A190/Rpb1 and A135/Rpb2

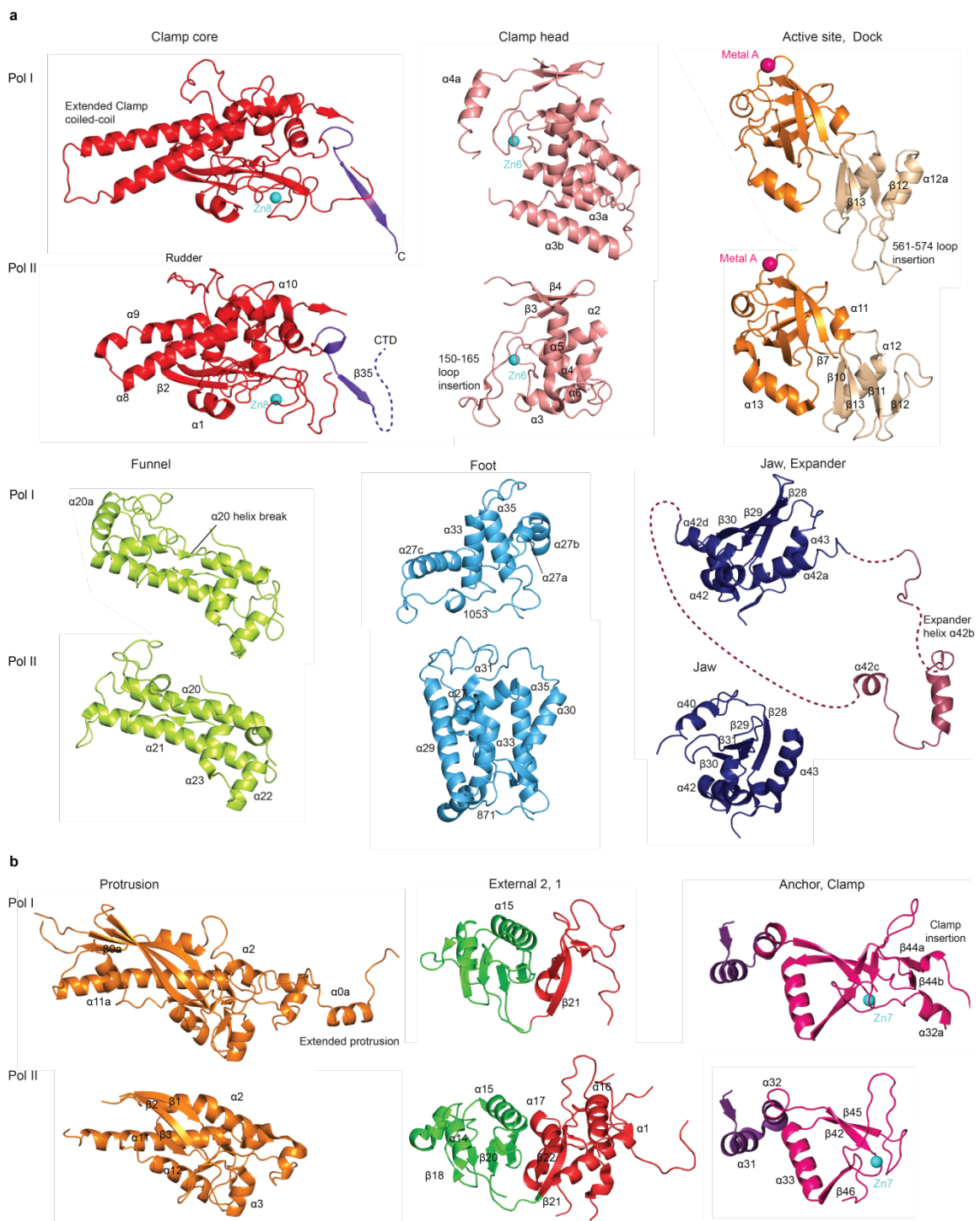


Figure 35. Detailed comparison of A190–A135 domains with their Rpb1–Rpb2 counterparts.

a Comparison of A190 domain structures (top) that differ significantly from their corresponding Pol II regions (bottom). Labelling of corresponding secondary structure elements is as for Pol II⁵⁸. New or lacking secondary structure elements are labelled. New elements were named according to the preceding Pol II element with small letters added alphabetically for subsequent elements. **b** Comparison of A135 domain structures (top) that differ significantly from their corresponding Pol II regions (bottom).

6.9 Evolutionary conservation of expander and connector elements

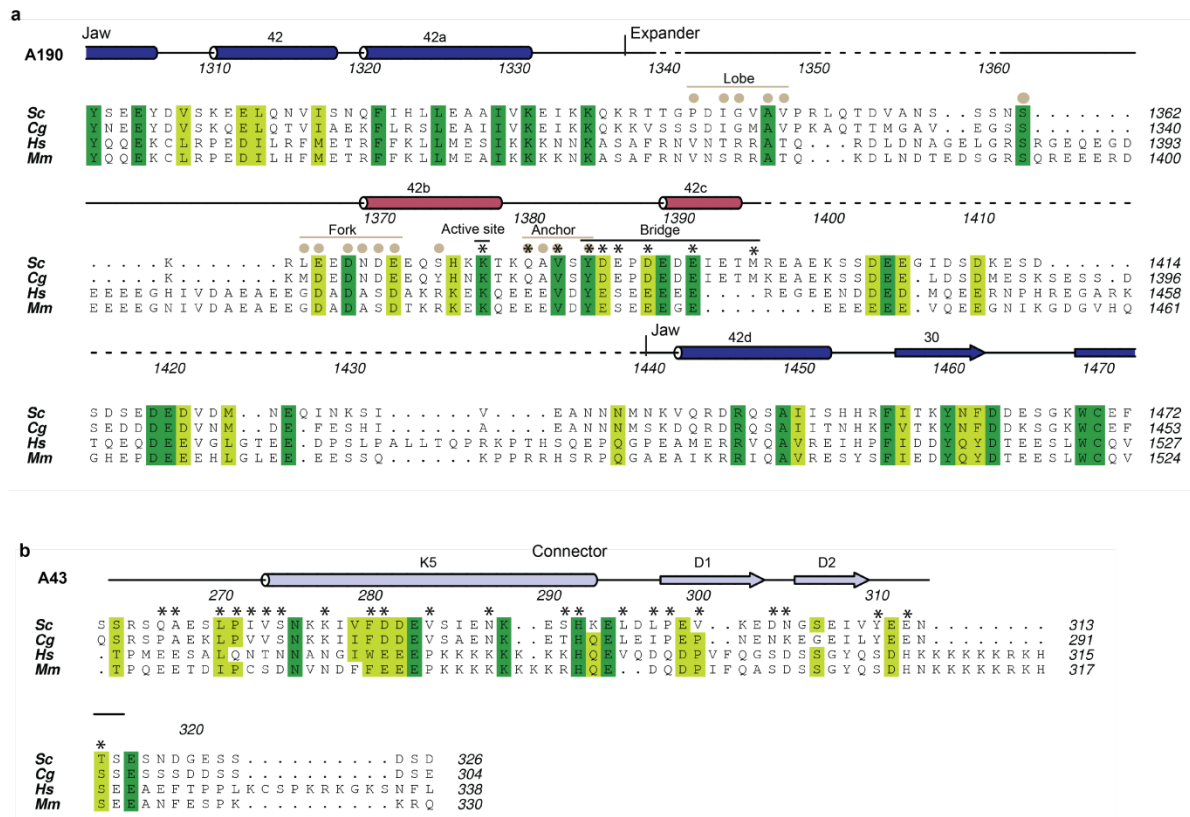


Figure 36. Sequence conservation of the expander and the connector element.

a Amino acid sequence alignment of the connector region in *S. cerevisiae* (*Sc*); *Candida glabrata* (*Cg*); *Homo sapiens* (*Hs*) and *Mus musculus* (*Mm*). Secondary structure elements are indicated above the alignment (K5 helix, cylinder; strands D1, D2; arrows). Residues that are involved in the interface with the Pol I clamp and cleft and showed a buried surface area in excess of 40\AA^2 are indicated with an asterisk above the alignment. Buried surfaces were calculated with the PISA server¹²⁴. A structure-based alignment of the A14–A43 stalk residues was published^{8,61} and is not included here. **b** Amino acid sequence alignment of the expander region in *S. cerevisiae*, *C. glabrata*, *H. sapiens* and *M. musculus*. Secondary structure elements are indicated above the alignment (helices, cylinders; strands, arrows). Residues that are involved in the interface with the Pol I cleft and showed a buried surface area in excess of 40\AA^2 are indicated with an asterisk above the alignment. Buried surfaces were calculated with the PISA server¹²⁴.

6.10 Expander mutations do not display a growth defect in *S. cerevisiae* on YPD medium

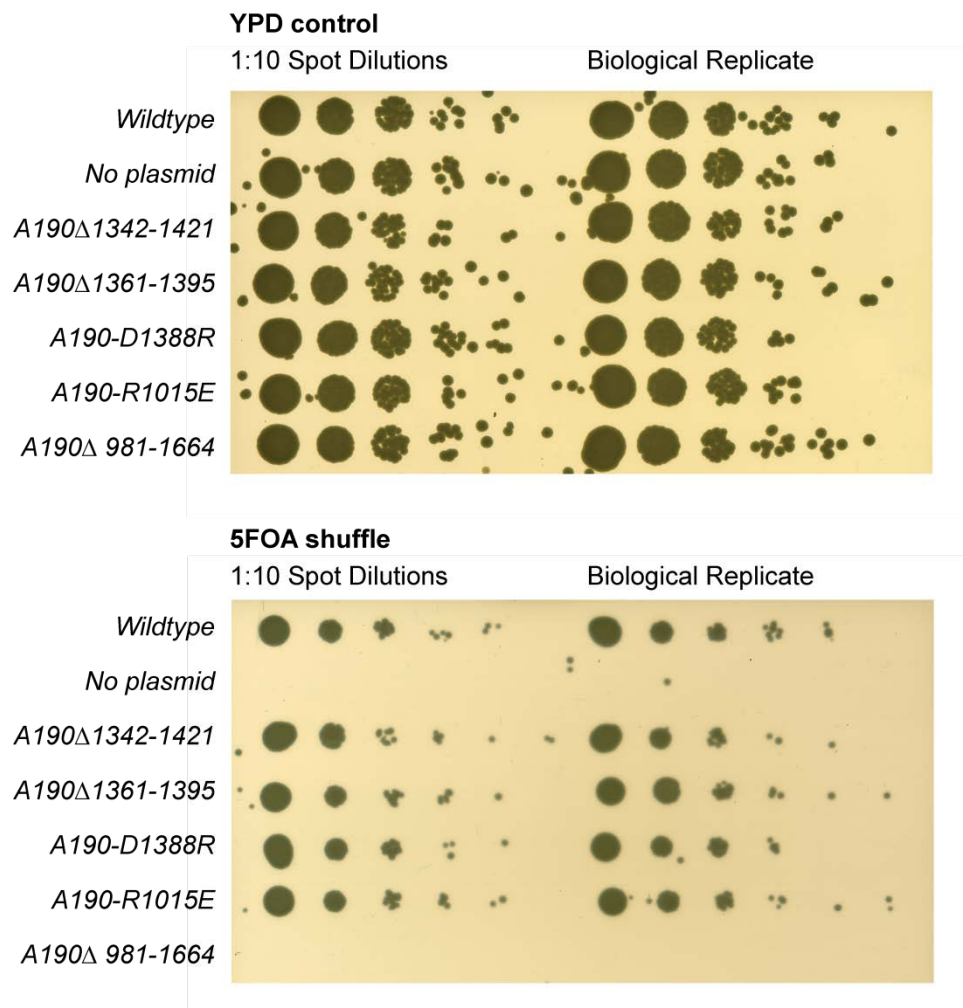


Figure 37. Mutation of the expander element does not result in a growth defect on YPD medium.

The expander element was mutated at different positions. None of them exhibited an obvious growth defect. If repeated at 30°C, 37°C or under stress conditions, no effect took place as well (data not shown).

7. Abbreviations

°C	Degree celsius	PIC	Pre initiation complex
FAM	6-carboxy-fluoresceine	Pol	RNA polymerase
Å	Ångstrom	rmsd	root mean square deviation
Amp	Ampicillin	RNAP	RNA polymerase
AU	asymmetric unit	RT	Room temperature
Bp	base pairs	s	seconds
Cam	Chloramphenicol	SAD	Single-wavelength anomalous diffraction
CE	Core element	SEC	Size exclusion chromatography
CF	Core factor	SDS	Sodium-Dodecyl-Sulphate
CV	Column volume	SLS	Swiss Light Source
DSS	Di-succimidyl suberate	Strep	Streptomycin
DTT	Dithiothreitol	TCA	Trichloroacetic acid
EM	Electron microscopy	TCEP	Tris(2-carboxyethyl)phosphine
ESRF	European Synchrotron Radiation Facility	Tet	Tetracyclin
g	g-force	TOR	Target of rapamycin
G418	Geneticin	TPB	TATA-binding protein
h	hours	UAF	Upstream activating factor
HRP	Horseradish peroxidase	UE	Upstream element
IGS	Intergenic space	v/v	Volume per volume
Kan	Kanamycin	w/v	Weight per volume
LB	Luria-Bertani medium	YPD	Yeast extract peptone dextrose medium
MAD	Multi-wavelength anomalous diffraction		
min	minutes		
NCS	Non-crystallographic symmetry		
NI	normal litres		
NOR	Nucleolar organizer region		
NTP	Nucleoside triphosphate		
OD ₆₀₀	Optical density at 600nm		
PAGE	Polyacrylamide gel electrophoresis		
PDB	Protein Data Bank		
PEG	Polyethylen glycol		
PI	Protease inhibitor mix		